Single-molecule detection of transient dimerization of opioid receptors 1: Homodimers' effect on signaling and internalization

Peng Zhou[1], Taka A. Tsunoyama[1], Rinshi S. Kasai[2,3,4], Koichiro M. Hirosawa[4], Ziya Kalay[5], Amine Aladag[1], Takahiro K. Fujiwara[5], Simone Pigolotti[6], and Akihiro Kusumi[1,5]

[1]Membrane Cooperativity Unit, Okinawa Institute of Science and Technology Graduate University, Onna-son, Okinawa 904-0495, Japan. [2]Institute for Life and Medical Sciences, Kyoto University, Kyoto 606-8507, Japan. [3]Division of Advanced Bioimaging, National Cancer Center Research Institute, Tokyo 104-0045, Japan. [4]Institute for Glyco-core Research (iGCORE), Gifu University, Gifu 501-1193, Japan. [5]Institute for Integrated Cell-Material Sciences (WPI-iCeMS), Kyoto University, Kyoto 606-8501, Japan. [6]Biological Complexity Unit, Okinawa Institute of Science and Technology Graduate University, Onna-son, Okinawa 904-0495, Japan.

Graphical Abstract

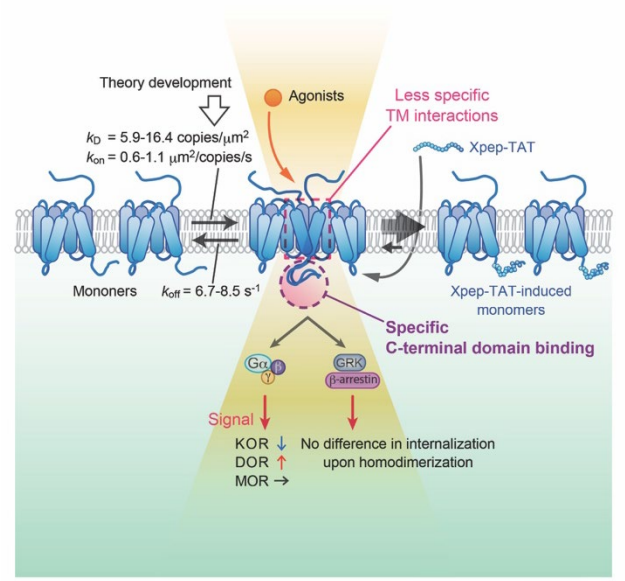

Highlights

- Opioid receptors rapidly interconvert between monomers and transient homodimers
- We developed theories for evaluating the dimer k_{off} and K_D in the plasma membrane
- C-terminal cytoplasmic domains are involved in specific homodimerization
- Homodimer blocking peptides modulate signaling but not receptor internalization

SUMMARY

Opioid receptors (ORs) are critical for endogenous and synthetic analgesics. Their homodimerization is considered important for their pharmacological diversities, but whether they form homodimers remains controversial. Here, we established that the three classical ORs, μ-, κ-, and δ-ORs (MOR, KOR, and DOR, respectively) undergo repeated transient (120-180 ms) homodimerizations every few seconds. This was done by using single-molecule imaging and developing theories for analyzing single-molecule colocalization data, which provide the key parameters, homodimer-monomer dissociation equilibrium constants and rate constants. Their 9-26 amino-acid C-terminal cytoplasmic domains, without sequence similarities, are involved in specific homodimerization, whereas the transmembrane domains provide less specific affinities. Using the membrane-permeable peptides mimicking the C-terminal homodimerization sequences which block homodimerizations, functions of monomers and homodimers were dissected. KOR and DOR homodimers, but not MOR homodimers, activate downstream G-proteins differently from monomers upon agonist addition, without influencing OR internalization. These findings could guide strategies to enhance OR-based analgesia.

60 **INTRODUCTION**

61 Three classical opioid receptors (ORs), μ-, κ-, and δ-ORs (MOR, KOR, and DOR, respectively),
62 are distributed across the central and peripheral nervous systems and play important roles in
63 regulating pain perception, hedonic homeostasis, mood, and well-being.[1,2] ORs are
64 prototypical class A G-protein-coupled receptors (GPCRs), and serve as key receptors for a
65 variety of endogenous and synthetic analgesics. These OR subtypes play critical roles in pain
66 therapeutics, and at the same time, in the development of tolerance to and dependence on
67 analgesics, which are likely associated with activations of the inhibitory G-protein and β-
68 arrestin pathways in complex manners.[2-7]

69 The diversity of OR conformations and their interactions with other proteins not only
70 drives various cellular physiological responses but also contributes to a spectrum of brain
71 circuit responses, both beneficial and adverse.[7-15] Hence, a profound understanding of the
72 mechanisms by which ORs' distinct downstream responses are induced is essential for the
73 development of analgesic drugs with minimized side effects. In addition, receptor
74 dimerization and clustering are often key steps for triggering the downstream signaling
75 cascades in other receptor signaling.[16,17]

76 The pharmacological diversities of ORs might be enhanced by their propensity to form
77 homodimers[18,19] and heterodimers.[20-23] Agonist-induced homodimer formation significantly
78 influences the balance of MOR's downstream G-protein and β-arrestin pathways.[24] Other
79 studies suggested that dimerization, both homo and hetero, might modulate or be modulated
80 by biased agonism, highlighting its significance in receptor signaling (for example, see
81 Refs[25,26] for homodimers and Refs[27-29] for heterodimers). For the β2-adrenergic receptor,
82 another class A GPCR, homodimers are responsible for generating the basal receptor signal in
83 the absence of agonists, a key common characteristic of GPCRs.[30] Furthermore, OR
84 heterodimerization is important for their cooperative functions, as supported by functional
85 and pharmacological studies.[31-36] Therefore, understanding both the homo- and hetero-
86 dimerizations of ORs, as well as those of other class-A GPCRs, is fundamental to deciphering
87 their functional regulation mechanisms.[26,37-45]

88 Despite such extensive research, the very existence of homo- and hetero-dimers of ORs,
89 particularly at physiological expression levels, remains controversial.[46] Previous detection of

90 homodimers of DOR,[18,47,48] MOR,[47,48] and KOR,[22,48] and heterodimers of all OR pairs[48]
91 contrasts with recent single-molecule imaging studies. These studies, performed at
92 physiological expression levels in the plasma membrane (PM) of living cells, in contrast to the
93 results obtained under the conditions of overexpression in cells and very high concentrations
94 in vitro, which are often necessary for the use of bulk observation methods, showed that
95 MOR,[49,50] DOR,[50] and KOR[51] are predominantly monomeric. Therefore, they concluded that
96 previously observed dimerization and its functional and pharmacological consequences would
97 be artifacts due to the employment of very high OR concentrations. Meanwhile, other single-
98 molecule investigations detected the nanodomains of KOR and MOR[52] as well as the transient
99 MOR dimerization[53] or that only after the agonist DAMGO binding, but not morphine.[24]
100 To address the overexpression issue and resolve these controversies, determining the
101 dimer-monomer equilibrium constant K_D is imperative, as it is unaffected by the expression
102 levels. In addition, since several GPCR homodimers are apparently metastable with lifetimes
103 on the order of 0.1-1 s,[30,37,53-57] estimating the dimer dissociation and association rate
104 constants, k_{off} and k_{on}, respectively, is essential for establishing the comprehensive
105 description of the dynamic dimer-monomer equilibrium of ORs. Such insights would enable us
106 to unequivocally determine whether ORs form homo- and hetero-dimers and to what extent
107 under various expression conditions, including both the lower and higher regions of
108 physiological expression levels in different cells in various brain regions. Furthermore,
109 identifying specific binding sites for homo- and hetero-dimerizations, given the high amino
110 acid similarities among the three classical ORs, would be interesting from the protein-
111 interaction viewpoint and highly beneficial for developing reagents that modify dimerizations.
112 In the present research, we addressed these issues, using advanced single-molecule
113 imaging, tracking, and analysis. The single-molecule approach was selected for its ability to
114 directly visualize receptor molecules' dimerization and dissociation in living cells. To extract
115 the dimer-monomer equilibrium constant, K_D, and rate constants, k_{off} and k_{on}, from single-
116 molecule imaging data, we developed two novel theories: one to evaluate k_{off} from the
117 distribution of single-molecule colocalization durations (instead of intuitive methods employed
118 previously), and another to estimates K_D (k_{on} can be calculated as k_{off}/K_D).

We present our findings in two back-to-back papers. This paper focuses on homodimers, while the companion paper addresses heterodimers.[58] In this paper, we report that all three ORs engage in continual, repeated, transient homodimerizations at 37°C, with K_Ds of 5.87 ± 0.56, 15.24 ± 1.54, and 16.42 ± 0.53 copies/μm^2 for KOR, MOR, and DOR, respectively. The homodimer lifetimes are in the range of 120-180 ms (dimer dissociation rate constants in the range of 6.71 to 8.47 s^{-1}), unequivocally demonstrating that even at low physiological expression levels, the three ORs form transient homodimers. Furthermore, we identified that the ≈9-26 amino acid sequences in the cytoplasmic C-terminal domains, without sequence similarities, are involved in the distinct homodimerizations of the three ORs, in line with the previous DOR homodimerization data,[18] whereas the transmembrane domains might promote both homo- and heterodimerizations in a less specific manner, in partial agreement with previous results.[37,59-66]

Building on these amino-acid sequences, we developed peptides that suppress OR homodimerization within live cells. This has allowed us to distinguish the functions of OR dimers from monomers, which could not be done before. OR monomerization by these peptides enhances and diminishes agonist-induced signals downstream from G proteins for KOR and DOR, respectively, without influencing agonist-induced internalization. Meanwhile, monomerization had no discernible effect on MOR signaling or internalization. These findings may inform novel strategies in developing more effective and safer pain treatments.

138 # RESULTS

139 **All three ORs continually interconvert between transient homodimers and**
140 **monomers: analysis by colocalization index based on the pair cross-correlation**
141 **function (PCCF)**

142 ORs conjugated with the SNAPf tag protein at their N-termini (SNAPf-ORs) were expressed in
143 the PM of CHO-K1 cells, which do not express ORs.[67] These SNAPf-tagged molecules were
144 functional (Figures S1A and S1B) and labeled with the fluorescent membrane-impermeable
145 SNAP ligands, SNAP-Surface 549 and SNAP-CF660R, with 60% and 61% efficiencies,
146 respectively (Figures S1C-S1E). For the experiments examining OR homodimerization, we
147 simultaneously labeled a SNAPf-OR (for example, SNAPf-KOR) with both SNAP-Surface 549
148 and SNAP-CF660R so that the number densities of the two probes on the PM were about the
149 same, with spot densities of 0.5 ± 0.25 spots/μm^2 for each color (total spot number densities
150 of 1.0 ± 0.5 spots/μm^2; for conciseness, we will describe as ≈1 spot/μm^2 throughout this
151 report), and then performed simultaneous dual-color single-molecule observations at normal
152 video rate (30 Hz) at 37°C, using a home-built total internal reflection fluorescence (TIRF)
153 microscope.[68,69]

154 Virtually all of the SNAPf-OR fluorescent spots exhibited diffusion in the PM, but in
155 addition, they often exhibited temporary colocalization and co-diffusion (STAR Methods),[57]
156 suggesting the frequent formation of transient homodimers (Movies S1 and S2; Figure 1A).
157 We focused on simultaneous two-color experiments, due to the ease of image analysis. For
158 the single-color imaging data, see Figure S2A and S2B, which show an example of repeated
159 homodimerizations of a KOR molecule with different partner KOR molecules, consistent with
160 the observations made with other GPCRs.[55-57]

161 To quantitatively examine the extent of the colocalization of two single molecules, we
162 employed a "colocalization index", which parameterizes the propensity of a pair of magenta
163 and green molecules to become localized within 100 nm. Namely, the colocalization index is
164 defined from the pair cross-correlation function (PCCF) histogram for the SNAP-Surface 549
165 (green) and SNAP-CF660R (magenta) spots (Figure 1B),[70] as the ratio of PCCF (0-100 nm) vs.
166 PCCF (400-500 nm) (Figures S2C-S2E). When a molecular interaction does not exist, the
167 colocalization index is equal to one within experimental uncertainty. When it does exist, the

index becomes significantly greater than 1. As a negative control (including incidental colocalization), the 180°-rotated magenta image was superimposed on the green image (see Figure S2D, grey histogram in Figure 1B), providing a colocalization index of ≈1. KOR, MOR, and DOR exhibited significantly higher colocalization indexes than the negative controls (Figure 1C), suggesting that they form homodimers (and possibly greater oligomers when the expression levels are enhanced).

Homodimer dissociation rate constant k_{off} (inverse of the dimer lifetime) can be obtained from single-molecule colocalization experiments

To evaluate the homodimer lifetimes, each time we found the colocalization event of spots with different colors within a threshold distance R = 200 nm (see Note S1, which shows that the selection of R does not affect the measured k_{off} value, although it could affect its SEM),[56,57,68,69] its duration was measured. By measuring the durations of >1,500 events (in ⩾ 17 cells; all statistical parameters are summarized in Table S1), we obtained the distribution of colocalization durations (Figure 1D).

To evaluate the homodimer dissociation rate constant k_{off} (inverse of the homodimer lifetime) from the distribution of colocalized durations, we developed a theory based on the diffusion equation that predicts the distribution of colocalization durations (Note S1). The crucial result of this theory is that, from the histogram of the *colocalization* durations, we can rigorously estimate the homodimer dissociation rate constant k_{off} and thus the homodimer lifetime τ_2. This result holds despite the fact that the generally used colocalization threshold distance is ≈200 nm, which is much greater than the molecular scale of 3~10 nm. The theory shows that, at a time resolution of 33 ms and under the conditions of quite limited signal-to-noise ratios in our experiments, the histogram of the colocalization durations can be fitted with the sum of two exponential functions, where the two decay constants represent the incidental colocalization lifetime ($1/\alpha$) and the inverse of the dissociation rate constant ($1/k_{off}$).

Previously, we[56,57,69] and others[53-55] depended on intuitive methods to obtain the homodimer lifetimes from optical colocalization data. However, due to the theory developed

here, we now have a firm basis to obtain the homodimer dissociation rate constant k_{off} from the distribution of single-molecule colocalization durations.

Brief outline of the theory to evaluate k_{off} from the single-molecule colocalization duration distribution (Note S1)

In dual-color single-molecule tracking, a colocalization is defined as an event in which two spots are located closer than a threshold distance R. Starting from the 2D diffusion equation, we found that the distribution of the dwell times in the threshold circle without binding (incidental lifetime τ_{inci}; i.e., incidental colocalization duration, Figure 1E) is expressed by

$$p_d(t) \approx \sum_{n=1}^{\infty} \frac{2D\epsilon{\mu_n}^2}{R^3} e^{-\frac{D{\mu_n}^2 t}{R^2}} \approx \alpha e^{-\alpha t} \quad , \tag{9}$$

where D is the diffusion coefficient, R is the threshold distance, ε is a regularization factor, and μ_n is the n-th real positive 0 of the Bessel function (Equation numbers in the main text are matched with those in Notes S1 and S2 for easy reference). Under our experimental conditions, the first term is sufficient to describe the distribution, providing a single exponential function with a decay time constant of $R^2/D\mu_1^2 = 1/\alpha$, which is the incidental colocalization lifetime (τ_{inci}). We indeed found that the colocalization time distribution for incidental colocalizations obtained for the overlay on the 180°-rotated image (Figure S2D) could be fitted with a single exponential function (using both Akaike's and Bayesian information criteria; AIC and BIC, respectively) (Figure 1D).

The dwell time in the threshold circle with binding (T; i.e., colocalization duration, Figure 1E) is given by the sum of τ_{inci} added to the sum of multiple binding durations, τ_i.

$$T = \tau_{\mathrm{inci}} + \sum_{i=1}^{n} \tau_i \quad . \tag{10}$$

Here, the terms in the sum correspond to possible multiple binding events during a dwell; i.e., to obtain the correct k_{off} value, we will need to consider the cases where the observed colocalization durations are the results of multiple binding events.

Combining these results, we obtain the dwell time distribution in the threshold circle.

$$P(T) = \frac{\alpha k_{\mathrm{off}}}{\Gamma}\left\{\left[1 - \frac{(\Delta - \Gamma)}{2k_{\mathrm{off}}}\right] e^{-\frac{T}{2}(\Delta-\Gamma)} - \left[1 - \frac{(\Delta + \Gamma)}{2k_{\mathrm{off}}}\right] e^{-\frac{T}{2}(\Delta+\Gamma)}\right\} \quad , \tag{21}$$

where $\Delta = (\alpha + k_{\text{off}} + k_{\text{on}})$ and $\Gamma = \sqrt{\Delta^2 - 4\alpha k_{\text{off}}}$.

At a time resolution of 33 ms and under the conditions of the quite limited signal-to-noise ratios in our experiments, we obtain

$$(\Delta - \Gamma)/2 \approx k_{\text{off}} \quad , \tag{30}$$

$$(\Delta + \Gamma)/2 \approx \alpha \quad . \tag{31}$$

This result explains why the histogram of the colocalization durations can be fitted by the sum of two exponential functions. Most importantly, it permits to identify the two decay constants with the incidental colocalization lifetime ($1/\alpha = \tau_{inci}$) and the inverse of the dissociation rate constant ($1/k_{\text{off}}$), as anticipated.

OR homodimer dissociation rate constant k_{off} and true homodimer lifetime

As shown in Figure 1D, we were able to fit the three histograms for KOR, MOR, and DOR, obtained from the correctly overlaid images, with the sum of two exponential functions, as predicted by equations 30 and 31. The fitting provided two time constants, τ_1 and τ_2 ($\tau_1 \leq \tau_2$). The histogram obtained from the rotated overlay images could be fitted with a single exponential function, which provided the time constant τ_{inci} (= $1/\alpha$) (the numbers of significant exponential terms were always confirmed by both AIC and BIC in this work). We found that $\tau_1 \approx \tau_{\text{inci}}$ for all three ORs. The longer decay time constant obtained from the histogram for the correctly overlaid images (τ_2) provides k_{off} (= $1/\tau_2$; Note S1). As such, using this theory, by simply plotting the histogram of the colocalization durations, we can obtain the correct homodimer dissociation rate constant k_{off} (by taking account of the multiple binding-dissociation cycles).

The homodimer lifetimes of KOR, MOR, and DOR were estimated to be 178 ± 5, 122 ± 3, and 120 ± 3 ms, respectively, from the histograms shown in Figure 1D (after correction for the trackable duration lifetimes of the two fluorescent probes). These lifetimes are considerably shorter than that reported for KOR (≈1.8 s at room temperature, perhaps ≈20°C).[53] This difference might be predominantly explained by the lower temperatures employed in the previous study (20°C), whereas our observations were performed at 37°C. In addition, it is possible that our imaging and analysis methods are more sensitive to short-term colocalization events, compared with previous investigations.

249

250 **Determination of OR homodimer-monomer equilibrium constant (K_D) from PCCF**

251 In the literature, the question of whether ORs (or GPCRs or any other membrane proteins)
252 form homodimers or not has been extensively debated. However, the facts of the matter are
253 that many membrane proteins would form homodimers and clusters anyway at higher
254 expression levels, and that the physiological expression levels vary greatly from cell to cell.
255 Therefore, the critical point should be to quantitatively estimate the homodimer affinity; i.e.,
256 to evaluate the homodimer dissociation (homodimer-monomer) equilibrium constant K_D.
257 Here, we developed a theory (Note S2) for evaluating K_D from the PCCF of the OR
258 fluorescently-labeled in two colors (PCCF in the form of a histogram, as shown in Figures 1B
259 and S2E), under conditions where the expression levels are low and so the presence of
260 oligomers greater than dimers could be neglected. The K_D values evaluated from the PCCF by
261 this method are quite accurate because we employed the expression conditions of ≈1
262 fluorescent spot/μm^2 (Figures S3C and S3E): Within this range, the colocalization index barely
263 depended on the expression levels when K_D >6.5 copies/μm^2 (see the simulation results
264 shown in Figures S3A-S3E, particularly Figure S3C). At these copy number densities, we
265 hardly detected oligomers greater than dimers.

266 The values of K_D were 5.87 ± 0.56, 15.24 ± 1.54, and 16.42 ± 0.53 copies/μm^2 for
267 KOR, MOR, and DOR at 37°C, respectively (Figure 2A and 2B; K_D was first determined for
268 each movie using the PCCF and the number of fluorescent spots obtained from the movie,
269 fixed fluorescent labeling efficiencies of 0.60 for SNAP- SNAP-Surface549 and 0.61 for SNAP-
270 CF660R, and fitting parameters of K_D and the precision of overlaying two-color movies plus
271 single-molecule localizations for the two fluorescent probes, and then the arithmetic mean (±
272 SEM) K_D was obtained using K_Ds determined for all the movies; the number of movies are
273 provided in Table S1, like other statistical parameters). These K_D values mean that KOR is
274 more likely to exist as homodimers than MOR and DOR (the main results are summarized in
275 Table 1 and their statistical test results are in Table S1). Our estimated values of K_D for the
276 MOR and KOR homodimers found here exhibited much smaller errors compared with previous
277 estimates (for MOR[53], 27.43 ± 11.75 copies/μm^2; and for KOR[50], 32 ± 15 copies/μm^2), and
278 their mean values are smaller by factors of approximately 1.7 and 4.9, respectively. In

279 contrast, these K_D values are greater than the K_D's of β2AR and FPR homodimers (1.6 and 3.6
280 copies/μm^2, respectively).[30,57] The K_D values for CD28, the constitutive disulfide-linked dimer
281 control molecule,[71] and the transmembrane domain of the LDL receptor (TM^{LDLR}), the
282 monomer control molecule,[57] are 0.041 ± 0.072 and 132 ±21 copies/μm^2, respectively,
283 providing the basic dynamic range (4400x) for this method to evaluate K_D values (although
284 the value for CD28 is a nominal value, representing the experimental limitation). Our results
285 indicate that the KOR homodimer affinities are higher than those of DOR and MOR, and thus
286 partially explain previous data showing that KOR, but not DOR or MOR, forms homodimers at
287 low membrane densities.[50] In the following part of this report and in the companion paper,
288 we use the colocalization index when showing the direct experimental data is preferrable,
289 whereas we show the K_D values when providing the fundamental constants is desirable.
290 Under our standard experimental conditions, the colocalization index is simply related to K_D as
291 shown in Figure 2C, and K_D can be roughly evaluated using the graphs shown there, although
292 we performed actual fitting for the PCCF for each cell to obtain the K_D value for each cell (the
293 final K_D value and its SEM were obtained as the arithmetic mean of the K_Ds for all the
294 observed cells).

295 Using k_{off} and K_D, k_{on} can be calculated as k_{off}/K_D (equation 1). Direct determination of
296 k_{on} from single-molecule movies is only possible when the labeling efficiency is 100%. This is
297 because the fluorescent spots that appear to be monomers (protomers) of A and B molecules
298 might be dimers of labeled and non-labeled molecules. For the correction to evaluate the
299 actual numbers of protomers, one would need to know K_D, and thus k_{on} cannot be
300 determined independently from K_D. The percentages (in copy numbers) of molecules
301 (protomers) that exist as dimers at various expression levels (number density of molecules)
302 were calculated from the obtained K_D values (Figure 2D). Their overall variations are in the
303 range of 3.4-59% of protomers in homodimers over the ORs' predicted physiological
304 expression ranges of 0.3 - 10 copies/μm^2.[46,49,53]

305 Therefore, substantial amounts of homodimers would exist in various nerve tissues at
306 any time. The expected average protomer copy numbers existing as monomers and
307 homodimers per cell at various expression levels are shown in Figure 2B and 2D. However, all
308 of these homodimers are forming and dispersing all the time, with lifetimes shorter than 0.2 s

309 (Figure 1D). Once dissociated into monomers, they will again form homodimers, often with
310 different partner molecules (Figure S2A and S2B), which will occur more readily at higher
311 expression levels. Therefore, although at any moment, 10-21% of ORs might exist as
312 homodimers at the expression levels we employed (≈1 copy/μm^2), the actual molecules
313 existing as dimers are turning over all the time, and within a few seconds (even at an
314 expression level of 1 copy/μm^2; calculated as $1/k_{off} + 1/[k_{on} \times 1]$), virtually all of the
315 molecules experience the periods of homodimers and monomers.
316 A previous biochemical study detected DOR homodimers[18] and a single-molecule
317 imaging study using a fluorescently-conjugated MOR antagonist detected MOR homodimers,[53]
318 in agreement with our results. Meanwhile, at apparent variance with our results, previous
319 single-molecule examinations demonstrated that MOR and KOR tend to exist as monomers
320 even at 20°C, at expression levels between 0.1 and 0.3 copies/μm^2.[24,51] Since we employed
321 somewhat higher number densities of ≈1 OR spot/μm^2, the discrepancy might simply be due
322 to the number densities of homodimers found in an image. This underscores the critical
323 importance of evaluating the homodimer-monomer dissociation equilibrium constant K_D,
324 rather than simply detecting homodimers.[57]
325

326 **The 9-26 amino-acid sequences in the C-terminal cytoplasmic domains play**
327 **critical roles in OR homodimerization**

328 To advance our understanding of OR homodimerization mechanism, we determined the OR
329 domains and amino acid sequences responsible for homodimerization. First, we examined the
330 involvement of the extracellular N-terminal domains in homodimerization, using the N-
331 terminal deletion mutants (KOR(Δ1-53), MOR(Δ1-51), and DOR(Δ1-35)). Given that the
332 amino-acid homologies in the N-terminal domains among the three ORs are quite low (Figure
333 S4A), we considered a possibility that they might be used to distinguish particular homo-
334 and/or hetero-dimers. These amino-acid sequence ranges were selected partly because the
335 removal of the entire N-terminal extracellular domains blocked the OR expression in the PM,
336 probably due to the deletion of the signal sequences. In addition, these deletion mutants
337 were previously used in X-ray crystallography studies to determine the structures of the
338 remaining parts of ORs.[72-75]

339 The N-terminal deletion mutants of the three ORs all exhibited diffusion behaviors
340 similar to those of the wild types (without immobilization or clustering) and virtually the same
341 colocalization indexes as those of the wild types (Figure 1C). These results clearly indicate
342 that the N-terminal extracellular domains are not responsible for homodimerization (see the
343 companion paper about the N-terminal domain involvement in heterodimer formation).
344 We next examined the involvement of the C-terminal cytoplasmic domains. Their
345 amino-acid homologies are also low, and in addition, a previous biochemical analysis
346 indicated that the 15-amino acid stretch in the C-terminal domain is responsible for DOR
347 homodimerization.[18] We examined systematically varied C-terminal deletion mutants (Figures
348 3A and 3B). They hardly exhibited immobility or clustering, and their colocalization indexes
349 showed that KOR's aa 365-380, MOR's aa 358-382, and DOR's aa 357-372 are critical for
350 homodimerization (Figure 3B and Table S1). For DOR, this amino-acid sequence agrees with
351 the previous biochemical data.[18] Meanwhile, the mean colocalization index values never
352 decreased to the index values comparable to those for rotated overlays (≈1) (Figure 3B) or a
353 monomer control molecule TM^{LDLR} (≈1.1) (Figure 2A), suggesting the possibility that there
354 might be other weaker homodimerization site(s), which might be the TM domains, as
355 previously suggested for ORs[46,73,74,76-79] and other class A GPCRs.[37,59,60,62-65] However, as
356 shown in Figure S4A; the aa identities of TM domains among the three ORs are quite high,
357 and thus the homo-interaction between TM domains might be less specific. We will revisit the
358 TM interactions for homodimerization later.
359 The distribution (histogram) of the colocalization *durations* for each representative
360 deletion mutant, KOR(Δ365-380), MOR(Δ358-382), or DOR(Δ357-372), could be fitted by a
361 single exponential function, rather than the sum of two exponential functions (based on both
362 AIC and BIC). The decay time constants were only slightly longer than the incidental
363 colocalization lifetimes (Figure 3C); i.e., the τ_2 component, representing the homodimer
364 lifetime fraction, is small and /or the τ_2 is short, and thus the τ_2 component could not be
365 resolved from the incidental colocalization lifetime decay component.
366 By introducing point mutations in these critical regions for homodimerization and their
367 surrounding regions (Figure 3A), we found that a few to several basic/acidic residues, as well
368 as proline residues, are involved in the OR homodimerization (for particular amino acids, see

369 the colocalization indexes shown in Figure 3D), suggesting that the electrostatic interactions
370 and the overall structure of the cytoplasmic C-terminal domain could be important for
371 homodimerization. Indeed, the IUPred2 scores (energy-estimation-based predictions for
372 ordered and disordered residues; http://iupred2a.elte.hu)[80,81] indicated that the C-terminal
373 region could be weakly intrinsically disordered (Figure S4B), and the scores decreased (more
374 ordered) with these point mutations (Figure S4C). Accordingly, in addition to the specific,
375 relatively strong amino-acid interactions, multiple specific, but weak interactions, made
376 possible by the flexible intrinsically disordered regions (IDRs) of the ORs' C-terminal regions,
377 might facilitate the OR homodimerization. Such a mechanism resembling liquid-liquid phase
378 separation was previously found for the dimerization of the transcription factor PU.1.[82]
379 Furthermore, the IDRs in the C-terminal regions might be necessary to bring the specific
380 binding sites closer so that the actual binding can occur.[83]
381
382 **Peptides mimicking the homodimerization sites block homodimer formation**
383 We then examined whether peptides with the same amino-acid sequences as those of the
384 deleted parts of the mutants could block homodimerization. The use of these peptides was
385 critical for unequivocally demonstrating that the specific amino-acid sequences in the C-
386 terminal regions of KOR, MOR, and DOR are responsible for homodimerizations, because the
387 deletion and point mutations might have induced conformational changes of the true
388 homodimer interaction sites, thus inhibiting homodimerization. Furthermore, if we could
389 develop such homodimerization blockers, they could become extremely useful tools to dissect
390 the functions of OR monomers and homodimers, and might inform future developments of
391 more effective analgesic treatments with fewer side effects and less tolerance development.
392 We employed two approaches. The first one involved the expression of peptides with
393 the same amino-acid sequences as those of the deleted parts of the mutants, conjugated to
394 the C-terminus of mGFP (named mGFP-Kpep, Mpep, and Dpep, collectively called mGFP-
395 Xpeps; numbers in parentheses following mGFP-Xpeps indicate the amino-acid residue ranges
396 in the wild-type ORs) in CHO-K1 cells stably expressing SNAPf-KOR, MOR, or DOR,
397 respectively (Figures 4A and 4B). The concentration of the cytoplasmic mGFP-Xpep was
398 measured by confocal fluorescence microscopy, based on calibration with various

399 concentrations of purified mGFP protein dissolved in Ham's F12 observation medium in the
400 glass-base dish (Figure S5A; see STAR Methods).
401 The OR homo-colocalization index in the cells expressing various concentrations of
402 mGFP-Xpep in the cytoplasm (homogeneously distributed throughout the cytoplasm; Figure
403 4B) exhibited a clear tendency to decrease with an increase of the specific mGFP-Xpep
404 concentration in the cytoplasm from 0 to 7.8 μM for all three ORs (Figure 4C), whereas the
405 control mGFP-peptides (mGFP-Dpep for KOR and MOR and mGFP-Kpep for DOR) had no
406 effect (Figure 4C). Consistently, the distributions of the colocalization *durations* in cells
407 expressing 3.8-7.8 μM mGFP-Xpeps could be fitted by a single exponential function, rather
408 than the sum of two exponential functions (based on both AIC and BIC; Figure 4D), and the
409 decay time constants became similar to those for the C-terminal deletion mutants (compare
410 Figure 4D with Figure 3C; Table 1).
411 As the second approach, the K-, M-, and D-peps were conjugated with the fluorescent
412 dye 5-FAM at their N-termini for visualization, and with the TAT sequence (YGRKKRRQRRR)
413 (using a G10 linker sequence) at their C-termini for membrane permeabilization (FAM-Xpep-
414 TAT; see STAR Methods), and added to cells preincubated with 150 μM pyrenebutyrate for 5
415 min (Figures 4E and 4F).[84] The FAM-peptide-TATs exhibited diffuse spatial distributions
416 throughout the cytosol (Figure 4F). The cells containing 2.9-3.4 μM FAM-Xpep-TAT (see
417 Figure S5B for the concentration calibration; in the following, we describe this concentration
418 range as ≈3 μM for conciseness) were selected and the effects of these cytoplasmic peptides
419 on the OR homodimerization were examined. The results indicated that ≈3 μM FAM-peptide-
420 TAT significantly blocked the homo-dimerization (Figure 4G; Table 1), consistent with the
421 data obtained using mGFP-Xpeps (Figure 4C). The control FAM-Xpep-TATs (FAM-Dpep-TAT
422 for KOR and MOR and FAM-Kpep-TAT for DOR) did not affect the colocalization indexes. The
423 effects on colocalization durations were consistent with these results and with those obtained
424 by expressing mGFP-Xpeps (Figure 4H; compare with Figure 4D; Table 1).
425 The Xpep concentrations required for blocking homodimer formation might appear quite
426 high (≈3 μM), compared with the ≈30-nM-level dissociation constants of various agonists and
427 antagonists for ORs. However, note that the latter is the value for simple binding of the
428 ligand to the receptor, whereas the former addresses the extremely efficient dimerization

429 propensities of membrane molecules in the two-dimensional (2D) PM. The efficiency of
430 dimerization in 2D space was previously found to be higher by a factor of 10^6 than that in 3D
431 space.[85]

432 The effects of the presence of ≈3 μM FAM-Xpep-TATs in the cytoplasm on the
433 homodimer K_D, k_{off}, and k_{on} values are summarized in Figure 4I. In addition to K_D and k_{on},
434 FAM-Xpep-TATs increased k_{off} (enhanced dimer dissociation), indicating that the OR
435 homodimerization cannot be described by simple first-order kinetics (simple binding reaction
436 at the C-terminal domains), perhaps due to the conformational changes of the C-terminal
437 domains induced by the peptide binding and/or to the presence of weaker secondary binding
438 sites such as TM domains (Figure 5, which will be discussed later). Nevertheless, we think the
439 present simplified approach is useful as the starting point for quantitative understanding of
440 the dynamic equilibrium between OR homodimers and monomers.
441

442 **Agonists modulate monomer-dimer interconversions, and FAM-Xpep-TAT peptides**
443 **reduce their effects**

444 The addition of representative agonists, U-50488 for KOR, [D-Ala^2, N-Me-Phe^4, Gly^5-ol]-
445 enkephalin acetate salt (DAMGO) for MOR, and SNC-80 for DOR, at 0.2 μM (a concentration
446 sufficient to ligate virtually all OR molecules) affected the homodimerizations of the three ORs
447 differently (observed during 2-5 min after agonist addition rather than after longer incubation
448 because these agonists induce OR internalizations, which become evident after 5 min;
449 discussed later in this report). The agonist-bound KOR exhibited less homodimerization (lower
450 colocalization index), whereas the agonist-bound MOR and DOR exhibited more
451 homodimerization (Figure 4G and Table 1), although these results might vary depending on
452 the particular agonist.[18,24] For example, the DOR agonists, DADLE, DSLET, and DPDPE, were
453 previously found to induce fewer homodimers,[18] but in the present research, another DOR
454 agonist SNC-80 was found to increase the homodimer fraction, suggesting that the
455 dimerization propensity depends on each agonist. We only examined one agonist for each OR
456 subtype, because an extensive examination of the agonist effects on OR homodimerization is
457 beyond the scope of the present work.

458 The colocalization indexes of the agonist-bound ORs were reduced by the addition of
459 FAM-Xpep-TAT for all ORs, but in different ways depending on the OR type (Figure 4G). The
460 colocalization index of the agonist-bound KOR, which exhibited a smaller index as compared
461 with that of non-ligated KOR, was further reduced by the presence of FAM-Kpep-TAT
462 (although with no statistical significance). The colocalization index of the agonist-bound MOR
463 was reduced in the presence of FAM-Mpep-TAT to a level near that for MOR with the FAM-
464 Mpep-TAT without the agonist. The colocalization index of the agonist-bound DOR was
465 reduced in the presence of FAM-Dpep-TAT, but was still greater than that of wild-type DOR in
466 the absence of the agonist. The reason for this higher tendency to form homodimers even in
467 the presence of FAM-Dpep-TAT is unknown, but we propose that the agonist-induced
468 conformational changes enhanced the interaction in the TM domains, because DOR
469 homodimerization also involves TM-domain interactions (see Figure 5, which will be discussed
470 in the next subsection). The effects of the agonists and homodimer blocker peptides on the
471 colocalization *durations* were consistent with the colocalization index data (Figure 4H), and
472 the agonists' effects on the homodimer K_D, k_{off}, and k_{on}, as well as the percentages of OR
473 protomers existing as homodimers are summarized in Figure 4I. The actual copy numbers of
474 OR protomers existing as monomers and homodimers at various total numbers of OR
475 molecules in the entire PM in a cell are summarized in Table S2.
476

477 **MOR's transmembrane domain 1 ($TM1^{MOR}$) is involved in MOR homodimerization**
478 **with less specificity**

479 Specific C-terminal cytoplasmic domain deletions/mutations and the addition of peptides with
480 the same amino acid sequences as the deleted sequences greatly reduced the OR
481 homodimers' colocalization indexes, but never to be compatible with 1 found for rotated
482 overlays or 1.1 found for the monomer control molecule TM^{LDLR} (Figure 2A). Therefore, we
483 considered the existence of other OR sites for homodimer formation. Since the involvement of
484 transmembrane domains in OR homo- and hetero-dimerization has been
485 proposed,[33,34,37,46,73,74,76-79] and the first OR transmembrane domain (TM1) is often mentioned
486 in the literature,[46,73,74,78,79] we examined the involvement of MOR's TM1 domain ($TM1^{MOR}$) in
487 MOR homodimerization (Figure 5A).

488 Colocalization indexes indicated that $TM1^{MOR}$ interacts with another $TM1^{MOR}$ and MOR, as
489 well as, importantly, with DOR (Figure 5B; the fluorescent spot number densities of the two
490 molecules in the PM were always adjusted to ≈1 spot/μm^2, and thus the number ratio was
491 approximately 1:1). These results suggest that $TM1^{MOR}$ is involved in MOR homodimerization
492 by the $TM1^{MOR}$-$TM1^{MOR}$ interaction, as well as, surprisingly, in MOR-DOR heterodimerization.
493 These results are supported by the observation of the colocalization *durations* (Figure 5C).
494 In contrast, in the homodimer blocking experiments where $TM1^{MOR}$ is expressed ≈10x
495 more than MOR or DOR (Figure 5D), $TM1^{MOR}$ moderately suppressed both MOR and DOR
496 homodimers (positive controls, Mpep and Dpep, respectively: negative controls, TM^{LDLR} = the
497 TM domain of LDL receptor and Xpeps specific for different OR homodimers; Figure 5E).
498 Particularly, $TM1^{MOR}$ reduced both MOR and DOR homodimers, whereas Mpep reduced MOR
499 homodimers and not DOR homodimers and Dpep reduced DOR homodimers and not MOR
500 homodimers. Taken together, we conclude that the interaction specificity of $TM1^{MOR}$ is limited
501 as shown from its ability to interact with both MOR and DOR (Figures 5B and 5E). The results
502 showing that $TM1^{MOR}$ suppresses both MOR-MOR and DOR-DOR homodimerization indicate
503 that $TM1^{MOR}$ is involved in both MOR homodimerization and MOR-DOR heterodimerization
504 (also refer to Figure 5C in the companion paper for the involvement of $TM1^{MOR}$ for MOR-DOR
505 heterodimerization). These results further indicate that $TM1^{MOR}$ might not be useful as a
506 specific blockers for MOR homodimerization or MOR-DOR heterodimerization.
507

508 **No major effects of Xpeps on the agonist-induced OR internalization**

509 We specifically blocked OR homodimers by the addition of Xpeps (FAM-Xpep-TATs), and
510 examined the effects on the agonist-induced OR internalization. Since all experiments were
511 performed at expression levels of ≈1 OR spot/μm^2, the percentages of the OR protomers
512 existing as homodimers are 10-21% without any addition, 3.2-4.4% after the addition of
513 FAM-Xpep-TATs, and 10-18% after the agonist addition, which is decreased to 2.9-8.6% after
514 the further addition of FAM-Xpep-TATs (see the column of 1 copy/μm^2 in Figure 4I).
515 OR internalization might be involved in opioid side effects and tolerance development.
516 Here, it was monitored by using the membrane-*im*permeable fluorescence quencher, Mn(III)
517 meso-tetra(4-sulfonatophenyl)porphine (Mn^{3+}-TSP). This quencher only suppresses

518 fluorescence emission from the SNAP-Surface 549 dye on the SNAPf-OR on the cell surface,
519 but not that in the cytoplasm.[86]
520 Accordingly, by subtracting the signal intensity after the quencher addition from that
521 before the addition, we evaluated the percentages of OR molecules remaining in the PM
522 (Figures 6A and S6).
523 The time courses of the decrease in the numbers of ORs remaining in the PM during 35
524 min (due to their internalization) were examined in both the presence and absence of 0.2 μM
525 agonists and ≈3 μM Xpeps in the cytoplasm (Figure 6B; Tables 1 and S1). All the time-course
526 data obtained under various conditions could be fitted with a single exponential function plus
527 a constant. The constant provides the OR fraction whose internalization is undetectable by
528 the 35-min observations, and the exponential decay constant provides the residency lifetime
529 in the PM for the OR component whose internalization was detectable by this observation
530 scheme (Tables 1 and S1). Without agonist, the three ORs all exhibited non-internalized
531 fractions in the range of 91-97% (for an observation period of 35 min). The internalized
532 molecules found during the 35-min observations showed characteristic dwell lifetimes (inverse
533 of internalization rates) between 24 and 45 min. The homodimer-blocking peptides, FAM-
534 Xpep-TATs, did not significantly affect the OR internalization (Figure 6B and Table 1).
535 The addition of agonists employed in this investigation greatly increased the fractions of
536 detectable internalizations and the internalization rates for all three ORs (Figure 6B and Table
537 1), although it decreases the percentages of KOR protomers existing as homodimers from 21
538 to 10% but increases the percentages from 11 to 18% and 10 to 17% for MOR and DOR,
539 respectively (Figure 4I). The FAM-Xpep-TATs reduced the homodimer percentages to 2.9,
540 3.3, and 8.6% for the engaged KOR, MOR, and DOR, respectively (Figure 4I). The
541 internalization observations indicated that for the engaged KOR, the addition of FAM-Kpep-
542 TAT induced only slightly faster internalization, whereas for the engaged MOR and DOR, no
543 differences in internalization were detectable after the addition of FAM-Mpep-TAT and FAM-
544 Dpep-TAT (Figure 6B and Table 1).
545 The lack of effect (or only the slight effect) of FAM-Xpep-TATs on the agonist-induced
546 OR internalization is probably because monomers and homodimers are internalized at about
547 the same rate. This might be induced if the internalization rate of homodimers as an

548 internalization unit (two protomers together as a homodimer) might become about half of
549 that of monomers or if the complex processes involving GRK and β-arrestin 2(Smith et al.,
550 2021; Asher et al., 2022; Wess et al., 2023; Zhou et al., 2017) might remove the ORs bound
551 by these proteins from the monomer-dimer equilibrium in the bulk PM.[87-90] However, due
552 caution in the interpretation of these data is required because the Xpep-bound C-terminal
553 domain might inhibit or enhance the interaction with GRK and β-arrestin 2 (for the Gqi5
554 binding, see the next subsection).
555 In addition to CHO-K1 cells, T24 cells were employed for these experiments because
556 the expression level of β2-arrestin in T24 cells is higher than that in CHO-K1 cells(Ménard et
557 al., 1997),[91] and thus T24 cells might undergo more active internalization. However, T24 cells
558 exhibited internalization behaviors quite similar to those of CHO-K1 cells (Figure 6B; Tables
559 S1 and S3).
560
561 **Xpeps modulate KOR and DOR signals**
562 The agonist-induced signal downstream from the OR was examined by a widely used method
563 for Gi-coupled GPCRs, employing the artificial G protein Gqi5 (Figures 6C-6E; refer to the
564 caption to Figure S1A and STAR Methods).[41,92,93] The addition of the homodimer-blocking
565 FAM-Xpep-TATs alone (thus the monomerization of ORs alone) did not induce any detectable
566 Ca^{2+} mobilization (Figure 6F and Table 1). Meanwhile, the respective agonists triggered Ca^{2+}
567 mobilization. The effects of the homodimer-blocking peptides on the agonist-induced Ca^{2+}
568 mobilization were complex (both FAM-Xpep-TATs and mGFP-Xpeps produced similar effects
569 for all three ORs). In cells expressing KOR, MOR, or DOR, the homodimer-blocking peptides
570 (OR monomerization) enhanced, did not affect, and reduced the agonist-induced Ca^{2+}
571 mobilization, respectively (Figure 6F and Table 1). These results indicate that KOR and DOR
572 monomers trigger higher and lower signals than their respective homodimers, whereas MOR
573 monomers and homodimers induce the downstream signals at similar levels (without
574 influencing the agonist-induced internalization of all ORs; Figure 6B). In short,
575 homodimerization suppresses the ligand-induced signaling of KOR and enhances the ligand-
576 induced signaling of DOR.

577 It is possible that these results might be induced by the interfering effect of the bound
578 peptide on the binding of Gqi5 to ORs (Gqi5's binding site to ORs is the same as the original
579 Gαi) because the Gi binding to class A GPCRs involves various intracellular domains. [89,90,94-97]
580 However, since the Halo-tag protein bound to the C-termini of ORs do not affect OR-induced
581 Ca^{2+} responses (Figure S1B of the companion paper) and since the peptide binding induces
582 distinct effects on the three ORs, we think it likely that the effect of homodimer blocking
583 peptides on the agonist-induced Ca^{2+} signal can be interpreted based on its effect on OR
584 monomerization.
585 Furthermore, these results suggest that the homodimer-blocking peptide-TATs could be
586 used as reagents (drugs) to enhance or suppress the agonist-induced G-protein-biased
587 cellular responses for KOR and DOR, respectively, without affecting their internalization
588 (Figure 6B). However, note that these results are correct only for the employed agonists, and
589 the results would be agonist dependent.
590

591 **DISCUSSION**

592 For the first time, the three critical parameters describing the homodimer-monomer dynamic
593 equilibrium (K_D, k_{on}, and k_{off}) have been determined for the OR. This was done for the three
594 classical ORs before and after the addition of a representative agonist for each OR (Figures
595 2B and 4I). The results unequivocally demonstrated that the three classical ORs all form
596 transient metastable homodimers at physiological expression levels (0.3-10 copies/μm^2) at
597 37°C, and predicting that 3.4-59% of OR protomers would exist as homodimers in various
598 tissues both before and after the agonist binding (Figure 2D). Accurate evaluation of the
599 dimer dissociation rate constant (k_{off}) in the live-cell PM using single-molecule colocalization
600 data became possible by developing a theory (Note S1), and the dimer-monomer dissociation
601 equilibrium constant (K_D) could be obtained much more readily compared with the method
602 we developed previously.[57] These theories/methods enabled accurate quantitative evaluations
603 of k_{off} and K_D, and would be applicable to evaluate the dimerization kinetics and equilibrium
604 of any membrane molecules, as exemplified by their application to OR heterodimerization
605 described in the companion paper.[58] Accordingly, they represent major developments for
606 studies of molecular interactions in the PM in general.

607 A previous single-molecule imaging study of neurotensin receptor 1, a GPCR, in
608 reconstituted membranes containing only this receptor and a phospholipid revealed that it
609 forms homodimers. This result demonstrated that neurotensin receptor 1 homodimerization
610 occurs without the involvement of any other proteins[37] (however, see[24]), and suggested that
611 ORs might also form homodimers in a similar manner.

612 Importantly, all of these homodimers are forming and dispersing continually, with
613 lifetimes shorter than 0.2 s at 37°C (Figure 1D). When the homodimers dissociate into
614 monomers, they will again form homodimers with the same and other partner molecules.
615 Longer homodimer lifetimes on the order of 0.5-2 s or even 15 s have been reported, but
616 they were observed at lower temperatures such as RT and 20°C.[53-55] How the limited dimer
617 fractions and lifetimes modulate the downstream signaling and internalization is extensively
618 discussed in the companion paper (refer to Figure 7C and related main text in the companion
619 paper).

620 Specific 9-26 residue amino-acid sequences in the near-C-terminal cytoplasmic domains,
621 which lack sequence similarities among the three ORs, are involved in the distinct
622 homodimerizations of all three classical ORs (Figures 3B, 3C, and 4), and do not participate in
623 heterodimerization (Figures 2A and 3A in the companion paper). In addition to localized
624 electrostatic interactions between charged amino acid residues, the overall structures of the
625 cytoplasmic C-terminal domains, and particularly the intrinsically disordered structures of the
626 C-terminal regions, might be important for homodimerization.[82] The enhancement of
627 homodimerization by the intrinsically disordered region might not be due to liquid-liquid
628 phase separation, but rather to its ability to flexibly adopt various structures, bringing specific
629 binding sites into positions and orientations for optimal interactions.
630 In the literature on homo- and hetero-dimerization of GPCRs, including ORs, the TM
631 domains have been proposed or found to be responsible for homodimerization.[37,46,73,74,76-79]
632 In the present study, we experimentally and directly confirmed this using $TM1^{MOR}$, but we
633 also found that $TM1^{MOR}$ binding to ORs is likely to be quite non-specific, as found by its
634 binding to DOR as well as MOR, and its suppressive effect on both DOR and MOR
635 homodimerization. Blocking of DOR homodimerization of $TM1^{MOR}$ suggests that it is also
636 involved in DOR-MOR heterodimerization. Furthermore, we found that Xpeps failed to reduce
637 the OR homo-colocalization indexes to the level of a monomer control molecule TM^{LDLR}.
638 Therefore, we propose that TM-TM interactions enhance both the homo- and hetero-
639 dimerizations of ORs in less specific manners, whereas the cytoplasmic C-terminal domain
640 interactions provide the specificities for OR homodimerization.
641 To the best of our knowledge, the Xpep-TATs developed here are the first peptide-
642 based reagents that specifically reduce GPCR homodimerization. These homodimer-blocking
643 peptides can become important tools to dissect the functions of OR monomers and
644 homodimers. The use of the Xpeps revealed that DOR and KOR homodimers, but not MOR
645 homodimers, induce G-protein-dependent signals differently from their respective monomers
646 (Figure 6F), although both monomers and homodimers are internalized at the same rate
647 before and after agonist addition (Figure 6B). These results suggest that the C-terminal
648 domain conformations of the DOR and KOR homodimers might undergo allosteric changes
649 upon homodimerization, affecting their G-protein-based signaling. The possibility of the

650 involvement of allosteric conformational changes of ORs upon dimerization will be further
651 discussed in the companion paper (allosteric effects might be more important for DOR-MOR
652 heterodimers).
653 These homodimer blocking peptides could become the basis for designing modulators
654 and potentiators in opioid therapy to enhance the efficacy and suppress side effects such as
655 tolerance development, particularly for the opioids targeting KOR and DOR. The development
656 of agonists for favorable biased signaling is important,[98-102] but the modulation of the OR
657 homodimerization would provide another means to produce biased signaling. Since the Xpep-
658 TATs are soluble and yet membrane-permeable (Figure 4E-4H) and thus they are likely to
659 pass the blood-brain barrier, they could be readily delivered via intravenous injections or
660 nasal sprays. In addition, Xpep-TATs would not compete with agonist binding because they
661 bind to the cytoplasmic C-terminal domains. Taken together, our findings reported here have
662 greatly extended our knowledge of ORs' metastable homodimers and their formation
663 mechanisms and functions, which can inform novel GPCR drug development strategies of
664 modulating homodimerization.
665

666 ## LIMITATIONS OF THE STUDY

667 The results obtained here revealed that the G-protein-mediated downstream signals are
668 different between monomers and homodimers of KOR and DOR, suggesting that the agonist-
669 induced conformational changes of G-protein binding sites in the IL3 domain are distinct
670 between monomers and homodimers. More direct structural studies on this point are
671 necessary.
672 G-proteins could often be bound to ORs before agonist stimulation,[103-105] which might
673 affect OR homodimerization. This possibility has not been investigated in the present study.
674 In general, we will need to comprehensively understand the involvement of G protein and β-
675 arrestins, ORs' TM domains, and ORs' possible allosteric conformational changes in ORs'
676 homo- and hetero-dimerizations. This will give us more complete description of the
677 dimerization kinetics and equilibrium. Meanwhile, we believe that the present approach, using
678 a simple first-order kinetics, is useful at this research stage towards our comprehensive

679 understanding of homo- and hetero-dimerization of ORs as well as those of GPCRs and other
680 membrane molecules in general.
681 Since we used only one agonist for each OR subtype, further examinations using other
682 agonists will be important. The effects of peptides blocking homodimerization were only
683 tested in cells, but for pharmacological applications, we will need to perform *in vivo*
684 experiments, such as those using mice.
685

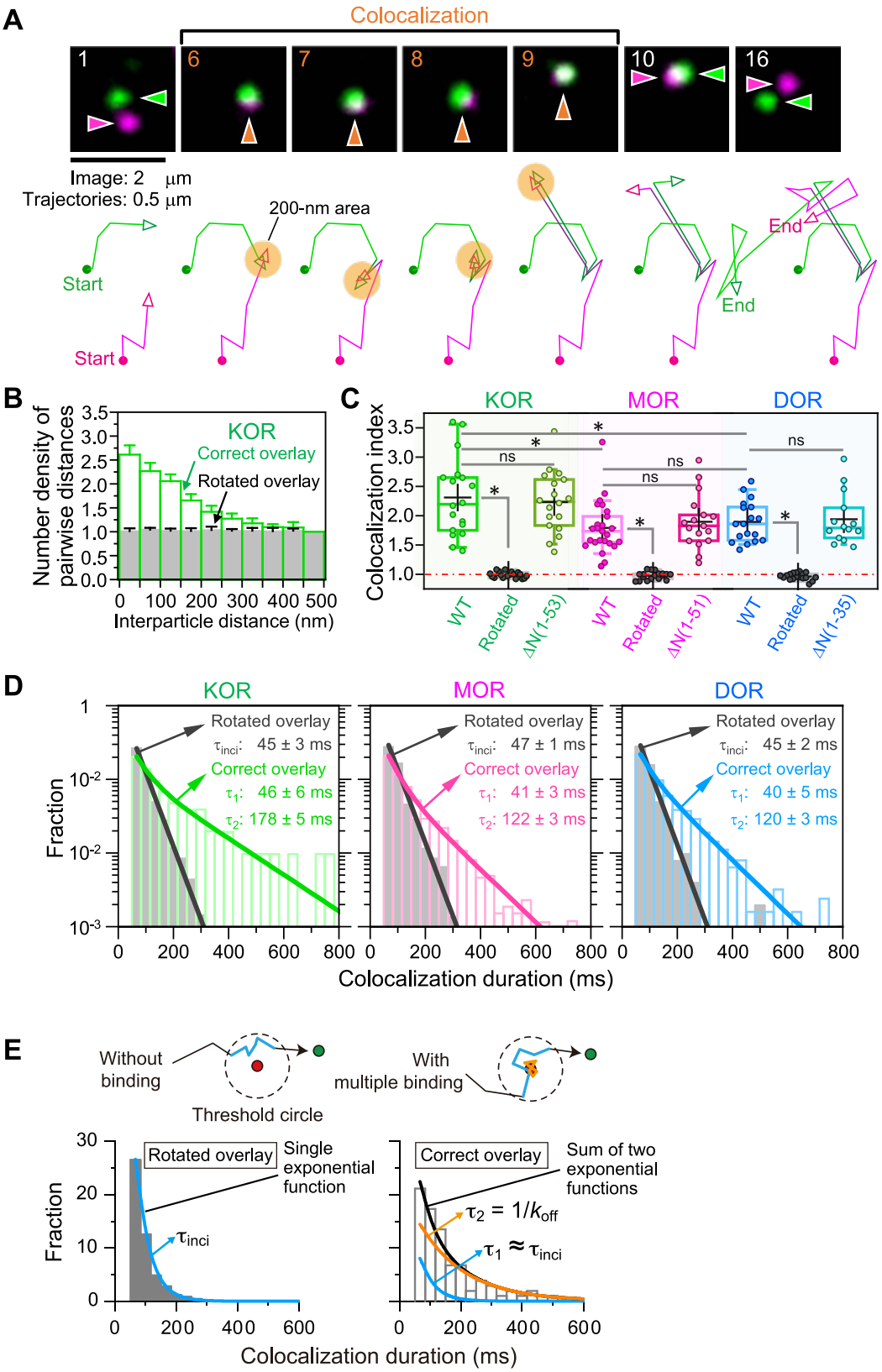

Figure 1. ORs in the PM form metastable homodimers with lifetimes of 120~150 ms, without involving the N-terminal extracellular domain.

689 (**A**) Typical image sequence of simultaneous two-color single fluorescent molecule observations,
690 showing transient homo-colocalization and co-diffusion of single molecules of SNAPf-KOR
691 tagged with SNAP-CF 660R (magenta) and SNAP-Surface 549 (green), with their trajectories.
692 (**B**) PCCFs for the SNAPf-KOR spots (mean ± SEM after area normalization; 18 movies). Green
693 and grey bars indicate the results of the correct and 180°-rotated overlays of the simultaneously
694 observed magenta and green images. The colocalization index is defined as the mean of PCCF
695 values for 0-100 nm divided by the mean of PCCF values for 400-500 nm (see Figures S2C-2E).
696 (**C**) Colocalization indexes showing that the three ORs undergo homo-colocalizations and that
697 OR homo-colocaliations are not affected by the deletions of the N-terminal extracellular
698 domains.
699 *Throughout this study, we employ the following conventions*: for the box plots, horizontal
700 bars, crosses, boxes, and whiskers indicate median values, mean values, interquartile ranges
701 (25–75%), and 10-90% ranges, respectively; for the bar graphs and tables, mean ± SEM values
702 are provided; and for the statistical analyses, * and ns represent significant ($p < 0.05$) and
703 non-significant ($p \geq 0.05$) differences, respectively. The p values were obtained by Tukey's
704 multiple comparison test, except the Brunner-Munzel test used for colocalization lifetimes. All
705 of the quantitative results are summarized in Table 1 and their statistical parameters (sample
706 size n and p values) are provided in Table S1.
707 (**D**) Histograms showing the distributions of colocalization *durations* for correct and rotated
708 overlays. The control histograms for rotated overlays (grey) were fitted by single exponential
709 functions (black), providing the lifetime of the incidental overlap events (τ_{inci}). The histograms
710 for correct overlays (colors) were fitted by the sum of two exponential functions: The faster
711 decay time (τ_1) was close to τ_{inci}, and the slower decay time provided the true homodimer
712 lifetime (τ_2; see Note S1 for the theory). The homodimer lifetimes, after correction for the
713 trackable duration lifetimes of the two fluorescent probes, are shown in the boxes
714 (summarized in Table 1).
715 (**E**) The method to determine the true dissociation rate constant (k_{off}), considering the
716 multiple binding events during an observed colocalization duration. See Note S1.
717

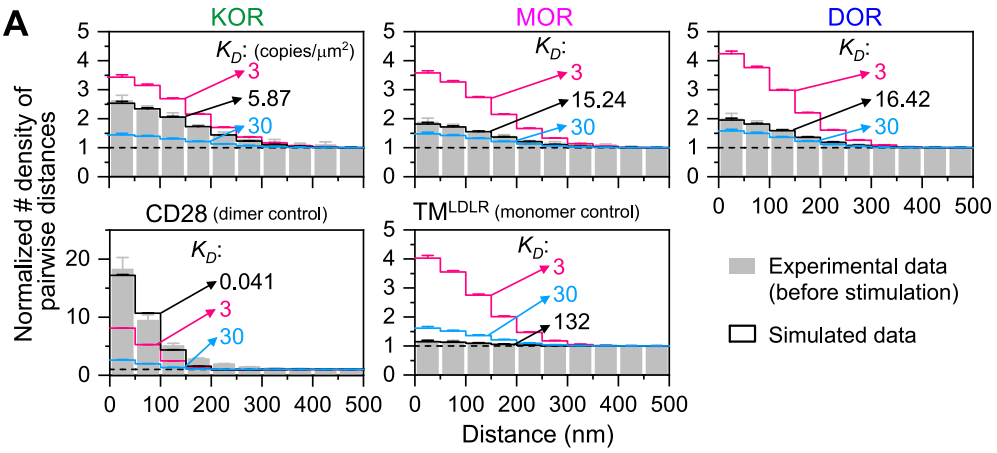

B

ORs	K_D (copies/μm²)	k_{off} (s⁻¹)	k_{on} (μm²/copies/s)	Predicted %OR protomers existing as dimers at different expression levels (copies/μm²)				
				0.3	1	3	10	30
KOR	5.87 ± 0.56	6.71 ± 1.17	1.14 ± 0.23	8.6	21	39	59	73
MOR	15.24 ± 1.54	8.47 ± 0.86	0.56 ± 0.08	3.7	11	23	43	61
DOR	16.42 ± 0.53	8.00 ± 0.96	0.49 ± 0.06	3.4	10	22	42	60
CD28	0.041 ± 0.072	N.D.	N.D.					
TM^LDLR	132 ± 21	N.D.	N.D.					

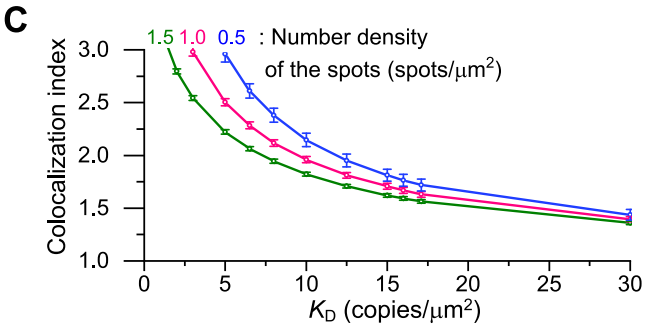

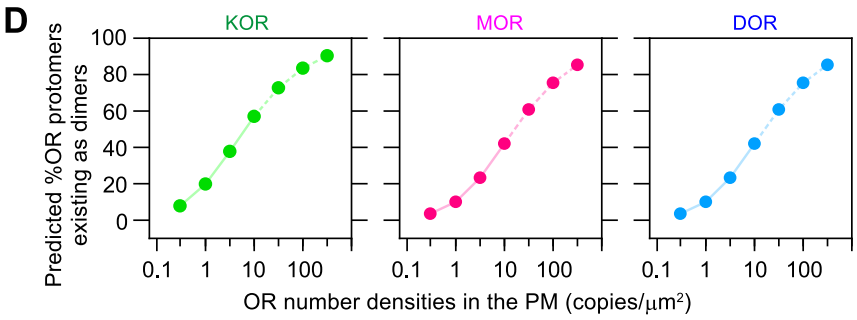

Figure 2. Dynamic OR homodimer-monomer equilibrium constants (K_Ds) and homodimer formation and dissociation rate constants (k_{on} and k_{off}, respectively), providing the %protomers existing as dimers as a function of the expression level.

722 (**A**) Experimental PCCFs for KOR, MOR, DOR, CD28, and TM^{LDLR} (the PCCF for KOR is the
723 same as that shown in Figure 1C) fitted with theoretical PCCFs (Eq. 24) in Note S2; the total
724 numbers of fluorescent spots, sN_{TA} and sN_{TB}, were determined from experiments; labeling
725 efficiency = 0.7 [Figure S1E]) using K_D and σ as fitting parameters. CD28 and TM^{LDLR} were
726 dimer and monomer references, respectively. The black lines indicate the best-fit functions,
727 and their K_D values are shown. The PCCFs with K_D values of 3 and 30 are also shown for
728 comparison.
729 (**B**) Summary of K_D, k_{off} and k_{on} values for the three ORs without agonist, and also for CD28
730 and TM^{LDLR}. N.D.: not done. Predicted percentages of OR protomers existing as dimers at
731 various expression levels calculated from the K_Ds are also shown. Physiological expression
732 levels found in the literature (1-10 copies/μm^2) are highlighted by a pink background (see the
733 main text).
734 (**C**) Colocalization index is simply related to K_D, if the labeling efficiency, the precision of
735 single-molecule localization plus image overlaying, and the number density of fluorescent
736 molecules in each movie were the same (0.7, 140 nm, and 0.5, 1, or 1.5 fluorescent
737 spots/μm^2, respectively). K_D can be roughly estimated from the colocalization index using
738 these curves.
739 (**D**) Predicted percentages of OR protomers existing as dimers, plotted as a function of
740 expression levels (without agonist). The curves indicate the mathematical functions calculated
741 from the K_D values, and solid curves are used for physiological expression levels found in the
742 literature (0.32-10 copies/μm^2). Tick marks between the exact digits represent ≈3.16x
743 ($10^{0.5}$x) of the smaller digit.
744
745

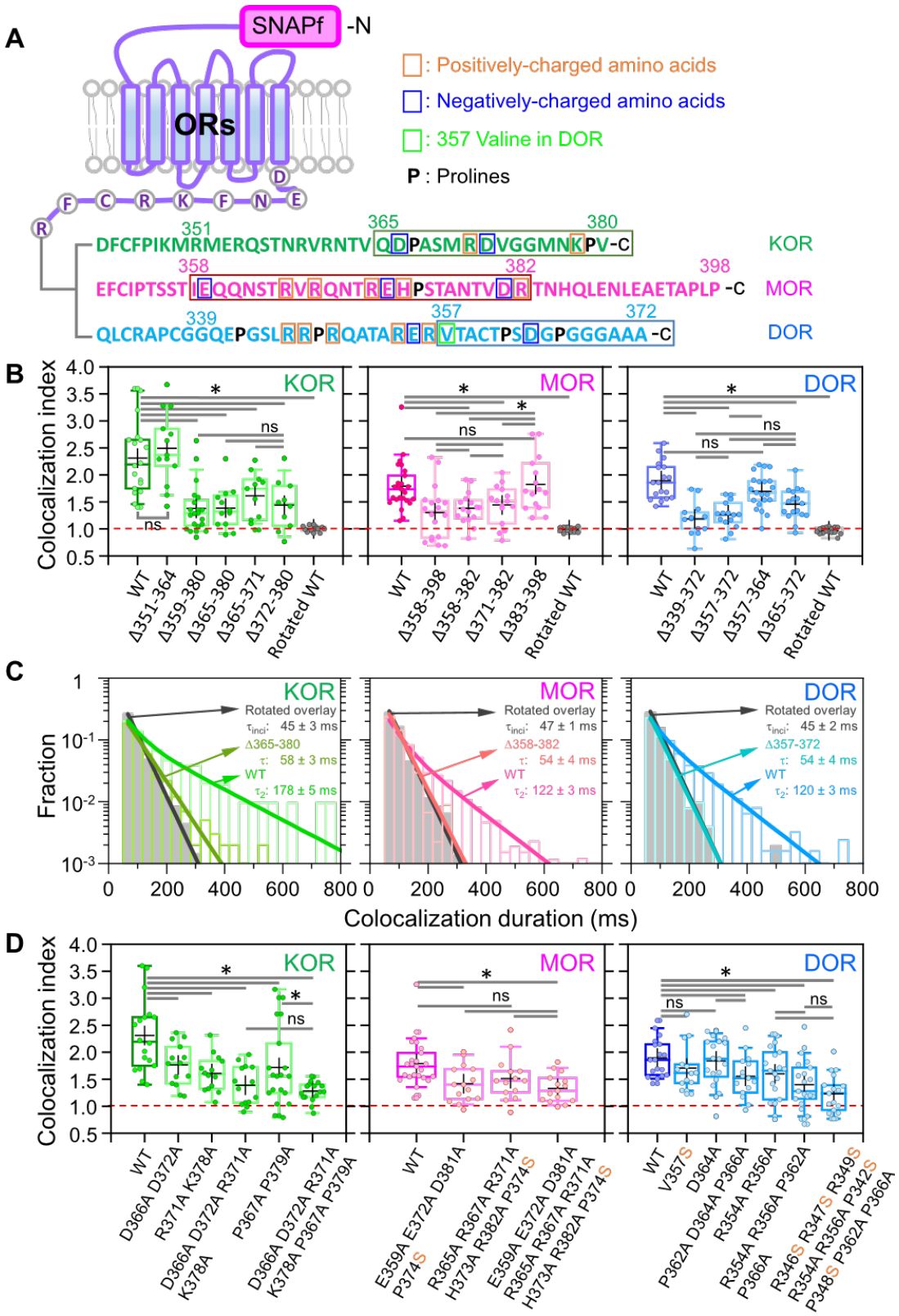

Figure 3. C-terminal cytoplasmic domains are predominantly responsible for OR homodimerization.

749 (**A**) Schematic figure showing the amino-acid sequences of the C-terminal cytoplasmic
750 domains of the three ORs. The sequences surrounded by rectangles were extensively
751 examined for their involvement in OR homodimerization.
752 (**B**) Colocalization indexes for WT and various C-terminal cytoplasmic deletion mutants,
753 showing that KOR aa 365-380, MOR aa 358-382, and DOR aa 357-372, with very low amino-
754 acid homologies, are critical for homodimerization.
755 (**C**) Histograms showing the distributions of colocalization *durations* for the C-terminal
756 cytoplasmic deletion mutants, KOR(Δ365-380), MOR(Δ358-382), and DOR(Δ357-372) (only
757 the results of correct overlays). WT-OR data are reproduced for comparison (for both correct
758 and rotated overlays; Figure 1D). Deletion mutants exhibited distributions that could be fitted
759 by single exponential functions, and their decay time constants τs (after correction for the
760 trackable duration lifetimes of the two fluorescent probes) are indicated in the boxes.
761 (**D**) The colocalization indexes of various C-terminal point mutants, indicating that the
762 charged groups and prolines in the C-terminal cytoplasmic domains play important roles in
763 OR homodimerization.
764

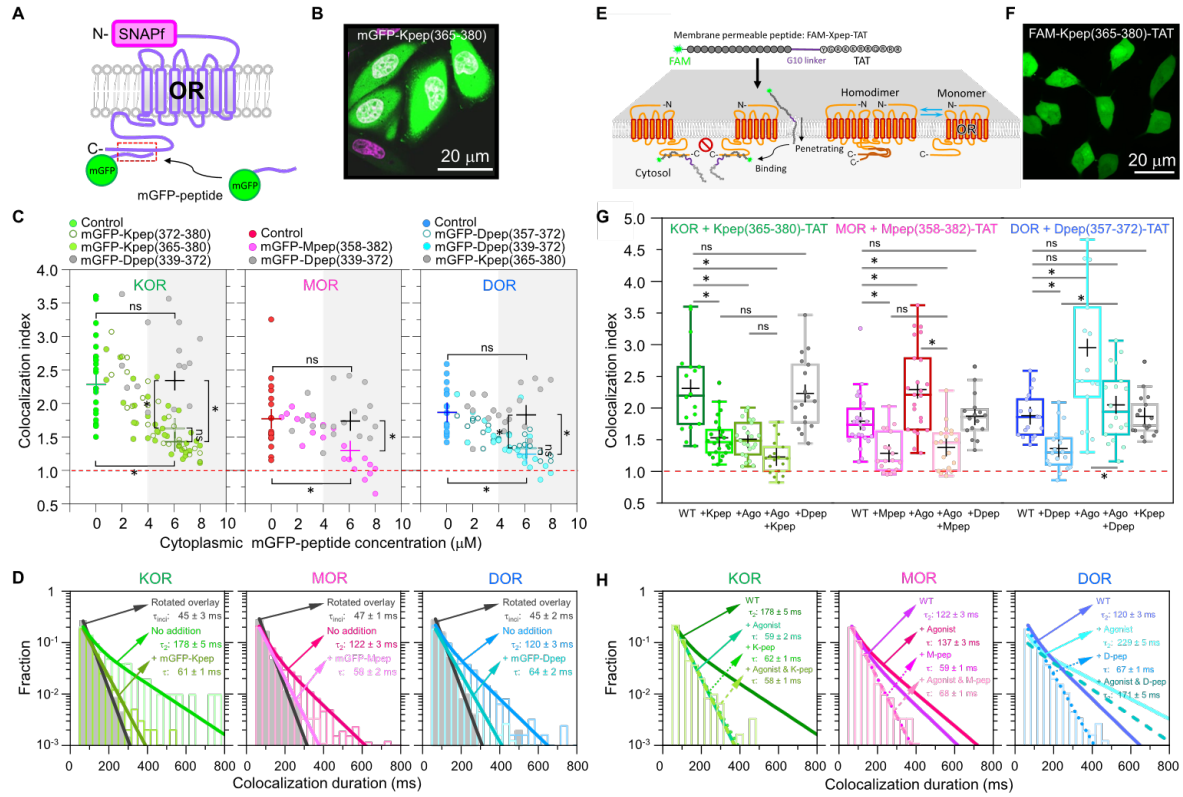

I

ORs	Agonist	Xpep	K_D (copies/μm²)	k_{off} (s⁻¹)	k_{on} (μm²/copies/s)	Predicted %OR protomers existing as dimers at different expression levels (copies/μm²)				
						0.3	1	3	10	30
KOR	–	–	5.87 ± 0.56	6.71 ± 1.17	1.14 ± 0.23	8.6	21	39	59	73
	–	+	58.02 ± 6.71	16.13 ± 0.26	0.28 ± 0.03	1.0	3.2	8.6	21	39
	+	–	15.81 ± 1.36	17.86 ± 0.32	1.13 ± 0.10	3.5	10	23	42	60
	+	+	65.05 ± 16.00	17.24 ± 0.30	0.27 ± 0.07	0.9	2.9	7.8	20	37
MOR	–	–	15.24 ± 1.54	8.47 ± 0.86	0.56 ± 0.08	3.7	11	23	43	61
	–	+	45.51 ± 7.92	16.95 ± 0.29	0.37 ± 0.07	1.3	4.0	11	25	43
	+	–	8.34 ± 0.58	5.35 ± 1.69	0.64 ± 0.21	6.8	18	34	54	70
	+	+	56.44 ± 8.15	14.71 ± 0.22	0.26 ± 0.04	1.0	3.3	8.8	22	39
DOR	–	–	16.42 ± 0.53	8.00 ± 0.96	0.49 ± 0.06	3.4	10	22	42	60
	–	+	41.21 ± 3.26	14.93 ± 0.22	0.36 ± 0.03	1.4	4.4	11	26	45
	+	–	7.69 ± 0.36	3.62 ± 0.25	0.47 ± 0.04	6.3	17	33	53	69
	+	+	19.56 ± 1.80	5.88 ± 0.17	0.30 ± 0.03	2.9	8.6	20	39	57

Figure 4. Specific C-terminal-domain peptides suppress OR homodimerization.

(**A**) Schematic figure showing the experimental design to examine the effects of mGFP-Xpeps expressed in the cell on OR homodimerization.

(**B**) Representative confocal image of CHO-K1 cells transfected with cDNAs encoding SNAPf-KOR (not visible here; only visible by single-molecule imaging conditions) and mGFP-Kpep (green), co-stained with the Live 650 Nuclear Stain (magenta; white nuclei indicate the entrance of mGFP-Kpep into the nuclei, whereas a magenta nucleus indicate the cell without mGFP-Kpep expression).

(**C**) The OR homo-colocalization index in each cell tends to decrease with an increase of the mGFP-Xpep concentration in the cytoplasm. The + keys at x = 0 and 6 μM mGFP-Xpep

776 indicate the mean value of the colocalization indexes without mGFP-Xpep expression and that
777 averaged over all the data points in the range of 3.8-7.8 μM mGFP-Xpep, respectively.
778 Significant reductions of the colocalization indexes in the presence of the mGFP-Xpeps, but
779 not the control mGFP-peptides, were found for all three ORs (Table 1).
780 (**D**) Histograms showing the *duration* distributions of transient homodimers of SNAPf-ORs in
781 cells co-expressing 3.8-7.8 μM mGFP-Xpeps (only the results of correct overlays; the value for
782 each bin is the mean of 18 cells), compared with those without co-expression (the same as
783 those shown in Figure 1D; for both correct and rotated overlays). For further details of these
784 graphs, see the caption to Figure 3C.
785 (**E**) Schematic figure showing the experimental design to examine the effect of the FAM-
786 Xpep-TATs incorporated in the cell on OR homodimerization.
787 (**F**) Representative confocal image of CHO-K1 cells containing an average of 3.4 μM FAM-
788 Kpep-TAT in the cytoplasm.
789 (**G, H**) Agonist addition (0.2 μM) suppressed KOR homodimerization, but enhanced the
790 homodimerization of MOR and DOR (colocalization indexes in **G** and durations of
791 colocalization events in **H**). The presence of ≈3 μM FAM-Xpep-TAT in the cytoplasm
792 suppressed homodimerization both before and 2-5 min after the agonist addition.
793 (**I**) Summary of K_D (homodimer-monomer equilibrium constant), k_{off} (dimer dissociation rate
794 constant), and k_{on} (dimer formation rate constant) for three ORs in the presence and absence
795 of ≈3 μM FAM-Xpep-TAT in the cytoplasm, both before and 2-5 min after the addition of
796 agonists. Predicted percentages of OR protomers existing as dimers at various expression
797 levels calculated from the K_Ds are also shown. Physiological expression levels found in the
798 literature are highlighted by a pink background (see the main text).
799

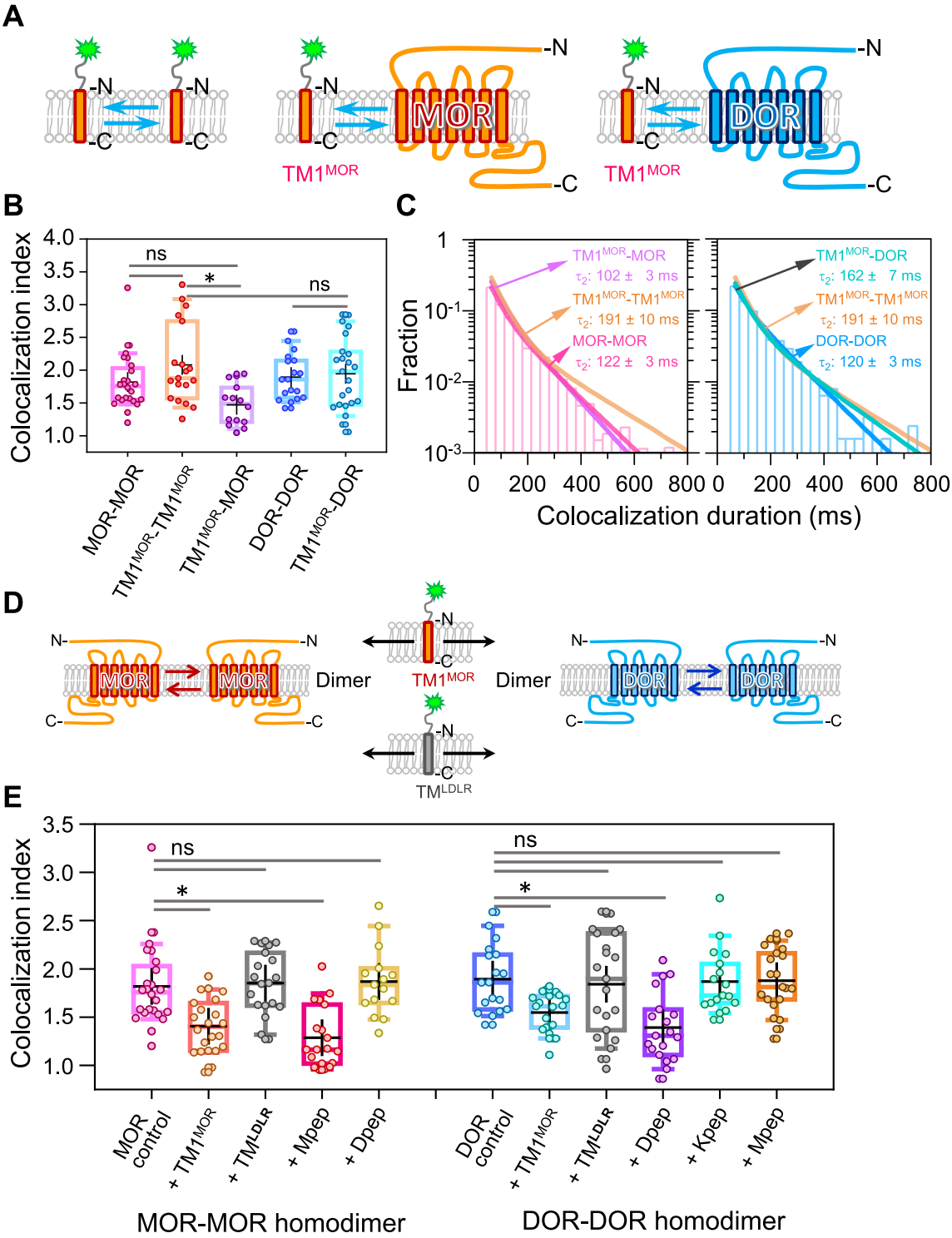

Figure 5. TM1^{MOR} suppresses both MOR and DOR homodimerization.

(**A**) Schematic figure showing the experimental design for examining the interaction (binding) of TM1^{MOR} with itself, MOR, and DOR.

804 (**B, C**) Colocalization indexes (**B**) and distributions of colocalization durations (**C**) showing
805 that $TM1^{MOR}$ forms metastable dimers with both MOR and DOR, suggesting that $TM1^{MOR}$
806 might be involved in MOR-MOR homodimerization as well as MOR-DOR heterodimerization
807 (see Figure 5 in the companion paper.[58]
808 (**D**) Schematic figure showing the experimental design for examining whether $TM1^{MOR}$ can
809 suppress homodimerizations of MOR and DOR.
810 (**E**) $TM1^{MOR}$ suppresses both MOR and DOR homodimerization, whereas Mpep and Dpep
811 specifically suppress MOR or DOR homodimerization, respectively.
812

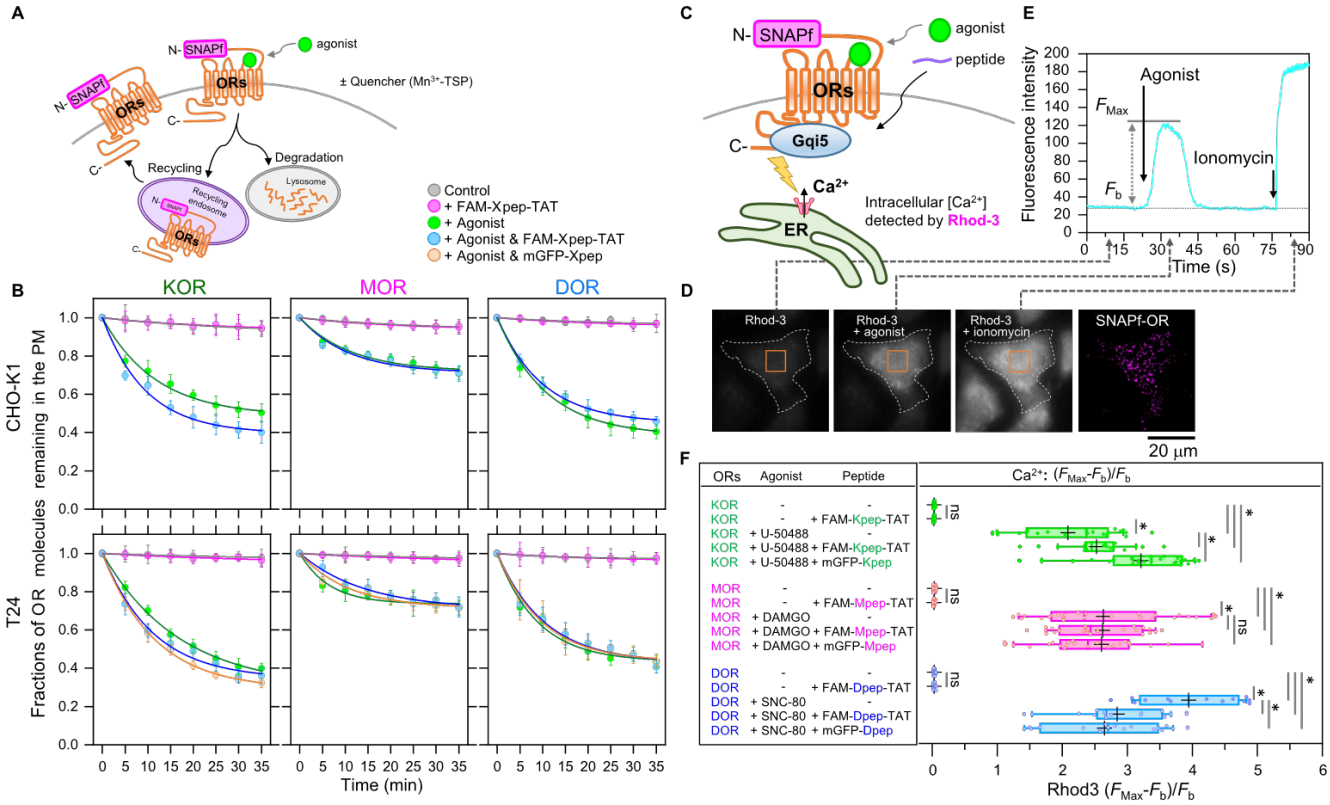

Figure 6. Xpeps hardly affect OR internalization in both the presence and absence of the agonist, whereas they enhanced, did not affect, or reduced the Ca^{2+} mobilization induced by the KOR, MOR, and DOR agonists, respectively.

(**A**) Schematic figure showing the experimental design for observing the internalization of OR (with possible recycling). Also see Figure S6**.**

(**B**) Time-dependent decreases of SNAPf-ORs on the PM due to their internalizations in CHO-K1 cells (top) and T24 cells (bottom) (mean ± SEM; 10 cells for each condition), before and after the addition of 0.2 μM agonist in the presence and absence of ≈3 μM FAM-Xpep-TATs and ≈6 μM mGFP-Xpeps in the cytoplasm. Photobleaching of the fluorescent probe is negligible because only one frame was recorded every 5 min. The time courses could be operationally fitted by single exponential functions, $y = C*\exp(-t/\tau_0) + (1-C)$, providing the fractions of OR molecules with detectable (C) and non-detectable (1 - C) internalizations for the observations up to 35 min, as well as the residency times (τ_0) for the internalized component.

828 (**C**) Schematic figure showing the experimental design for observing the Ca^{2+} mobilization
829 after the agonist stimulation. The Ca^{2+} mobilization was monitored by the Rhod-3
830 fluorescence intensity (see the caption to Figure S1A and STAR Methods).
831 (**D, E**) Typical fluorescence images of Rhod-3 in cells (**D**; orange rectangles = ROI) and the
832 time-dependent changes of the Rhod-3 signal intensity in the ROI (**E**), showing the changes
833 in the cytosolic Ca^{2+} concentration after the agonist stimulation. Cells with similar expression
834 levels of ORs (≈1 fluorescent spot/μm^2) were selected.
835 (**F**) Ca^{2+} mobilization at 75 s after the agonist addition, parametrized by using $[F_{Max}-F_b]/F_b$
836 (see **E**).
837

838 **Table 1. Summary of the colocalization indexes, homodimer lifetimes, fractions and**
839 **PM residency times of molecules with internalizations detectable by the 35-min**
840 **observations, and Ca^{2+} mobilization parameter, $(F_{Max}-F_b)/F_b$, in the presence and**
841 **absence of various modulators (0.2 μM agonists, ≈3 μM FAM-Xpep-TATs in the**
842 **cytoplasm, and ≈6 μM mGFP-Xpeps in the cytoplasm). The agonists employed here**
843 **were U-50488 for KOR, DAMGO for MOR, and SNC-80 for DOR.**
844

ORs	Additions	Colocalization Index (Mean ± SEM)	Homodimer Lifetime (Mean ± SEM) (ms)	Fraction of internalized molecules (%)	PM residency time of internalized molecules (min)	Ca^{2+} $(F_{Max}-F_b)/F_b$
KOR	Control	2.30 ± 0.2	178 ± 5	8.4 ± 4.1	32.1 ± 23.8	0.04 ± 0.01
	+ FAM-pep-TAT	1.53 ± 0.1^{*,Na}	62 ± 1^{*,Na}	6.9 ± 2.4^{Nc,†}	26.2 ± 15.4^{Nc,†}	0.05 ± 0.01^{Nc,†}
	+ mGFP-pep	1.41 ± 0.1^{*,Na}	61 ± 1^{*,Na}	-	-	-
	+ Agonist	1.48 ± 0.1*	59 ± 2*	51.4 ± 2.7*	11.9 ± 1.7*	1.96 ± 0.32*
	+ Agonist + FAM-pep-TAT	1.23 ± 0.1*,†	58 ± 1^{*,Na}	60.5 ± 2.5*,†	9.6 ± 1.2^{*,Na}	2.46 ± 0.21*,†
	+ Agonist + mGFP-pep	1.17 ± 0.1*,†	54 ± 2^{*,Na}	-	-	3.11 ± 0.17*,†
MOR	Control	1.82 ± 0.1	122 ± 3	6.4 ± 1.9	25.8 ± 12.6	0.03 ± 0.01
	+ FAM-pep-TAT	1.38 ± 0.1*,†	59 ± 1*,†	6.3 ± 1.0^{Nc,†}	22.1 ± 4.1^{Nc,†}	0.04 ± 0.01^{Nc,†}
	+ mGFP-pep	1.32 ± 0.1*,†	58 ± 2*,†	-	-	-
	+ Agonist	2.18 ± 0.2*	137 ± 3*	28.1 ± 1.7*	11.3 ± 1.9*	2.80 ± 0.21*
	+ Agonist + FAM-pep-TAT	1.38 ± 0.1*,†	68 ± 1*,†	28.9 ± 2.0^{*,Na}	10.7 ± 2.1^{*,Na}	2.78 ± 0.22^{*,Na}
	+ Agonist + mGFP-pep	1.34 ± 0.1*,†	67 ± 3*,†	-	-	2.80 ± 0.24^{*,Na}
DOR	Control	1.89 ± 0.1	120 ± 3	4.5 ± 3.5	29.8 ± 37.4	0.05 ± 0.01
	+ FAM-pep-TAT	1.36 ± 0.1*,†	67 ± 1*,†	4.9 ± 2.5^{Nc,†}	26.2 ± 22.6^{Nc,†}	0.05 ± 0.01^{Nc,†}
	+ mGFP-pep	1.29 ± 0.1*,†	64 ± 2*,†	-	-	-
	+ Agonist	3.00 ± 0.3*	229 ± 5*	61.6 ± 1.7*	10.8 ± 0.9*	3.85 ± 0.23*
	+ Agonist + FAM-pep-TAT	2.08 ± 0.2*,†	171 ± 5*,†	55.0 ± 1.0*,†	10.1 ± 0.5^{*,Na}	2.84 ± 0.20*,†
	+ Agonist + mGFP-pep	2.00 ± 0.2*,†	168 ± 5^{Nc,†}	-	-	2.65 ± 0.22*,†

845
846 * $^{(Nc)}$: Significant (insignificant) difference from the value for "Control".
847 † $^{(Na)}$: Significant (insignificant) difference from the value for "+ Agonist".
848

STAR METHODS

Detailed methods are provided in the online version of this paper and include the following:

KEY RESOURCES TABLE

RESOURCE AVAILABILITY

- Lead contact
- Materials availability
- Data and code availability

EXPERIMENTAL MODEL AND SUBJECT DETAILS

- Cell lines and culture
- Plasmids and cloning

METHOD DETAILS

- Transfections
- Cell treatments with agonists and FAM-Xpep-TATs
- Fluorescence labeling of ORs
- Microscope observations
- Single fluorescent-molecule imaging
- Evaluating colocalization durations
- Evaluating the colocalization index
- Monte-Carlo simulations
- Confocal imaging to study the effects of mGFP-Xpeps and FAM-Xpep-TATs on cells stably expressing ORs
- Ca^{2+} mobilization assay to examine OR activation
- Quantifying the internalization of SNAPf-ORs

QUANTIFICATION AND STATISTICAL ANALYSIS

- Statistical analysis

SUPPLEMENTAL INFORMATION

- Supplemental information can be found online at .....

ACKNOWLEDGMENTS

We thank Profs. H. Takeshima of Kyoto University, R. Schülz of the University of Münich, R. Y. Tsien of the University of California San Diego, Simon J. Savis of the University of Oxford, Michiyuki Matsuda of Kyoto University, and M. Sokabe of Nagoya University, School of Medicine, for their kind gifts of cDNAs encoding rat KOR and DOR, that encoding rat MOR, that encoding mCherry, that encoding CD28, plasmids of pPBpuro and pCMV-mPBase, and the human T24 epithelial cell line, respectively. We also thank Ms. Irina Meshcheryakova for technical help in preparing the cDNAs. This work was supported in part by Japan Society for the Promotion of Science (JSPS) Grants-in-Aid for Scientific Research (Kiban A to A.K. [21H04772], Kiban S to A.K. [16H06386], Kiban B to T.K.F. [16H04775, 20H02585], Kiban C to R.S.K. [17K07333], Wakate B to R.S.K. [26870292], Wakate to T.A.T. [21K15058], and Challenging Exploratory Research to T.K.F. [18K19001] and A.K. [22K19334]), a Grant-in-Aid from the Ministry of Education, Culture, Sports, Science and Technology of Japan (MEXT) for Transformative Research Areas (A) to T.K.F. (21H05252), and a JST grant ACT-X to T.A.T. (JPMJAX211B). WPI-iCeMS of Kyoto University is supported by the World Premiere Research Center Initiative (WPI) of MEXT.

AUTHOR CONTRIBUTIONS

P.Z., R.S.K., and A.K. conceived and formulated the project. A.K., T.A.T., T.K.F., and P.Z. developed the simultaneous dual-color single-molecule tracking station. P.Z., T.A.T., R.S.K., and A.K. designed biological experiments, and P.Z., with help from T.A.T., performed virtually all of the biological and microscopic experiments. T.K.F. developed and improved the in-house image analysis software. S.P. developed the theory for evaluating the k_{off} from the single-molecule experimental data (Note S1). K.M.H., T.A.T., and A.K. developed the colocalization index method, and T.A.T., Z.K., and A.K. developed the theory for linking the PCCF to the dimer dissociation equilibrium constant and performed Monte-Carlo simulations to prove the theory (Note S2). A.A. performed the OR sequence analysis to detect intrinsically disordered regions. A.K., P.Z., and T.A.T. wrote the manuscript, and all authors discussed the results and participated in the manuscript revisions.

DECLARATION OF INTERESTS

911 PZ and AK have a patent pending for Xpeps and Xpep-TATs. The remaining authors have no
912 conflicts of interest to declare.
913

914 # STAR Methods

915 ## Key resources table

REAGENT or RESOURCE	SOURCE	IDENTIFIER
Bacterial and virus strains		
E. coli HST08 Premium Competent Cells	Takara	Cat# 9128
Chemicals, peptides, and recombinant proteins		
U-50488	Sigma-Aldrich	Cat# D8040
DAMGO	Sigma-Aldrich	Cat# E7384
SNC-80	Sigma-Aldrich	Cat# S2812
Pyrenebutyrate	Sigma-Aldrich	Cat# 257354
Mn (III) meso-tetra(4-sulfonatophenyl)porphine chloride Mn^{3+}-TSP	Frontier Scientific	Cat# MnT1239
FAM-Kpep-TAT	Cosmo-Bio	N/A
FAM-Mpep-TAT	Cosmo-Bio	N/A
FAM-Dpep-TAT	Cosmo-Bio	N/A
EGFP protein	BioVision	Cat# 4999
SNAP-Surface 549 ligand	New England Biolabs	Cat# S9112S
SNAP-CF660R ligand	Shinsei Kagaku	N/A
SaraFluor650T Halo ligand	Goryo Chemical	Cat# A308-02
Critical commercial assays		
Gibson Assembly Master Mix	New England BioLabs	Cat# E2611L
Mycoplasma PCR Detection Kit	Beyotime Biotechnology	Cat# C0301S
VenorGeM Mycoplasma Detection Kit	Minerva Biolabs	Cat# MNV11-1100
SF Cell Line 4D-Nucleofector X Kit L	Lonza	Cat# V4XC-2012
Fluo 4-AM special packaging	Dojindo	Cat# F312
Rhod-3 Calcium Imaging Kit	Thermo Fisher Scientific	Cat# R10145
NucSpot Live 650	Biotium	Cat# 40082
Experimental models: Cell lines		
Human: T24	Masahiro Sokabe (Nagoya University)[106]	N/A
Chinese Hamster: CHO-K1	Dainippon Pharma Co., Ltd.	Cat# 03-402
Recombinant DNA		
Plasmid: pEGFP	Clontech	Cat# Z2370N
Plasmid: pmCherry	Clontech	Cat# Z2522N
Plasmid: pPBpuro	Michiyuki Matsuda (Kyoto University)[107]	N/A
Plasmid: pCMV-mPBase	Michiyuki Matsuda (Kyoto University)[107]	N/A
SNAPf	New England Biolabs	Cat# N9172S
Halo7	Promega	Cat# G9651
mEGFP	Clontech	Cat# Z2370N
mCherry	Roger Y Tsien (University of California San Diego)[108]	N/A
CD47	Eric C Brown (Genentech)[109]	N/A
CD28	Simon J Davis (University of Oxford)[110]	N/A

TM^{LDLR}	[57]	N/A
rat KOR	Hiroshi Takeshima (Kyoto University)[111]	N/A
rat MOR-GFP	Rüdiger Schulz (University of Munich)[112]	N/A
rat DOR	Hiroshi Takeshima (Kyoto University)[111]	N/A
GNA15	OriGene	CAT#: SC125360
mGFP-Kpep	This paper	N/A
mGFP-Mpep	This paper	N/A
mGFP-Dpep	This paper	N/A
SNAPf-TM1^{MOR}	This paper	N/A
SNAPf-TM1^{DOR}	This paper	N/A
Software and algorithms		
HSR v2.3.1.0	Hamamatsu Photonics	https://www.hamamatsu.com/jp/en.html
MCR v1.2.0.0	Hamamatsu Photonics	N/A
LabVIEW 2018 v18.0.1f4	National Instruments	RRID:SCR_014325 (https://www.ni.com/en-us.html)
MatLab 2019a v9.6.0	MathWorks	RRID:SCR_001622 (https://www.mathworks.com)
ImageJ (Fiji) v2.1.0	NIH[113]	RRID:SCR_002285 (https://imagej.net/software/fiji/)
Photoshop CC 2021 v22.4.2	Adobe	RRID:SCR_014199 (https://www.adobe.com)
Illustrator CC 2021 v.24.3	Adobe	RRID:SCR_010279 (https://www.adobe.com)
Origin 2017 v.b9.490.220	Origin Lab	RRID:SCR_014212 (https://www.originlab.com)
R studio v1.2.1335	R studio	RRID:SCR_000432 (https://www.rstudio.com)
Excel v16.51	Microsoft	https://www.microsoft.com/en-us/microsoft-365/excel

RESOURCE AVAILABILITY

Lead contact

Further information and requests for resources and reagents should be directed to and will be fulfilled by the lead contact.

Materials availability

Plasmids and cell lines generated in this study will be shared by the lead contact upon request.

Data and code availability

All data generated or analyzed for this study are available within the paper and its associated Supplementary Information. Any additional information required to reanalyze the data reported in this paper is available from the lead contact upon reasonable request. Superimpositions of image sequences obtained in two colors and tracking single-molecules for in-vitro observation data were performed using C++-based computer programs, produced in-house[114] and based on the well-established approaches. Source codes for this have been integrated into a large, complex software package. While

932 the software package cannot be extracted in a useful way, the entire software is available from the lead
933 contact upon reasonable request, who will provide guidance on how to use it, as its manual and
934 comments are written in Japanese.
935

936 # EXPERIMENTAL MODEL AND SUBJECT DETAILS

937 ## Cell lines and culture

938 CHO-K1 cells (Dainippon Pharma) and T24 cells (gift from Prof. M. Sokabe of Nagoya University)[106],
939 confirmed free of mycoplasma contamination by MycoAlert (Lonza), were routinely cultured in Ham's
940 Nutrient Mixture F12 (Sigma-Aldrich) supplemented with 10% (v/v) fetal bovine serum (FBS, Life
941 Technologies), 100 units/ml penicillin, and 0.1 mg/ml streptomycin, at 37˚C under a 5% CO_2
942 atmosphere in the incubator.
943

944 ## Plasmids and cloning

945 All of the newly generated cDNA constructs and other constructs obtained from outside sources,
946 including gifts and constructs from commercial sources, were sequenced to examine their exact DNA
947 sequences. To generate plasmids for expressing SNAPf-ORs in CHO-K1 cells, the tag protein SNAPf was
948 attached to the N-terminus of the ORs, an additional signal sequence of interleukin 6 was attached to
949 the N-terminus of the tag protein, and a 21 amino-acid linker (SGGGSGG x3) was inserted between
950 the ORs and the tag protein. A Site-Directed Mutagenesis Kit (New England Biolabs) was used to
951 generate the cDNAs encoding the OR point mutants.
952

953 # METHOD DETAILS

954 ## Transfections

955 Transfection of CHO-K1 cells with the cDNAs of interest was performed by electroporation, according
956 to the manufacturer's instructions (4D-Nucleofector, Lonza; SF Cell Line solution and program CHO-K1
957 for CHO-K1 cells). The transfected cells were seeded in glass-base dishes (35-mm in diameter with a
958 12-mm diameter glass window, 0.15-mm-thick glass; Iwaki, Tokyo; 2×10^5 cells/dish) and cultured for
959 24-48 h before fluorescence microscopy observations.
960

961 ## Cell treatments with agonists and FAM-Xpep-TATs

962 U-50488, DAMGO, and SNC-80 (Sigma-Aldrich), agonists for KOR, MOR and DOR, respectively, were
963 applied to the cells in the same way. The agonists were dissolved in DMSO (2 mM), and then diluted
964 with Hanks' balanced salt solution (HBSS, Nissui) buffered with 2 mM TES at pH 7.4 (T-HBSS), at a final
965 concentration of 200 µM. The agonist solution (1 µl) was added to the cells in 1 ml Ham's F12
966 observation medium (a final concentration of 200 nM) at 37˚C.
967 For the cellular incorporation of FAM-Xpep-TATs (custom-synthesized by Cosmo-Bio), the cells
968 were first incubated with 150 µM pyrenebutyrate (Sigma-Aldrich) in T-HBSS at 37˚C for 5 min, and
969 then 2 mM FAM-Xpep-TAT in T-HBSS was added at a final peptide concentration of 20 µM. After an
970 incubation at 37˚C for 10 min, the cells were washed three times with T-HBSS, and then fresh Ham's
971 F12 observation medium was added to the cells. The presence of FAM-Xpep-TAT in the cytoplasm was
972 confirmed by the addition of the membrane-impermeable quencher, trypan blue.[115]
973

974 ## Fluorescence labeling of ORs

975 The SNAPf-tagged wild-type and mutant ORs expressed in the PM (SNAPf tag located at the
976 extracellular N-terminus) were covalently conjugated by simultaneously incubating the cells with two
977 fluorescent SNAP ligands, SNAP-Surface 549 (New England Biolabs) and SNAP-CF660R (Shinsei
978 Kagaku), both at 300 nM, in the growth medium at 37˚C in the CO_2 incubator for 30 min. The cells
979 were washed three times with fresh medium (5-min incubation each time), and then the Ham's F12
980 observation medium was added. The labeling efficiency was determined by using the SNAPf-CD47-
981 mGFP protein expressed in the PM. CD47 is a monomeric 5-pass transmembrane protein expressed in
982 the PM.[116] We could not use ORs for this purpose because they form transient dimers, and thus
983 employed a monomeric CD47 (Figures S1C and S1D).
984 The labeling efficiency (the percentage of the SNAPf-tag protein labeled with the fluorescent
985 SNAP ligand) was determined in the following way. The percentage of fluorescent mGFP spots of
986 SNAPf-CD47-mGFP that was colocalized by the SNAP-dye spots were measured as a function the
987 concentration of the SNAP-dye-conjugated ligand in the medium, after a 30 min incubation at 30˚C.
988 Note that not every mGFP molecule was fluorescent, but since we examined whether the fluorescent
989 mGFP molecule identified in the image was colocalized by a SNAP-dye spot, the labeling efficiencies of
990 the SNAPf-protein tag can be evaluated without the influence of the fluorescence efficiency of mGFP.
991 Then the efficiency at each fluorescent ligand concentration was plotted against the dye
992 concentration (Figure S1E). We found that the plot could be fitted by a function of a single
993 exponential function plus a constant, providing the saturating labeling efficiency (constant) and the
994 characteristic labeling efficiency (exponential constant).
995 To obtain the labeling efficiency at a dye concentration of 300 nM for an incubation period of 30
996 min, the conditions used throughout this study, the determined exponential function was used for a
997 concentration of 300 nM. The fluorescence labeling efficiencies under our normal observation
998 conditions were found to be 60% and 61% for SNAP-Surface 549 and SNAP-CF660, respectively.
999
1000 **Microscope observations**
1001 All microscope observations were performed at 37˚C by placing the entire microscope, except for the
1002 far ends of the excitation arms and the detection arms, in a home-built microscope environment
1003 chamber made with thermo- and electric-field-insulating plastic sheets and equipped with four
1004 heating circulators (SKH0-112-OT, Kokensya, Tokyo, Japan). The Ham's F12 medium used for
1005 microscope observations was free of sodium bicarbonate and phenol red, and buffered with 2 mM N-
1006 [tris(hydroxymethyl)methyl]-2-aminoethanesulfonic acid (TES, Sigma-Aldrich) at pH 7.4 (called Ham's
1007 F12 observation medium).
1008
1009 **Single fluorescent-molecule imaging**
1010 Fluorescently labeled ORs expressed in the bottom PM (the PM facing the coverslip) at fluorescent-
1011 spot number densities of 0.5 ± 0.25 spots/μm^2 for each color (SNAP-Surface 549 and SNAP-CF660R;
1012 total spot number densities of 1.0 ± 0.5 spots/μm^2; for conciseness, we describe the number densities
1013 as ≈1 spot/μm^2 throughout this report) were observed at the level of single molecules at 37˚C, using a
1014 home-built objective lens-type TIRF microscope constructed on an inverted microscope (Olympus IX-
1015 83), with a 100x, 1.49 numerical aperture (NA) objective lens, optimized for the present research
1016 based on the instrument used previously.[68,117] ORs tagged with fluorescent probes were excited with
1017 TIR illumination using the following power densities: SNAP-Surface 549 at 561 nm (Coherent OBIS
1018 561-100 LS) at 0.35 $\mu W/\mu m^2$; and SNAP-CF660R at 642 nm (Omicron LuxXPlus 640-140) at 0.52
1019 $\mu W/\mu m^2$. The dual-color images were separated by a dichroic mirror ZT405/488/561/640rpc-UF3

1020 (Chroma) and projected into two detection arms with band-pass filters of 572.5-647.5 nm
1021 (ET600/50m; Chroma) for the SNAP-Surface 549 dye and 662.5-737.5 nm (ET700/75m; Chroma) for
1022 the SNAP-CF660R dye. In some experiments using mGFP-Xpeps and FAM-Xpep-TATs, an additional
1023 detection arm equipped with a dichroic mirror ZT405/488/561/640rpc-UF3 (Chroma) and a band-pass
1024 filter of 500.0-550.0 nm (ET525/50m; Chroma) was employed. The fluorescence signal in each channel
1025 was first detected and amplified by a two-stage microchannel-plate image intensifier (C9016-
1026 02MLP24; Hamamatsu Photonics), and the intensified image was projected onto the scientific CMOS
1027 camera (C11440-22CU; Hamamatsu Photonics), operated at 30 Hz, which was synchronized with the
1028 same intensifier-camera set(s) placed on another detection arm. The image sequences in each
1029 channel were superimposed after correction for spatial distortions, as described previously.[68] The
1030 positions (x and y coordinates) of all of the observed single fluorescent-molecules were determined
1031 by an in-house computer program, as described previously.[118]
1032
1033 **Evaluating colocalization durations**
1034 The colocalization of two fluorescent molecules was defined as the event where two fluorescent
1035 spots, representing these molecules, become localized within 200 nm of each other, as described
1036 previously.[57,68] Briefly, in single-color experiments using SNAP-Surface 549 (Figure S2), a spatial cross-
1037 correlation analysis was employed.[57] Using this method, we found that when two fluorescent spots,
1038 each representing a single molecule of SNAP-Surface 549, are located close together, the threshold
1039 distance for discriminating one or two spots occurred at 200 nm in the present experimental set up.
1040 Using this definition, colocalized trajectories were obtained and colocalization durations were
1041 estimated. In simultaneous two-color single fluorescent-molecule tracking experiments, using the dye
1042 pairs of SNAP-Surface 549 and SNAP-CF660R, the distance between the two molecules was directly
1043 measured from the locations (x, y-positions) of each molecule (with different colors). Even when
1044 examining pairs of different-colored molecules that are known to be truly associated, the probability
1045 of scoring the two molecules as associated is limited by the localization accuracies of each molecule
1046 and the accuracies of superimposing the two images. Based on the method developed previously[68]
1047 and the accuracies determined here, we found that, for truly associated molecules, the probability of
1048 scoring the two molecules as associated increases to 99% when using the criterion that the molecules
1049 lie within 200 nm of each other. Therefore, we used this criterion as the definition of colocalization in
1050 simultaneous two-color single-molecule observations. This distance of 200 nm coincided with the
1051 definition of colocalization in single-color experiments. Due to this coincidence, in the present
1052 research, we defined the colocalization of two fluorescent molecules as the event where the two
1053 fluorescent spots representing these molecules become localized within 200 nm from each other.
1054 Each time we found a green-magenta pair located within 200 nm (colocalization), we measured
1055 the duration in which their distances remained within 200 nm (colocalized duration) (for the results
1056 obtained by using two dye molecular species with different excitation/emission wavelengths, we call
1057 them green and magenta probes/movies for convenience in this report). After obtaining the
1058 colocalization durations for all of the colocalization events, we generated a histogram (distribution) of
1059 colocalization durations. The distribution of incidental colocalization durations was obtained by
1060 superimposing the magenta image sequences with the 180-degree rotated (doubly flipped) green
1061 image sequences (Figure S2D). For the precise analysis of these histograms, we first produced
1062 cumulative histograms and fitted them with a single exponential function ($C_0 - C_1\exp[-t/\tau_1]$) or the
1063 sum of two exponential functions ($C_0 - C_1\exp[-t/\tau_1] - C_2\exp[-t/\tau_2]$). The choice of the number of
1064 exponentials (including the cases of the sum of three exponential functions) was made based on

1065 Akaike's and Bayesian information criteria (they always agreed). Based on these functions, the
1066 functions describing the original histograms were derived and overlaid on the histograms.
1067 First, we found that the distribution of incidental colocalization durations could be fitted by a
1068 single exponential function, with a time constant representing the incidental colocalization lifetime
1069 τ_{inci}. Second, the distribution of colocalization durations was obtained for correctly superimposed
1070 magenta and green image sequences. This distribution could be fitted by the sum of two exponential
1071 decay functions (τ_1 and τ_2; $\tau_1 < \tau_2$,). These results are consistent with the theory developed here that
1072 predicts the distribution of colocalization durations based on the diffusion equation (Note S1). Since
1073 τ_1 was almost the same as τ_{inci} (Figure 1E), following the theory developed in Note S1, τ_2 provided the
1074 true homodimer lifetime (inverse of k_{off}; after correction for the trackable duration lifetimes of the
1075 two fluorescent probes). The trackable duration lifetime is obtained from the distribution of trajectory
1076 lengths, which would represent how long single molecules can be continuously tracked under the
1077 influences of photobleaching and loss of signals due to blinking and the entrance of the molecules
1078 into the PM areas located farther from the PM. The distributions could be fitted as single exponential
1079 functions providing trackable duration lifetimes (τ_{track}'s) of 16.3 ± 1.2 s (n = 500) for SNAP-Surface 549
1080 and 7.8 ± 0.6 s (n = 400) for SNAP-CF660R bound to SNAPf-MOR expressed in CHO-K1 cells observed
1081 at 30 Hz (Figure S1F). The correction was made by using the equation:
1082 $\tau(\text{corrected}) = [\tau(\text{observed})^{-1} - \tau_{track}(\text{dye 1})^{-1} - \tau_{track}(\text{dye 2})^{-1}]^{-1}$.
1083
1084 **Evaluating the colocalization index**
1085 For the quantitative evaluation of the extent of colocalization (representing both the frequency and
1086 lifetime of colocalization events) in simultaneous two-color single-molecule imaging movies, we
1087 defined a parameter called the colocalization index. This analysis method is essentially based on a pair
1088 cross-correlation analysis,[70] and the detailed method used in this research is explained in Figures S2C-
1089 S2E and S3.
1090
1091 **Monte-Carlo simulations**
1092 For the detailed method for Monte-Carlo simulations to examine the theory to obtain K_D from the pair
1093 cross-correlation function (PCCF) (Note S2), see the caption to Figure S3.
1094 The colocalization index depends on the number density of fluorescent spots in the PM. In the
1095 present experimental observations, we selected the cells exhibiting fluorescent spot number densities
1096 in the PM of 0.5 ± 0.25 spots/μm^2 for each color (SNAP-Surface 549 and SNAP-CF660R; total spot
1097 number densities of 1.0 ± 0.5 spots/μm^2; for conciseness, we describe the number densities as ≈1
1098 spot/μm^2 throughout this report). These densities were found to be reasonable by the Monte-Carlo
1099 simulation results, which indicated that, for the K_D greater than 6.5 copies/μm^2, the colocalization
1100 index does not vary sharply in the number density range of 0.5 - 1.5 spots/μm^2 (refer to Figure S3C).
1101 At the same time, we developed the theory to evaluate the dimer-monomer dissociation equilibrium
1102 constant K_D from the PCCF and the total number of spots in the image (refer to Note S2).
1103
1104 **Confocal imaging to study the effects of mGFP-Xpeps and FAM-Xpep-TATs on cells stably expressing**
1105 **ORs**
1106 CHO-K1 cells stably expressing ORs were transfected with mGFP-Xpeps. The cells were identified by
1107 the incubation with NucSpot Live 650 Nuclear Stain (Biotium), according to the protocol
1108 recommended by the manufacturer. After three washes with the complete medium, it was replaced
1109 with the Ham's F12 observation medium. The incorporation of the FAM-Xpep-TATs in the cells was

1110 performed as described in a previous subsection "Cell treatments with agonists and FAM-Xpep-TATs".
1111 Confocal fluorescence images were acquired on the same microscope station used for single-molecule
1112 imaging at 37˚C, equipped with an Olympus SR10 spinning-disc confocal super-resolution unit (with a
1113 Plan-Apochromat 100x oil immersion objective; NA = 1.49).
1114 GFP and FAM were excited at 488 nm and detected through a 505-530 nm band pass filter. The
1115 NucSpot Live 650 was excited at 642 nm and detected through a 662.5-737.5 nm long pass filter. The
1116 concentrations of cytoplasmic mGFP-Xpep and FAM-Xpep-TAT were evaluated using calibration
1117 curves, obtained by observing the purified EGFP protein (BioVision) and FAM-Xpep-TATs dissolved in
1118 Ham's F12 observation medium at various concentrations, with a focus at 5 µm above the cover-glass
1119 surface (Figure S5B).
1120

1121 **Ca^{2+} mobilization assay**

1122 Since the OR expression level varies from cell to cell, the signaling process must be observed at the
1123 level of individual cells. The ORs are coupled to the inhibitory trimeric G protein Gi, which induces the
1124 decrease of the cytoplasmic cAMP concentration by inhibiting adenylyl cyclase. However, using the
1125 cells with low OR expression levels employed for single-molecule observations (≈1 fluorescent
1126 spot/μm^2), the decrease of the cytoplasmic cAMP levels in individual cells from those in non-
1127 stimulated state was impossibly difficult to measure. Meanwhile, the increase of the cytoplasmic Ca^{2+}
1128 concentrations by the PLCβ activated by the Gq signaling pathway could be measured in individual
1129 cells.[41,92,93] Therefore, in this assay, Gαq was modified so that OR could be coupled to Gαq. Namely,
1130 the C-terminal five amino-acid sequence of Gαq, ECGLY, was replaced with that of Gαi2, DCGLF (this
1131 chimeric protein is called Gqi5), because the Gα protein binds to the specific GPCR by way of its short
1132 C-terminal sequence.[119] Therefore, we generated the CHO-K1 cell line stably expressing Gqi5, had it
1133 express the OR, and then observed the cytoplasmic Ca^{2+} mobilization upon agonist addition, using the
1134 Ca^{2+}-sensitive dyes (Figures 6C-6F and S1B). This method of using Gqi5 has been widely employed in
1135 the research of ORs[92] and other Gi-coupled GPCRs.[41,93]
1136 Briefly, CHO-K1 cells stably expressing Gqi5 were generated and transfected with the cDNAs
1137 encoding the wild-type and SNAPf-linked ORs. The Ca^{2+}-sensitive dyes Fluo-4 AM (Dojindo) and Rhod-
1138 3 AM (Thermo Fisher Scientific) were employed. Rhod-3 was used for the experiments with mGFP-
1139 Xpeps and FAM-Xpep-TATs, and Fluo-4 was used for the experiments that did not employ these
1140 homodimer-blocking reagents. These AM dyes were incorporated in the cell, according to the
1141 manufacturers' recommendations, using the following solutions: for Fluo-4, 4.6 µM Fluo-4 AM in T-
1142 HBSS containing 1.25 mM Probenecid (Dojindo) and 0.04 % (w/v) Pluronic F127 (Dojindo), and for
1143 Rhod-3, 10 µM Rhod-3 AM in T-HBSS containing 2.5 mM Probenecid and 1× PowerLoad™ (Thermo
1144 Fisher Scientific). These loading solutions (2 ml) were added to the cells and incubated in the dark at
1145 37˚C for 30 min, and then the cells were washed three times with T-HBSS.
1146 For the observations of the Ca^{2+} mobilization downstream of the SNAPf-tagged ORs, we
1147 selected cells expressing SNAPf-tagged ORs bound by SNAP-Surface 549 (or SNAP-CF660R for
1148 experiments using Rhod-3) at number densities of ≈1 fluorescent spot/μm^2 in the basal PM, using
1149 single-molecule detection (TIRF illumination) in the 561-nm channel (642-nm channel when we
1150 employed Rhod-3). These cells were then observed by epifluorescence illumination using the 488-nm
1151 channel to monitor the Fluo-4 signal (561-nm channel to observe the Rhod-3 signal and 488-nm
1152 channel for mGFP-Xpeps and FAM-Xpep-TATs). Agonist stimulation was performed by adding the
1153 DMSO solutions of agonists at a final concentration of 200 nM. To determine the saturation levels of
1154 the fluorescence signal intensity at higher concentrations of Ca^{2+}, 1 µM (final concentration)

1155 ionomycin (Wako) was added (which would increase the intracellular Ca^{2+} concentration to that
1156 outside the cells [1.3 mM]). The Fluo-4 and Rhod-3 image sequences were analyzed using the ImageJ
1157 software.
1158 For the comparison of the functions of the SNAPf-ORs with those of the wild-type ORs, we
1159 hoped to compare the cells expressing the SNAPf-ORs at the levels of ≈1 spot/μm^2 in the basal PM
1160 with the cells expressing the wild-type ORs at levels comparable to or higher than those of SNAPf-ORs,
1161 because the cells expressing the wild-type ORs should serve as the positive controls. For this purpose,
1162 the expression levels of wild-type ORs were monitored by using cells transfected with the cDNA
1163 linking the wild-type OR sequence to the mCherry sequence via the self-cleavable 2A linker sequence
1164 (mCherry-2A-OR). This way, mCherry is released from the OR into the cytoplasm at the ER, and the
1165 wild-type OR is then transported to the PM. The expression of wild-type OR was detected by the
1166 presence of mCherry in the cytoplasm using the epi-illumination at 561 nm (sensitivities much lower
1167 than single-molecule imaging, showing the presence of rather high concentrations of mCherry).
1168 Therefore, the expression of the wild-type OR used in this study is considered higher than that of
1169 SNAPf-ORs.
1170

1171 ## QUANTIFICATION AND STATISTICAL ANALYSIS

1172 All statistical analyses for *in vitro* experiments were performed with Tukey's multiple comparison test
1173 except for the analysis of the colocalization lifetime data, which was performed with the Brunner-
1174 Munzel test, using OriginPro 2019b for Windows and RStudio 1.2.1335 for Windows. P values less
1175 than 0.05 were considered statistically significant. The confocal images were processed and analyzed
1176 using Image J for Windows. Curve fitting was performed by OriginPro 2019b for Windows. The
1177 simulation study was performed using the in-house software based on MATLAB 2019a for Windows.
1178
1179

1180

REFERENCES

1. Darcq, E., and Kieffer, B.L. (2018). Opioid receptors: drivers to addiction? Nat. Rev. Neurosci. *19*, 499-514.
2. Valentino, R.J., and Volkow, N.D. (2018). Untangling the complexity of opioid receptor function. Neuropsychopharmacology *43*, 2514-2520.
3. Blythe, E.E., and von Zastrow, M. (2024). β-Arrestin-independent endosomal cAMP signaling by a polypeptide hormone GPCR. Nat. Chem. Biol. *20*, 323-332.
4. Flores-Espinoza, E., and Thomsen, A.R.B. (2024). Beneath the surface: endosomal GPCR signaling. Trends Biochem. Sci. *49*, 520-531.
5. Grimes, J., Lanoiselée, Y., Miljus, T., O'Brien, S.L., Stepniewski, T.M., Medel-Lacruz, B., Baidya, M., Makarova, M., Mistry, R., *et al.* (2023). Plasma membrane preassociation drives β-arrestin coupling to receptors and activation. Cell *186*, 2238-2255. E2220.
6. Mahoney, J.P., and Sunahara, R.K. (2016). Mechanistic insights into GPCR–G protein interactions. Curr. Opin. Struct. Biol. *41*, 247-254.
7. Schmid, C.L., Kennedy, N.M., Ross, N.C., Lovell, K.M., Yue, Z., Morgenweck, J., Cameron, M.D., Bannister, T.D., and Bohn, L.M. (2017). Bias factor and therapeutic window correlate to predict safer opioid analgesics. Cell *171*, 1165-1175.e1113.
8. Che, T., and Roth, B.L. (2023). Molecular basis of opioid receptor signaling. Cell *186*, 5203-5219.
9. Bruchas, M.R., and Roth, B.L. (2016). New technologies for elucidating opioid receptor function. Trends Pharmacol. Sci. *37*, 279-289.
10. Chan, H.C.S., McCarthy, D., Li, J., Palczewski, K., and Yuan, S. (2017). Designing safer analgesics via μ-opioid receptor pathways. Trends Pharmacol. Sci. *38*, 1016-1037.
11. Cong, X., Maurel, D., Déméné, H., Vasiliauskaité-Brooks, I., Hagelberger, J., Peysson, F., Saint-Paul, J., Golebiowski, J., Granier, S., and Sounier, R. (2021). Molecular insights into the biased signaling mechanism of the μ-opioid receptor. Mol. Cell *81*, 4165-4175. e4166.
12. Hauser, A.S., Attwood, M.M., Rask-Andersen, M., Schiöth, H.B., and Gloriam, D.E. (2017). Trends in GPCR drug discovery: new agents, targets and indications. Nat. Rev. Drug Discov. *16*, 829-842.
13. Spangler, S., and Bruchas, M.R. (2017). Tuning biased GPCR signaling for physiological gain. Cell *171*, 989-991.
14. Wacker, D., Stevens, R.C., and Roth, B.L. (2017). How ligands illuminate GPCR molecular pharmacology. Cell *170*, 414-427.
15. Brust, T.F., Morgenweck, J., Kim, S.A., Rose, J.H., Locke, J.L., Schmid, C.L., Zhou, L., Stahl, E.L., Cameron, M.D., Scarry, S.M., et al. (2016). Biased agonists of the kappa opioid receptor suppress pain and itch without causing sedation or dysphoria. Sci. Signal. *9*, ra117-ra117.
16. Bag, N., Wagenknecht-Wiesner, A., Lee, A., Shi, S.M., Holowka, D.A., and Baird, B.A. (2021). Lipid-based and protein-based interactions synergize transmembrane signaling stimulated by antigen clustering of IgE receptors. Proc. Natl. Acad. Sci. U.S.A. *118*,

1222 e2026583118.
1223 17. Wollman, A.J.M., Fournier, C., Llorente-Garcia, I., Harriman, O., Payne-Dwyer, A.L.,
1224 Shashkova, S., Zhou, P., Liu, T.-C., Ouaret, D., Wilding, J., et al. (2022). Critical roles for
1225 EGFR and EGFR–HER2 clusters in EGF binding of SW620 human carcinoma cells. J. R.
1226 Soc. Interface *19*, 20220088.
1227 18. Cvejic, S., and Devi, L.A. (1997). Dimerization of the delta opioid receptor: implication
1228 for a role in receptor internalization. J. Biol. Chem. *272*, 26959-26964.
1229 19. He, L., Fong, J., von Zastrow, M., and Whistler, J.L. (2002). Regulation of opioid receptor
1230 trafficking and morphine tolerance by receptor oligomerization. Cell *108*, 271-282.
1231 20. Fujita, W., Gomes, I., and Devi, L.A. (2014). Revolution in GPCR signalling: opioid
1232 receptor heteromers as novel therapeutic targets: IUPHAR review 10. Br. J. Pharmacol.
1233 *171*, 4155-4176.
1234 21. Gomes, I., Gupta, A., Filipovska, J., Szeto, H.H., Pintar, J.E., and Devi, L.A. (2004). A role
1235 for heterodimerization of μ and δ opiate receptors in enhancing morphine analgesia.
1236 Proc. Natl. Acad. Sci. U.S.A. *101*, 5135-5139.
1237 22. Jordan, B.A., and Devi, L.A. (1999). G-protein-coupled receptor heterodimerization
1238 modulates receptor function. Nature *399*, 697-700.
1239 23. Wang, D., Tawfik, V.L., Corder, G., Low, S.A., François, A., Basbaum, A.I., and Scherrer,
1240 G. (2018). Functional divergence of delta and mu opioid receptor organization in CNS
1241 pain circuits. Neuron *98*, 90-108.e105.
1242 24. Möller, J., Isbilir, A., Sungkaworn, T., Osberg, B., Karathanasis, C., Sunkara, V.,
1243 Grushevskyi, E.O., Bock, A., Annibale, P., Heilemann, M.*, et al.* (2020). Single-molecule
1244 analysis reveals agonist-specific dimer formation of μ-opioid receptors. Nat. Chem. Biol.
1245 *16*, 946-954.
1246 25. Ilien, B., Glasser, N., Clamme, J.-P., Didier, P., Piemont, E., Chinnappan, R., Daval, S.B.,
1247 Galzi, J.-L., and Mely, Y. (2009). Pirenzepine promotes the dimerization of muscarinic M1
1248 receptors through a three-step binding process. J. Biol. Chem.284, 19533-19543.
1249 26. Liu, J., Tang, H., Xu, C., Zhou, S., Zhu, X., Li, Y., Prézeau, L., Xu, T., Pin, J.-P., Rondard,
1250 P., et al. (2022). Biased signaling due to oligomerization of the G protein-coupled
1251 platelet-activating factor receptor. Nat. Commun. 13, 6365.
1252 27. Bhushan, R.G., Sharma, S.K., Xie, Z., Daniels, D.J., and Portoghese, P.S. (2004). A
1253 bivalent ligand (KDN-21) reveals spinal δ and κ opioid receptors are organized as
1254 heterodimers that give rise to δ1 and κ2 phenotypes. Selective targeting of δ–κ
1255 heterodimers. J. Med. Chem. 47, 2969-2972.
1256 28. Gomes, I., Fujita, W., Gupta, A., Saldanha, S.A., Negri, A., Pinello, C.E., Eberhart, C.,
1257 Roberts, E., Filizola, M., Hodder, P.*, et al.* (2013). Identification of a μ-δ opioid receptor
1258 heteromer-biased agonist with antinociceptive activity. Proc. Natl. Acad. Sci. U.S.A. *110*,
1259 12072-12077.
1260 29. Waldhoer, M., Fong, J., Jones, R.M., Lunzer, M.M., Sharma, S.K., Kostenis, E., Portoghese,
1261 P.S., and Whistler, J.L. (2005). A heterodimer-selective agonist shows in vivo relevance
1262 of G protein-coupled receptor dimers. Proc. Natl. Acad. Sci. U.S.A. *102*, 9050-9055.
1263 30. Kasai, R.S., Fujiwara, T.K., and Kusumi, A. (2020). Metastable GPCR dimers trigger the

1264 basal signal by recruiting G-proteins. bioRxiv, 2020.2002.2010.929588.
1265 31. Gomes, I., Fujita, W., Gupta, A., Saldanha, S.A., Negri, A., Pinello, C.E., Eberhart, C.,
1266 Roberts, E., Filizola, M., Hodder, P.*, et al.* (2013). Identification of a μ-δ opioid receptor
1267 heteromer-biased agonist with antinociceptive activity. Proc. Natl. Acad. Sci. U.S.A. *110*,
1268 12072-12077.
1269 32. Gupta, A., Mulder, J., Gomes, I., Rozenfeld, R., Bushlin, I., Ong, E., Lim, M., Maillet, E.,
1270 Junek, M., Cahill, C.M.*, et al.* (2010). Increased abundance of opioid receptor heteromers
1271 after chronic morphine administration. Sci. Signal. *3*, ra54-ra54.
1272 33. He, S.Q., Zhang, Z.N., Guan, J.S., Liu, H.R., Zhao, B., Wang, H.-B., Li, Q., Yang, H., Luo,
1273 J., Li, Z.-Y.*, et al.* (2011). Facilitation of μ-opioid receptor activity by preventing δ-opioid
1274 receptor-mediated codegradation. Neuron *69*, 120-131.
1275 34. Jacobs, B.A., Pando, M.M., Jennings, E., Chavera, T.A., Clarke, W.P., and Berg, K.A.
1276 (2018). Allosterism within δ opioid-κ opioid receptor heteromers in peripheral sensory
1277 neurons: regulation of κ opioid agonist efficacy. Mol. Pharmacol. *93*, 376-386.
1278 35. Jacobs, B.A., Pando, M.M., Jennings, E.M., Jamshidi, R.J., Zamora, J.C., Chavera, T.S.,
1279 Clarke, W.P., and Berg, K.A. (2019). Signaling characteristics and functional regulation
1280 of delta opioid-kappa opioid receptor (DOP-KOP) heteromers in peripheral sensory
1281 neurons. Neuropharmacology *151*, 208-218.
1282 36. Olson, K.M., Keresztes, A., Tashiro, J.K., Daconta, L.V., Hruby, V.J., and Streicher, J.M.
1283 (2018). Synthesis and evaluation of a novel bivalent selective antagonist for the mu-
1284 delta opioid receptor heterodimer that reduces morphine withdrawal in mice. J. Med.
1285 Chem. *61*, 6075-6086.
1286 37. Dijkman, P.M., Castell, O.K., Goddard, A.D., Munoz-Garcia, J.C., de Graaf, C., Wallace,
1287 M.I., and Watts, A. (2018). Dynamic tuneable G protein-coupled receptor monomer-
1288 dimer populations. Nat. Commun. *9*, 1710.
1289 38. Ferré, S., Ciruela, F., Woods, A.S., Lluis, C., and Franco, R. (2007). Functional relevance
1290 of neurotransmitter receptor heteromers in the central nervous system. Trends Neurosci.
1291 *30*, 440-446.
1292 39. Fribourg, M., Moreno, J.L., Holloway, T., Provasi, D., Baki, L., Mahajan, R., Park, G., Adney,
1293 S.K., Hatcher, C., Eltit, J.M.*, et al.* (2011). Decoding the signaling of a GPCR heteromeric
1294 complex reveals a unifying mechanism of action of antipsychotic drugs. Cell *147*, 1011-
1295 1023.
1296 40. George, S.R., O'Dowd, B.F., and Lee, S.P. (2002). G-Protein-coupled receptor
1297 oligomerization and its potential for drug discovery. Nat. Rev. Drug Discov. *1*, 808-820.
1298 41. Han, Y., Moreira, I.S., Urizar, E., Weinstein, H., and Javitch, J.A. (2009). Allosteric
1299 communication between protomers of dopamine class A GPCR dimers modulates
1300 activation. Nat. Chem. Biol. *5*, 688-695.
1301 42. Kasai, R.S., and Kusumi, A. (2014). Single-molecule imaging revealed dynamic GPCR
1302 dimerization. Current Opinion in Cell Biology *27*, 78-86.
1303 43. Milligan, G., Ward, R.J., and Marsango, S. (2019). GPCR homo-oligomerization. Curr.
1304 Opin. Cell Biol. *57*, 40-47.
1305 44. Navarro, G., Cordomí, A., Casadó-Anguera, V., Moreno, E., Cai, N.-S., Cortés, A., Canela,

1306 E.I., Dessauer, C.W., Casadó, V., Pardo, L.*, et al.* (2018). Evidence for functional pre-
1307 coupled complexes of receptor heteromers and adenylyl cyclase. Nat. Commun. *9*, 1242.
1308 45. Toneatti, R., Shin, J.M., Shah, U.H., Mayer, C.R., Saunders, J.M., Fribourg, M., Arsenovic,
1309 P.T., Janssen, W.G., Sealfon, S.C., López-Giménez, J.F.*, et al.* (2020). Interclass GPCR
1310 heteromerization affects localization and trafficking. Sci. Signal. *13*, eaaw3122.
1311 46. Meral, D., Provasi, D., Prada-Gracia, D., Möller, J., Marino, K., Lohse, M.J., and Filizola, M.
1312 (2018). Molecular details of dimerization kinetics reveal negligible populations of
1313 transient μ-opioid receptor homodimers at physiological concentrations. Sci. Rep. *8*,
1314 7705.
1315 47. George, S.R., Fan, T., Xie, Z., Tse, R., Tam, V., Varghese, G., and O'Dowd, B.F. (2000).
1316 Oligomerization of mu- and delta-opioid receptors: generation of novel functional
1317 properties. J. Biol. Chem. *275*, 26128-26135.
1318 48. Wang, D., Sun, X., Bohn, L.M., and Sadée, W. (2005). Opioid receptor homo- and
1319 heterodimerization in living cells by quantitative bioluminescence resonance energy
1320 transfer. Mol. Pharmacol. *67*, 2173-2184.
1321 49. Asher, W.B., Geggier, P., Holsey, M.D., Gilmore, G.T., Pati, A.K., Meszaros, J., Terry, D.S.,
1322 Mathiasen, S., Kaliszewski, M.J., McCauley, M.D.*, et al.* (2021). Single-molecule FRET
1323 imaging of GPCR dimers in living cells. Nat. Methods *18*, 397-405.
1324 50. Cechova, K., Lan, C., Macik, M., Barthes, N.P.F., Jung, M., and Ulbrich, M.H. (2021). Kappa
1325 but not delta or mu opioid receptors form homodimers at low membrane densities. Cell.
1326 Mol. Life Sci. *78*, 7557-7568.
1327 51. Drakopoulos, A., Koszegi, Z., Lanoiselée, Y., Hübner, H., Gmeiner, P., Calebiro, D., and
1328 Decker, M. (2020). Investigation of inactive-state κ opioid receptor homodimerization via
1329 single-molecule microscopy using new antagonistic fluorescent probes. J. Med. Chem.
1330 *63*, 3596-3609.
1331 52. Rogacki, M.K., Golfetto, O., Tobin, S.J., Li, T., Biswas, S., Jorand, R., Zhang, H., Radoi,
1332 V., Ming, Y., Svenningsson, P., et al. (2018). Dynamic lateral organization of opioid
1333 receptors (kappa, mu_{wt} and mu_{N40D}) in the plasma membrane at the nanoscale level.
1334 Traffic *19*, 690-709.
1335 53. Gentzsch, C., Seier, K., Drakopoulos, A., Jobin, M.-L., Lanoiselée, Y., Koszegi, Z., Maurel,
1336 D., Sounier, R., Hübner, H., Gmeiner, P.*, et al.* (2020). Selective and wash-resistant
1337 fluorescent dihydrocodeinone derivatives allow single-molecule imaging of μ-opioid
1338 receptor dimerization. Angew. Chem. Int. Ed. *59*, 5958-5964.
1339 54. Calebiro, D., Rieken, F., Wagner, J., Sungkaworn, T., Zabel, U., Borzi, A., Cocucci, E., Zürn,
1340 A., and Lohse, M.J. (2013). Single-molecule analysis of fluorescently labeled G-protein–
1341 coupled receptors reveals complexes with distinct dynamics and organization. Proc. Natl.
1342 Acad. Sci. U.S.A. *110*, 743-748.
1343 55. Hern, J.A., Baig, A.H., Mashanov, G.I., Birdsall, B., Corrie, J.E.T., Lazareno, S., Molloy,
1344 J.E., and Birdsall, N.J.M. (2010). Formation and dissociation of M1 muscarinic receptor
1345 dimers seen by total internal reflection fluorescence imaging of single molecules. Proc.
1346 Natl. Acad. Sci. U.S.A. *107*, 2693-2698.
1347 56. Kasai, R.S., Ito, S.V., Awane, R.M., Fujiwara, T.K., and Kusumi, A. (2018). The class-A

1348 GPCR dopamine D2 receptor forms transient dimers stabilized by agonists: detection by
1349 single-molecule tracking. Cell Biochem. Biophys. *76*, 29-37.
1350 57. Kasai, R.S., Suzuki, K.G.N., Prossnitz, E.R., Koyama-Honda, I., Nakada, C., Fujiwara, T.K.,
1351 and Kusumi, A. (2011). Full characterization of GPCR monomer-dimer dynamic
1352 equilibrium by single molecule imaging. J. Cell Biol. *192*, 463-480.
1353 58. Zhou, P., Kasai, R.S., Fujita W., Tsunoyama, T.A., Ueda H., Pigolotti, S., Fujiwara, T.K.,
1354 and Kusumi, A. (2024). Single-molecule detection of transient dimerization of opioid
1355 receptors 2: Heterodimer blockage enhances morphine analgesia. Companion paper.
1356 59. Cai, X., Bai, B., Zhang, R., Wang, C., and Chen, J. (2017). Apelin receptor homodimer-
1357 oligomers revealed by single-molecule imaging and novel G protein-dependent signaling.
1358 Sci. Rep. *7*, 40335.
1359 60. Harikumar, K.G., Dong, M., Cheng, Z., Pinon, D.I., Lybrand, T.P., and Miller, L.J. (2006).
1360 Transmembrane segment peptides can disrupt cholecystokinin receptor oligomerization
1361 without affecting receptor function. Biochemistry *45*, 14706-14716.
1362 61. Harikumar, K.G., Pinon, D.I., and Miller, L.J. (2007). Transmembrane segment IV
1363 contributes a functionally important interface for oligomerization of the Class II G
1364 protein-coupled secretin receptor. J. Biol. Chem. *282*, 30363-30372.
1365 62. Hebert, T.E., Moffett, S., Morello, J.-P., Loisel, T.P., Bichet, D.G., Barret, C., and Bouvier,
1366 M. (1996). A peptide derived from a β2-Adrenergic receptor transmembrane domain
1367 inhibits both receptor dimerization and activation. J. Biol. Chem. *271*, 16384-16392.
1368 63. Hernanz-Falcón, P., Rodríguez-Frade, J.M., Serrano, A., Juan, D., del Sol, A., Soriano, S.F.,
1369 Roncal, F., Gómez, L., Valencia, A., Martínez-A, C., et al. (2004). Identification of amino
1370 acid residues crucial for chemokine receptor dimerization. Nat. Immunol. *5*, 216-223.
1371 64. Jastrzebska, B., Chen, Y., Orban, T., Jin, H., Hofmann, L., and Palczewski, K. (2015).
1372 Disruption of rhodopsin dimerization with synthetic peptides targeting an interaction
1373 interface. J. Biol. Chem. *290*, 25728-25744.
1374 65. McMillin, S.M., Heusel, M., Liu, T., Costanzi, S., and Wess, J. (2011). Structural basis of
1375 M3 muscarinic receptor dimer/oligomer Formation. J. Biol. Chem. 286, 28584-28598.
1376 66. Petersen, J., Wright, S.C., Rodríguez, D., Matricon, P., Lahav, N., Vromen, A., Friedler, A.,
1377 Strömqvist, J., Wennmalm, S., Carlsson, J., et al. (2017). Agonist-induced dimer
1378 dissociation as a macromolecular step in G protein-coupled receptor signaling. Nat.
1379 Commun. *8*, 226.
1380 67. Pan, Y.X. (2003). Expression of opioid receptors in mammalian cell lines. In opioid
1381 research: methods and protocols, Z.Z. Pan, ed. (Totowa, NJ: Humana Press), pp. 17-28.
1382 68. Koyama-Honda, I., Ritchie, K., Fujiwara, T., Iino, R., Murakoshi, H., Kasai, R.S., and
1383 Kusumi, A. (2005). Fluorescence imaging for monitoring the colocalization of two single
1384 molecules in living cells. Biophys. J. *88*, 2126-2136.
1385 69. Koyama-Honda, I., Fujiwara, T.K., Kasai, R.S., Suzuki, K.G.N., Kajikawa, E., Tsuboi, H.,
1386 Tsunoyama, T.A., and Kusumi, A. (2020). High-speed single-molecule imaging reveals
1387 signal transduction by induced transbilayer raft phases. J. Cell Biol. *219*.
1388 70. Stone, M.B., and Veatch, S.L. (2015). Steady-state cross-correlations for live two-colour
1389 super-resolution localization data sets. Nat. Commun. *6*, 7347.

71. Evans, E.J., Esnouf, R.M., Manso-Sancho, R., Gilbert, R.J.C., James, J.R., Yu, C., Fennelly, J.A., Vowles, C., Hanke, T., Walse, B., et al. (2005). Crystal structure of a soluble CD28-Fab complex. Nat. Immunol. *6*, 271-279.
72. Granier, S., Manglik, A., Kruse, A.C., Kobilka, T.S., Thian, F.S., Weis, W.I., and Kobilka, B.K. (2012). Structure of the δ-opioid receptor bound to naltrindole. Nature *485*, 400-404.
73. Huang, W., Manglik, A., Venkatakrishnan, A.J., Laeremans, T., Feinberg, E.N., Sanborn, A.L., Kato, H.E., Livingston, K.E., Thorsen, T.S., Kling, R.C.*, et al.* (2015). Structural insights into μ-opioid receptor activation. Nature *524*, 315-321.
74. Manglik, A., Kruse, A.C., Kobilka, T.S., Thian, F.S., Mathiesen, J.M., Sunahara, R.K., Pardo, L., Weis, W.I., Kobilka, B.K., and Granier, S. (2012). Crystal structure of the μ-opioid receptor bound to a morphinan antagonist. Nature *485*, 321-326.
75. Wu, H., Wacker, D., Mileni, M., Katritch, V., Han, G.W., Vardy, E., Liu, W., Thompson, A.A., Huang, X.P., Carroll, F.I.*, et al.* (2012). Structure of the human κ-opioid receptor in complex with JDTic. Nature *485*, 327-332.
76. Ferré, S., Casadó, V., Devi, L.A., Filizola, M., Jockers, R., Lohse, M.J., Milligan, G., Pin, J.-P., and Guitart, X. (2014). G protein–coupled receptor oligomerization revisited: functional and pharmacological perspectives. Pharmacol. Rev. *66*, 413.
77. Johnston, J.M., Aburi, M., Provasi, D., Bortolato, A., Urizar, E., Lambert, N.A., Javitch, J.A., and Filizola, M. (2011). Making structural sense of dimerization interfaces of delta opioid receptor homodimers. Biochemistry *50*, 1682-1690.
78. Marino, K.A., Prada-Gracia, D., Provasi, D., and Filizola, M. (2016). Impact of lipid composition and receptor conformation on the spatio-temporal organization of μ-opioid receptors in a multi-component plasma membrane model. PLoS Comput. Biol. *12*, e1005240.
79. Provasi, D., Boz, M.B., Johnston, J.M., and Filizola, M. (2015). Preferred supramolecular organization and dimer interfaces of opioid receptors from simulated self-association. PLOS Computat. Biol. *11*, e1004148.
80. Mészáros, B., Erdős, G., and Dosztányi, Z. (2018). IUPred2A: context-dependent prediction of protein disorder as a function of redox state and protein binding. Nucleic Acids Res. *46*, W329-W337.
81. Erdős, G., and Dosztányi, Z. (2020). Analyzing protein disorder with IUPred2A. Current protocols in bioinformatics *70*, e99.
82. Xhani, S., Lee, S., Kim, H.M., Wang, S., Esaki, S., Ha, V.L.T., Khanezarrin, M., Fernandez, G.L., Albrecht, A.V., Aramini, J.M.*, et al.* (2020). Intrinsic disorder controls two functionally distinct dimers of the master transcription factor PU.1. Sci. Adv. *6*, eaay3178.
83. Kusumi, A., Tsunoyama, T.A., Suzuki, K.G.N., Fujiwara, T.K., and Aladag, A. (2024) Transient, nano-scale, liquid-like molecular assemblies coming of age. Curr. Opinion Cell Biol. *89,* 102394.
84. Inomata, K., Ohno, A., Tochio, H., Isogai, S., Tenno, T., Nakase, I., Takeuchi, T., Futaki, S., Ito, Y., Hiroaki, H.*, et al.* (2009). High-resolution multi-dimensional NMR spectroscopy of proteins in human cells. Nature *458*, 106-109.

1432 85. Grasberger, B., Minton, A.P., DeLisi, C., and Metzger, H. (1986). Interaction between
1433 proteins localized in membranes. Proc. Natl. Acad. Sci. U.S.A. *83*, 6258-6262.
1434 86. Keppler A, Pick H, Arrivoli C, Vogel H, Johnsson K. (2004) Labeling of fusion proteins
1435 with synthetic fluorophores in live cells. Proc. Natl. Acad. Sci. U.S.A. *101*(27):9955-9959.
1436 87. Smith, J.S., Pack, T.F., Inoue, A., Lee, C., Zheng, K., Choi, I., Eiger, D.S., Warman, A.,
1437 Xiong, X., Ma, Z., et al. (2021). Noncanonical scaffolding of Gαi and β-arrestin by G
1438 protein–coupled receptors. Science *371*, eaay1833.
1439 88. Asher, W.B., Terry, D.S., Gregorio, G.G.A., Kahsai, A.W., Borgia, A., Xie, B., Modak, A.,
1440 Zhu, Y., Jang, W., Govindaraju, A., et al. (2022). GPCR-mediated β-arrestin activation
1441 deconvoluted with single-molecule precision. Cell *185*, 1661-1675.e1616.
1442 89. Wess, J., Oteng, A.B., Rivera-Gonzalez, O., Gurevich, E.V., and Gurevich, V.V. (2023).
1443 β-arrestins: structure, function, physiology, and pharmacological perspectives.
1444 Pharmacol. Rev. *75*, 854-884.
1445 90. Zhou, X.E., He, Y., de Waal, P.W., Gao, X., Kang, Y., Van Eps, N., Yin, Y., Pal, K.,
1446 Goswami, D., White, T.A., et al. (2017). Identification of phosphorylation codes for
1447 arrestin recruitment by G protein-coupled receptors. Cell *170*, 457-469.e413.
1448 91. Ménard, L., Ferguson, S., Zhang, J., Lin, F., Lefkowitz, R., Caron, M., and Barak, L. (1997).
1449 Synergistic regulation of beta2-adrenergic receptor sequestration: intracellular
1450 complement of beta-adrenergic receptor kinase and beta-arrestin determine kinetics of
1451 internalization. Mol. Pharmacol. *51*, 800-808.
1452 92. Camarda, V., and Calo′, G. (2013). Chimeric G proteins in fluorimetric calcium assays:
1453 Experience with opioid receptors. In Calcium Signaling Protocols, D.G. Lambert, and R.D.
1454 Rainbow, eds. (Totowa, N.J.: Humana Press), pp. 293-306.
1455 93. Yokoyama, T., Kato, N., and Yamada, N. (2003). Development of a high-throughput
1456 bioassay to screen melatonin receptor agonists using human melatonin receptor
1457 expressing CHO cells. Neurosci. Lett. *344*, 45-48.
1458 94. Hauser, A.S., Kooistra, A.J., Munk, C., Heydenreich, F.M., Veprintsev, D.B., Bouvier, M.,
1459 Babu, M.M., and Gloriam, D.E. (2021). GPCR activation mechanisms across classes and
1460 macro/microscales. Nat. Struct. Mol. Biol. *28*, 879-888.
1461 95. Zhou, Q., Yang, D., Wu, M., Guo, Y., Guo, W., Zhong, L., Cai, X., Dai, A., Jang, W.,
1462 Shakhnovich, E.I., et al. (2019). Common activation mechanism of class A GPCRs. Elife
1463 *8*. 10.7554/eLife.50279.
1464 96. Mafi, A., Kim, S.K., and Goddard, W.A., 3rd (2020). Mechanism of β-arrestin recruitment
1465 by the μ-opioid G protein-coupled receptor. Proc. Natl. Acad. Sci. U.S.A. *117*, 16346-
1466 16355.
1467 97. Koehl, A., Hu, H., Maeda, S., Zhang, Y., Qu, Q., Paggi, J.M., Latorraca, N.R., Hilger, D.,
1468 Dawson, R., Matile, H., et al. (2018). Structure of the μ-opioid receptor–Gi protein
1469 complex. Nature *558*, 547-552.
1470 98. Che, T., Dwivedi-Agnihotri, H., Shukla, A.K., and Roth, B.L. (2021). Biased ligands at
1471 opioid receptors: current status and future directions. Sci. Signal. *14*, eaav0320.
1472 99. Violin, J.D., Crombie, A.L., Soergel, D.G., and Lark, M.W. (2014). Biased ligands at G-
1473 protein-coupled receptors: promise and progress. Trends Pharmacol. Sci. *35*, 308-316.

1474 100. Manglik, A. (2020). Molecular Basis of Opioid Action: From Structures to New
1475 Leads. Biol. Psychiatry *87*, 6-14.
1476 101. De Neve, J., Barlow, T.M.A., Tourwé, D., Bihel, F., Simonin, F., and Ballet, S. (2021).
1477 Comprehensive overview of biased pharmacology at the opioid receptors: biased ligands
1478 and bias factors. RSC Med. Chem. *12*, 828-870.
1479 102. Huang, Y.H., Lin, S.Y., Ou, L.C., Huang, W.C., Chao, P.K., Chang, Y.C., Chang, H.F.,
1480 Lee, P.T., Yeh, T.K., Kuo, Y.H., et al. Discovery of a mu-opioid receptor modulator that in
1481 combination with morphinan antagonists induces analgesia. Cell Chem. Biol.
1482 10.1016/j.chembiol.2024.06.013.
1483 103. Audet, N., Galés, C., Archer-Lahlou, É., Vallières, M., Schiller, P.W., Bouvier, M., and
1484 Pineyro, G. (2008). Bioluminescence resonance energy transfer assays reveal ligand-
1485 specific conformational changes within preformed signaling complexes containing δ-
1486 opioid receptors and heterotrimeric G proteins *. J. Biol. Chem. *283*, 15078-15088.
1487 104. Ayoub, M.A., Trinquet, E., Pfleger, K.D.G., and Pin, J.-P. (2010). Differential
1488 association modes of the thrombin receptor PAR1 with Gαil, Gα12, and β-arrestin 1.
1489 FASEB J. *24*, 3522-3535.
1490 105. Bondar, A., and Lazar, J. (2017). The G protein G_{i1} exhibits basal coupling but not
1491 preassembly with G protein-coupled receptors. J. Biol. Chem. *292*, 9690-9698.
1492 106. Naruse, K., Sai, X., Yokoyama, N., and Sokabe, M. (1998). Uni-axial cyclic stretch
1493 induces c-src activation and translocation in human endothelial cells via SA channel
1494 activation. FEBS Lett. *441*, 111-115.
1495 107. Nakamura, A., Oki, C., Kato, K., Fujinuma, S., Maryu, G., Kuwata, K., Yoshii, T.,
1496 Matsuda, M., Aoki, K., and Tsukiji, S. (2020). Engineering orthogonal, plasma membrane-
1497 specific SLIPT systems for multiplexed chemical control of signaling pathways in living
1498 single cells. ACS Chem. Biol. *15*, 1004-1015.
1499 108. Shaner, N.C., Campbell, R.E., Steinbach, P.A., Giepmans, B.N.G., Palmer, A.E., and
1500 Tsien, R.Y. (2004). Improved monomeric red, orange and yellow fluorescent proteins
1501 derived from *Discosoma* sp. red fluorescent protein. Nat. Biotechnol. *22*, 1567-1572.
1502 109. Lindberg, F.P., Gresham, H.D., Schwarz, E., and Brown, E.J. (1993). Molecular
1503 cloning of integrin-associated protein: an immunoglobulin family member with multiple
1504 membrane-spanning domains implicated in alpha v beta 3-dependent ligand binding. J.
1505 Cell Biol. *123*, 485-496.
1506 110. James, J.R., Oliveira, M.I., Carmo, A.M., Iaboni, A., and Davis, S.J. (2006). A
1507 rigorous experimental framework for detecting protein oligomerization using
1508 bioluminescence resonance energy transfer. Nat. Methods *3*, 1001-1006.
1509 111. Fukuda, K., Kato, S., Mori, K., Nishi, M., and Takeshima, H. (1993). Primary
1510 structures and expression from cDNAs of rat opioid receptor δ-and μ-subtypes. FEBS
1511 Lett. *327*, 311-314.
1512 112. Schulz, R., Wehmeyer, A., and Schulz, K. (2002). Opioid receptor types selectively
1513 cointernalize with G protein-coupled receptor kinases 2 and 3. J. Pharmacol. Exp. Ther.
1514 *300*, 376.
1515 113. Schindelin, J., Arganda-Carreras, I., Frise, E., Kaynig, V., Longair, M., Pietzsch, T.,

Preibisch, S., Rueden, C., Saalfeld, S., Schmid, B., et al. (2012). Fiji: an open-source platform for biological-image analysis. Nat. Methods 9, 676-682.

114. Fujiwara, T.K., Takeuchi, S., Kalay, Z., Nagai, Y., Tsunoyama, T.A., Kalkbrenner, T., Iwasawa, K., Ritchie, K.P., Suzuki, K.G.N., and Kusumi, A. (2023). Development of ultrafast camera-based single fluorescent-molecule imaging for cell biology. J. Cell Biol. *222*.

115. Cowen, T., Haven, A.J., and Burnstock, G. (1985). Pontamine sky blue: A counterstain for background autofluorescence in fluorescence and immunofluorescence histochemistry. Histochemistry *82*, 205-208.

116. Tsunoyama, T.A., Watanabe, Y., Goto, J., Naito, K., Kasai, R.S., Suzuki, K.G.N., Fujiwara, T.K., and Kusumi, A. (2018). Super-long single-molecule tracking reveals dynamic-anchorage-induced integrin function. Nat. Chem. Biol. *14*, 497-506.

117. Murakoshi, H., Iino, R., Kobayashi, T., Fujiwara, T., Ohshima, C., Yoshimura, A., and Kusumi, A. (2004). Single-molecule imaging analysis of Ras activation in living cells. Proc. Natl. Acad. Sci. U.S.A. *101*, 7317-7322.

118. Fujiwara, T.K., Iwasawa, K., Kalay, Z., Tsunoyama, T.A., Watanabe, Y., Umemura, Y.M., Murakoshi, H., Suzuki, K.G.N., Nemoto, Y.L., Morone, N.*, et al.* (2016). Confined diffusion of transmembrane proteins and lipids induced by the same actin meshwork lining the plasma membrane. Mol. Biol. Cell *27*, 1101-1119.

119. Conklin, B.R., Farfel, Z., Lustig, K.D., Julius, D., and Bourne, H.R. (1993). Substitution of three amino acids switches receptor specificity of Gqα to that of Giα. Nature *363*, 274-276.

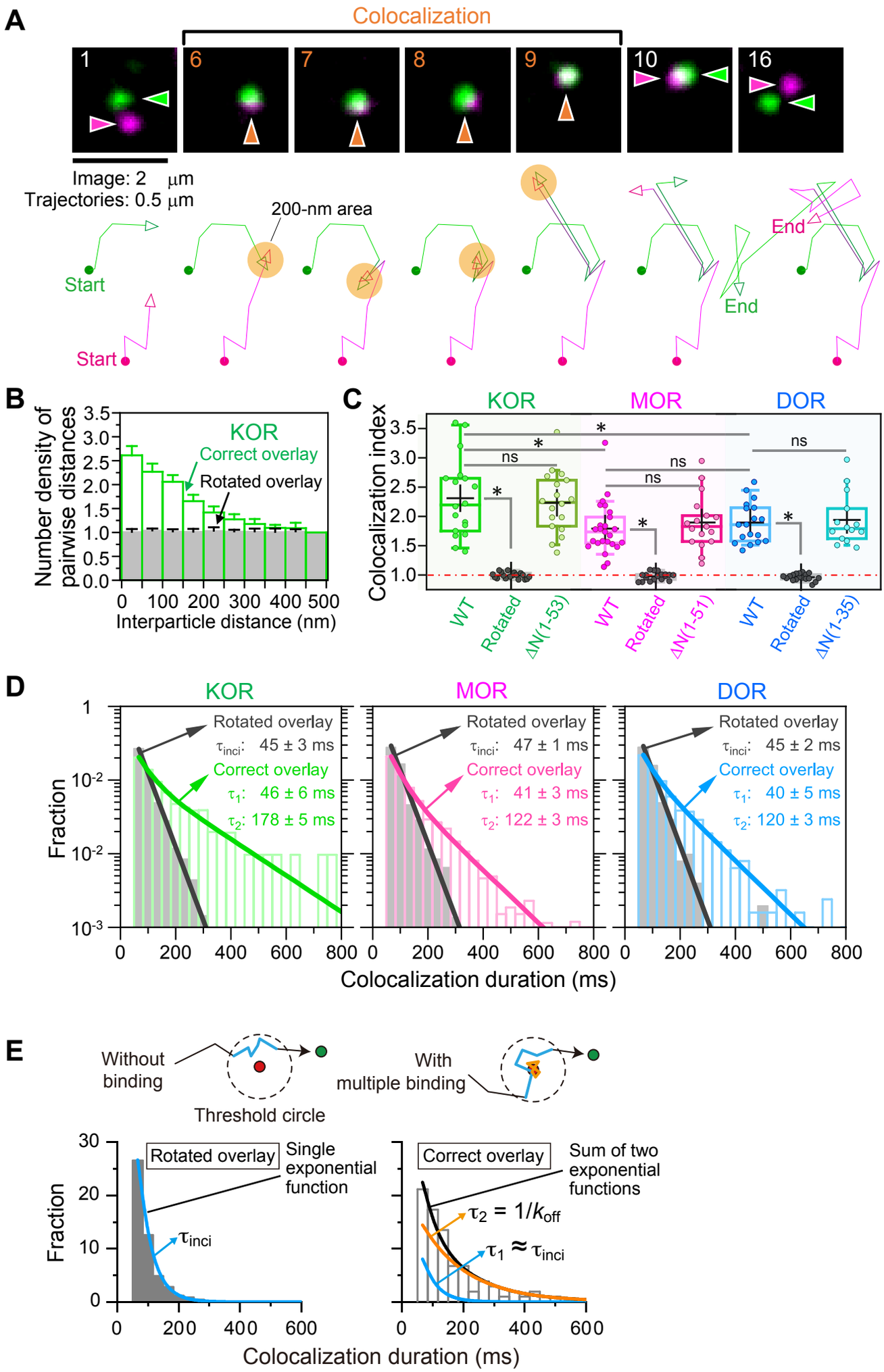
A
Colocalization
1
6
7
8
9
10
16
Image: 2 μm
Trajectories: 0.5 μm
200-nm area
Start
Start
End
End
B
Number density of pairwise distances
KOR
Correct overlay
Rotated overlay
Interparticle distance (nm)
C
KOR
MOR
DOR
Colocalization index
ns
*
WT
Rotated
ΔN(1-53)
WT
Rotated
ΔN(1-51)
WT
Rotated
ΔN(1-35)
D
KOR
MOR
DOR
Fraction
Rotated overlay
τinci: 45 ± 3 ms
Correct overlay
τ1: 46 ± 6 ms
τ2: 178 ± 5 ms
Rotated overlay
τinci: 47 ± 1 ms
Correct overlay
τ1: 41 ± 3 ms
τ2: 122 ± 3 ms
Rotated overlay
τinci: 45 ± 2 ms
Correct overlay
τ1: 40 ± 5 ms
τ2: 120 ± 3 ms
Colocalization duration (ms)
E
Without binding
With multiple binding
Threshold circle
Rotated overlay
Single exponential function
τinci
Correct overlay
Sum of two exponential functions
τ2 = 1/koff
τ1 ≈ τinci
Fraction
Colocalization duration (ms)

Figure 1

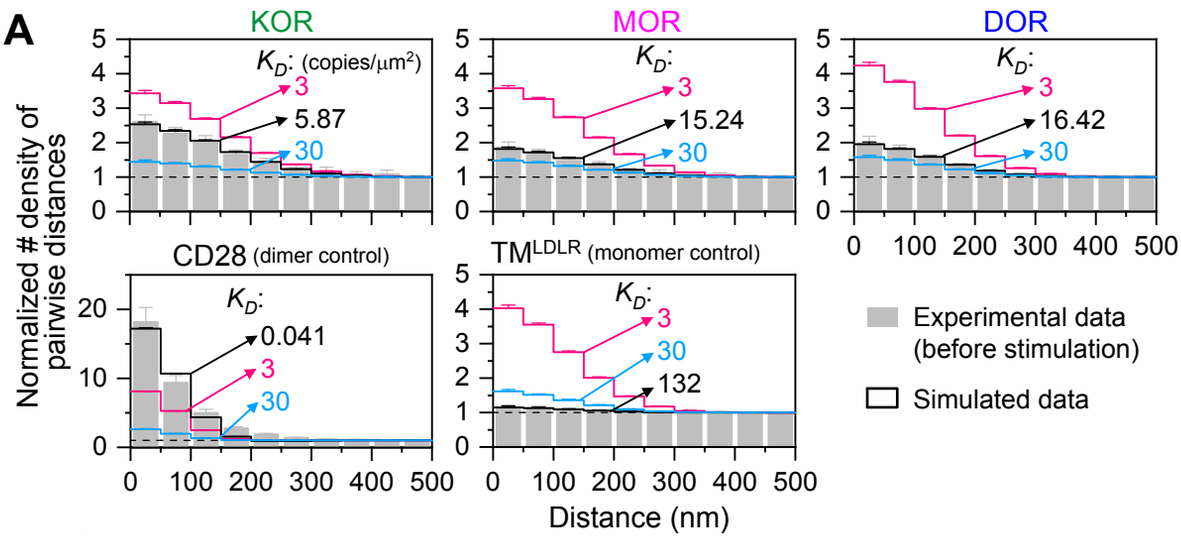

B

ORs	K_D (copies/μm²)	k_{off} (s⁻¹)	k_{on} (μm²/copies/s)	Predicted %OR protomers existing as dimers at different expression levels (copies/μm²)				
				0.3	1	3	10	30
KOR	5.87 ± 0.56	6.71 ± 1.17	1.14 ± 0.23	8.6	21	39	59	73
MOR	15.24 ± 1.54	8.47 ± 0.86	0.56 ± 0.08	3.7	11	23	43	61
DOR	16.42 ± 0.53	8.00 ± 0.96	0.49 ± 0.06	3.4	10	22	42	60
CD28	0.041 ± 0.072	N.D.	N.D.					
TM^LDLR	132 ± 21	N.D.	N.D.					

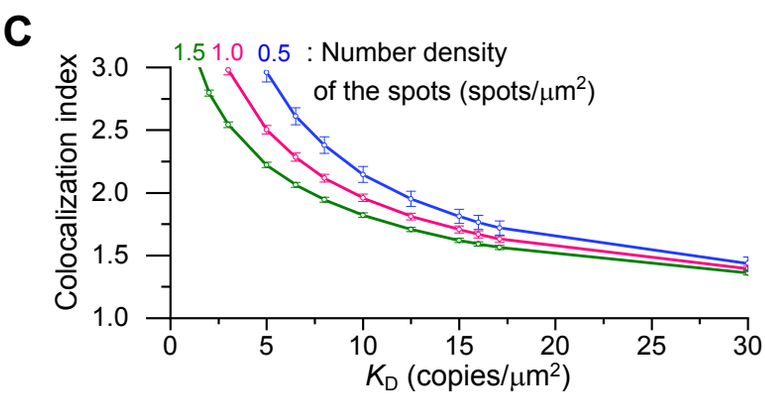

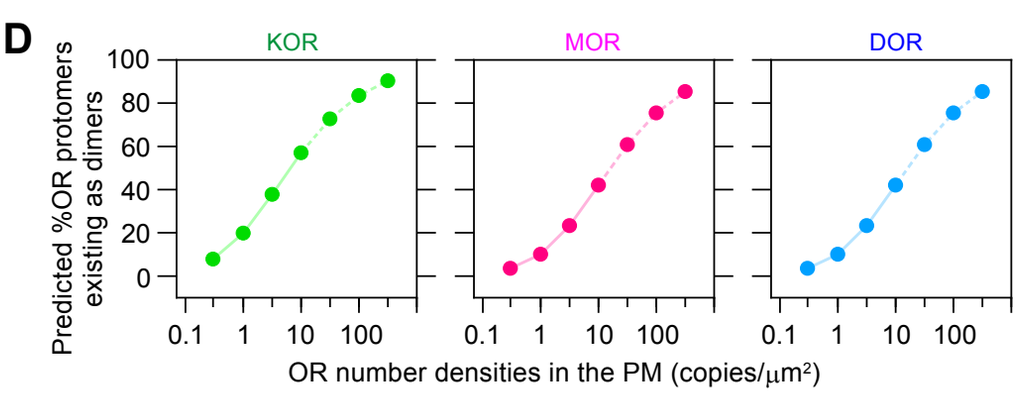

Figure 2

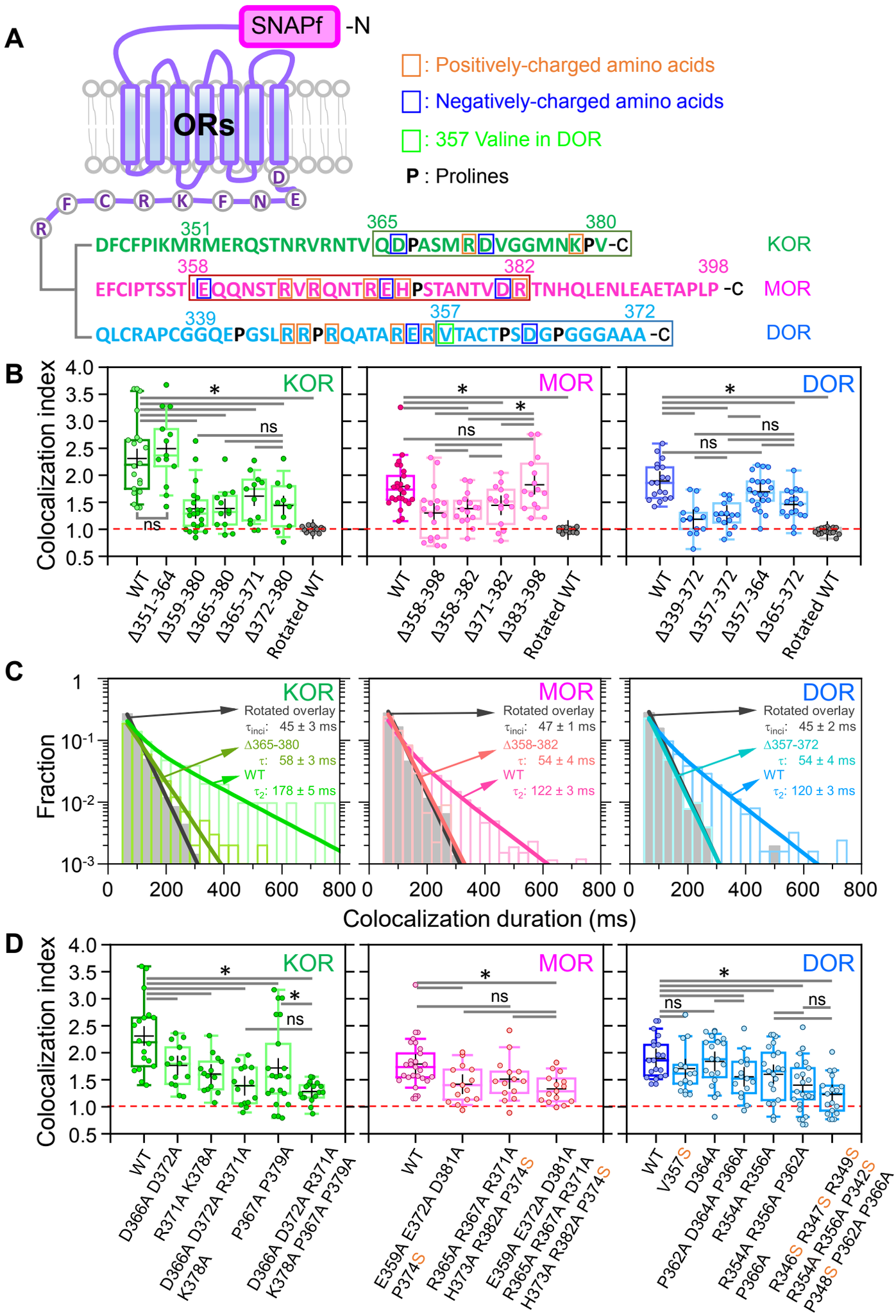
A
SNAPf
-N
ORs
: Positively-charged amino acids
: Negatively-charged amino acids
: 357 Valine in DOR
P : Prolines
R F C R K F N E D
351 365 380
DFCFPIKMRMERQSTNRVRNTV QDPASMRDVGGMNKPV-C KOR
358 382 398
EFCIPTSSTIEQQNSTRVRQNTREHPSTANTVDRTNHQLENLEAETAPLP -C MOR
339 357 372
QLCRAPCGGQEPGSLRRPRQATAREREVTACTPSDGPGGGAAA -C DOR
B
Colocalization index
KOR
MOR
DOR
ns
*
WT
Δ351-364
Δ359-380
Δ365-380
Δ365-371
Δ372-380
Rotated WT
Δ358-398
Δ358-382
Δ371-382
Δ383-398
Δ339-372
Δ357-372
Δ357-364
Δ365-372
C
Fraction
Rotated overlay
τinci: 45 ± 3 ms
Δ365-380
τ: 58 ± 3 ms
WT
τ2: 178 ± 5 ms
τinci: 47 ± 1 ms
Δ358-382
τ: 54 ± 4 ms
τ2: 122 ± 3 ms
τinci: 45 ± 2 ms
Δ357-372
τ: 54 ± 4 ms
τ2: 120 ± 3 ms
Colocalization duration (ms)
D
D366A D372A
R371A K378A
D366A D372A R371A K378A
P367A P379A
D366A D372A R371A K378A P367A P379A
E359A E372A D381A P374S
R365A R367A R371A H373A R382A P374S
E359A E372A D381A R365A R367A R371A H373A R382A P374S
V357S
D364A
P362A D364A P366A
R354A R356A
R354A R356A P362A P366A
R346S R347S R349S
R354A R356A P342S P348S P362A P366A

Figure 3

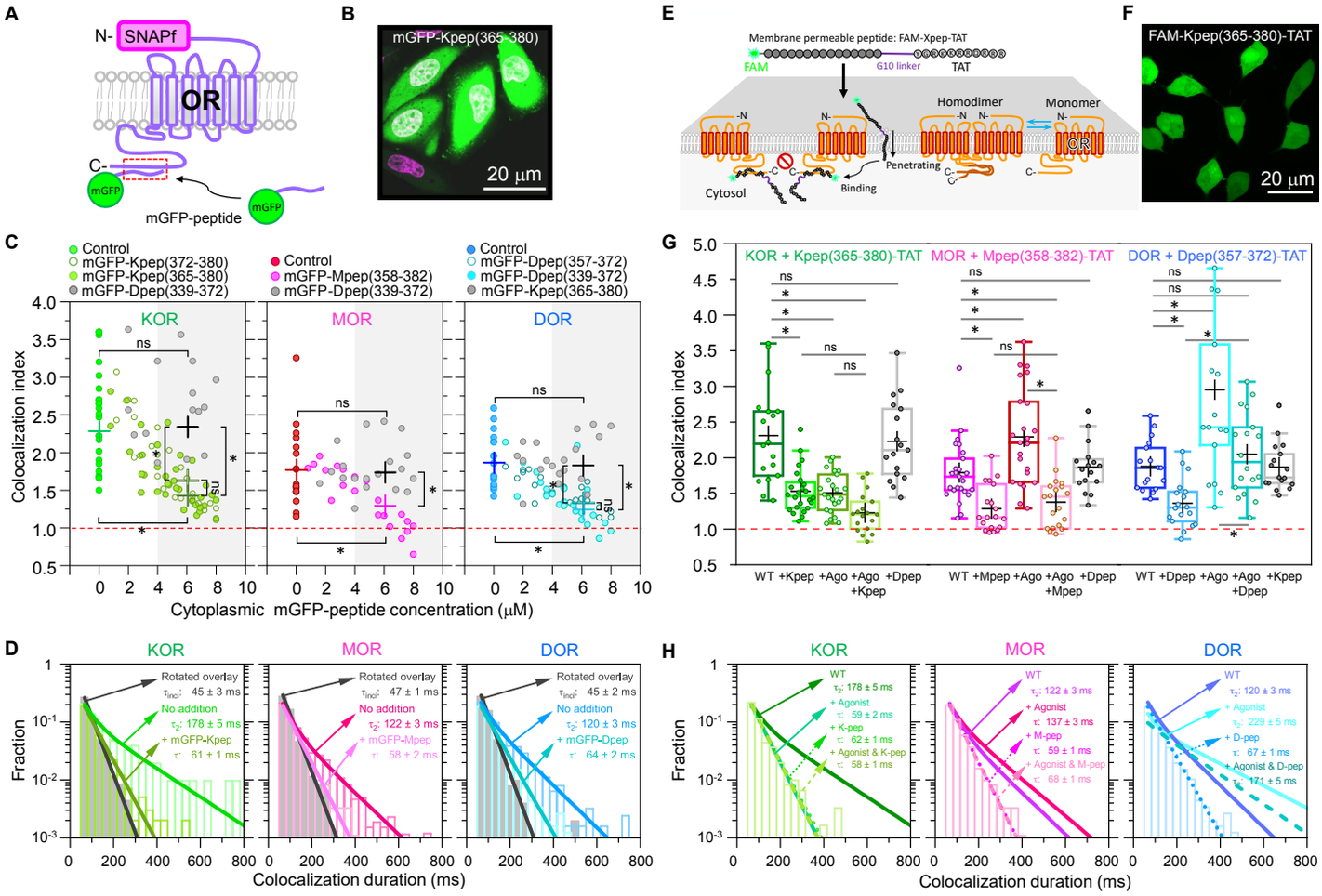

I

ORs	Agonist	Xpep	K_D (copies/μm²)	k_{off} (s⁻¹)	k_{on} (μm²/copies/s)	Predicted %OR protomers existing as dimers at different expression levels (copies/μm²)				
						0.3	1	3	10	30
KOR	–	–	5.87 ± 0.56	6.71 ± 1.17	1.14 ± 0.23	8.6	21	39	59	73
	–	+	58.02 ± 6.71	16.13 ± 0.26	0.28 ± 0.03	1.0	3.2	8.6	21	39
	+	–	15.81 ± 1.36	17.86 ± 0.32	1.13 ± 0.10	3.5	10	23	42	60
	+	+	65.05 ± 16.00	17.24 ± 0.30	0.27 ± 0.07	0.9	2.9	7.8	20	37
MOR	–	–	15.24 ± 1.54	8.47 ± 0.86	0.56 ± 0.08	3.7	11	23	43	61
	–	+	45.51 ± 7.92	16.95 ± 0.29	0.37 ± 0.07	1.3	4.0	11	25	43
	+	–	8.34 ± 0.58	5.35 ± 1.69	0.64 ± 0.21	6.8	18	34	54	70
	+	+	56.44 ± 8.15	14.71 ± 0.22	0.26 ± 0.04	1.0	3.3	8.8	22	39
DOR	–	–	16.42 ± 0.53	8.00 ± 0.96	0.49 ± 0.06	3.4	10	22	42	60
	–	+	41.21 ± 3.26	14.93 ± 0.22	0.36 ± 0.03	1.4	4.4	11	26	45
	+	–	7.69 ± 0.36	3.62 ± 0.25	0.47 ± 0.04	6.3	17	33	53	69
	+	+	19.56 ± 1.80	5.88 ± 0.17	0.30 ± 0.03	2.9	8.6	20	39	57

Figure 4

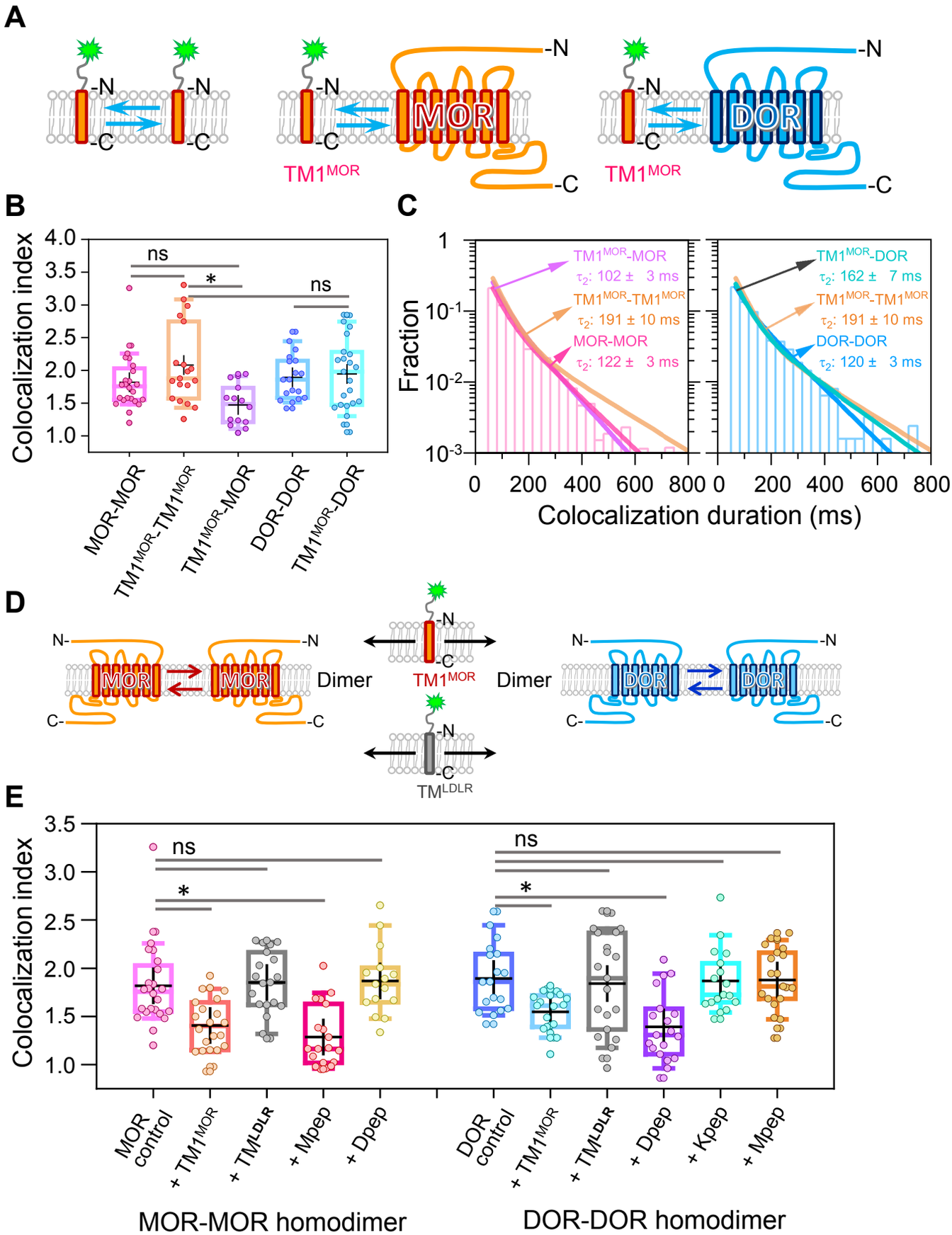
A
-N
-C
MOR
DOR
TM1MOR
B
Colocalization index
ns
*
MOR-MOR
TM1MOR-TM1MOR
TM1MOR-MOR
DOR-DOR
TM1MOR-DOR
C
Fraction
TM1MOR-MOR
τ2: 102 ± 3 ms
TM1MOR-TM1MOR
τ2: 191 ± 10 ms
MOR-MOR
τ2: 122 ± 3 ms
TM1MOR-DOR
τ2: 162 ± 7 ms
DOR-DOR
τ2: 120 ± 3 ms
Colocalization duration (ms)
D
N-
C-
Dimer
TMLDLR
E
MOR control
+ TM1MOR
+ TMLDLR
+ Mpep
+ Dpep
DOR control
+ Kpep
MOR-MOR homodimer
DOR-DOR homodimer

Figure 5

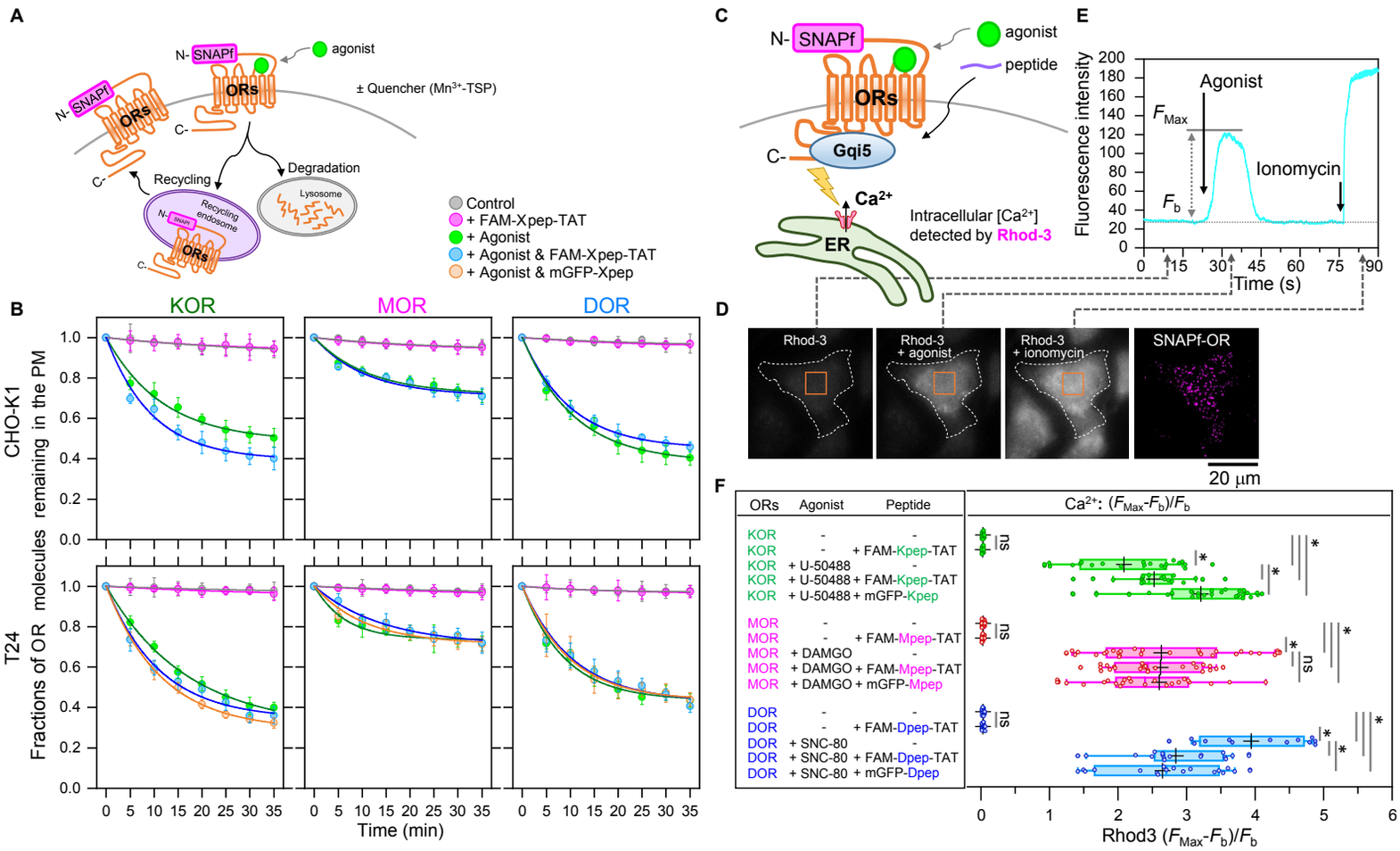
A
N- SNAPf
agonist
ORs
± Quencher (Mn3+-TSP)
C-
Recycling
Degradation
Lysosome
Recycling endosome
Control
+ FAM-Xpep-TAT
+ Agonist
+ Agonist & FAM-Xpep-TAT
+ Agonist & mGFP-Xpep
B
KOR
MOR
DOR
CHO-K1
T24
Fractions of OR molecules remaining in the PM
Time (min)
C
N- SNAPf
agonist
peptide
ORs
C-
Gqi5
Ca2+
ER
Intracellular [Ca2+] detected by Rhod-3
E
Fluorescence intensity
Agonist
FMax
Fb
Ionomycin
Time (s)
D
Rhod-3
Rhod-3 + agonist
Rhod-3 + ionomycin
SNAPf-OR
20 µm
F
ORs Agonist Peptide
KOR - -
KOR - + FAM-Kpep-TAT
KOR + U-50488 -
KOR + U-50488 + FAM-Kpep-TAT
KOR + U-50488 + mGFP-Kpep
MOR - -
MOR - + FAM-Mpep-TAT
MOR + DAMGO -
MOR + DAMGO + FAM-Mpep-TAT
MOR + DAMGO + mGFP-Mpep
DOR - -
DOR - + FAM-Dpep-TAT
DOR + SNC-80 -
DOR + SNC-80 + FAM-Dpep-TAT
DOR + SNC-80 + mGFP-Dpep
Ca2+: (FMax-Fb)/Fb
ns
Rhod3 (FMax-Fb)/Fb

Figure 6

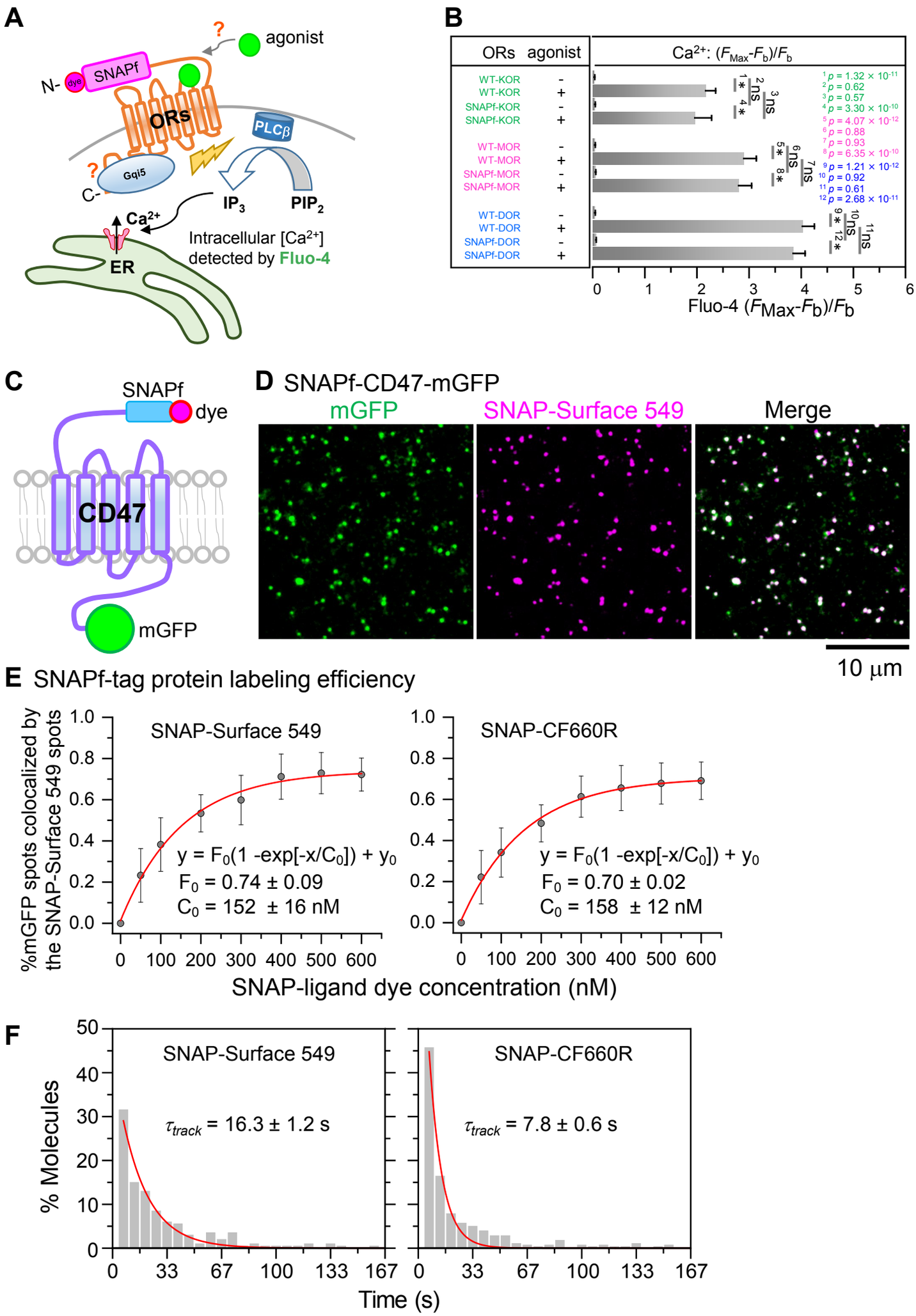
A
agonist
N-
dye
SNAPf
ORs
PLCβ
Gqi5
C-
IP3
PIP2
Ca2+
ER
Intracellular [Ca2+] detected by Fluo-4
B
ORs agonist
Ca2+: (FMax-Fb)/Fb
WT-KOR -
WT-KOR +
SNAPf-KOR -
SNAPf-KOR +
WT-MOR -
WT-MOR +
SNAPf-MOR -
SNAPf-MOR +
WT-DOR -
WT-DOR +
SNAPf-DOR -
SNAPf-DOR +
1 p = 1.32 × 10-11
2 p = 0.62
3 p = 0.57
4 p = 3.30 × 10-10
5 p = 4.07 × 10-12
6 p = 0.88
7 p = 0.93
8 p = 6.35 × 10-10
9 p = 1.21 × 10-12
10 p = 0.92
11 p = 0.61
12 p = 2.68 × 10-11
Fluo-4 (FMax-Fb)/Fb
C
SNAPf
dye
CD47
mGFP
D SNAPf-CD47-mGFP
mGFP
SNAP-Surface 549
Merge
10 μm
E SNAPf-tag protein labeling efficiency
SNAP-Surface 549
y = F0(1 -exp[-x/C0]) + y0
F0 = 0.74 ± 0.09
C0 = 152 ± 16 nM
SNAP-CF660R
y = F0(1 -exp[-x/C0]) + y0
F0 = 0.70 ± 0.02
C0 = 158 ± 12 nM
%mGFP spots colocalized by the SNAP-Surface 549 spots
SNAP-ligand dye concentration (nM)
F
SNAP-Surface 549
τtrack = 16.3 ± 1.2 s
SNAP-CF660R
τtrack = 7.8 ± 0.6 s
% Molecules
Time (s)

Fig. S1

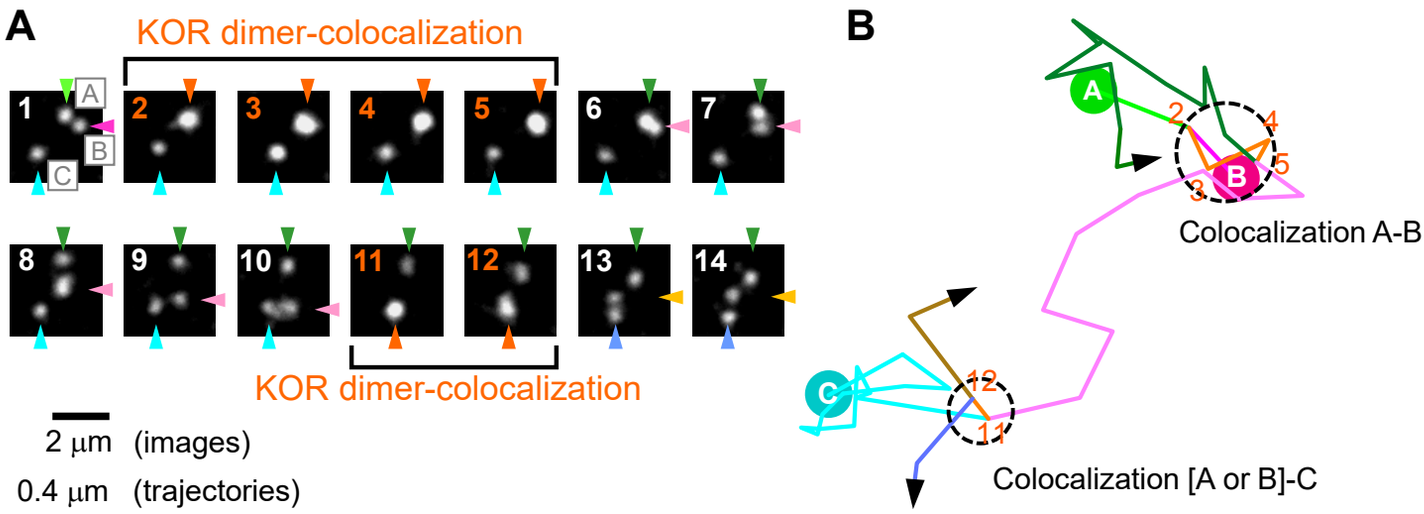
A
KOR dimer-colocalization
1
2
3
4
5
6
7
8
9
10
11
12
13
14
A
B
C
KOR dimer-colocalization
2 μm (images)
0.4 μm (trajectories)
B
A
B
C
2
3
4
5
11
12
Colocalization A-B
Colocalization [A or B]-C

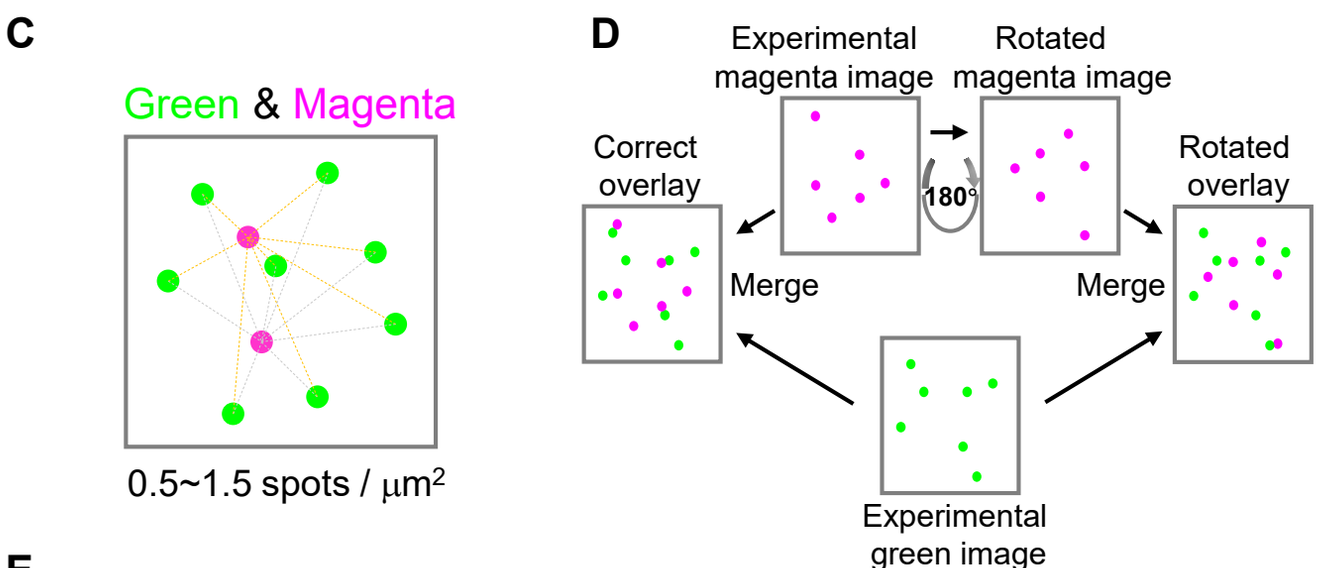
C
Green & Magenta
0.5~1.5 spots / μm²
D
Experimental magenta image
Rotated magenta image
Correct overlay
Rotated overlay
180°
Merge
Merge
Experimental green image

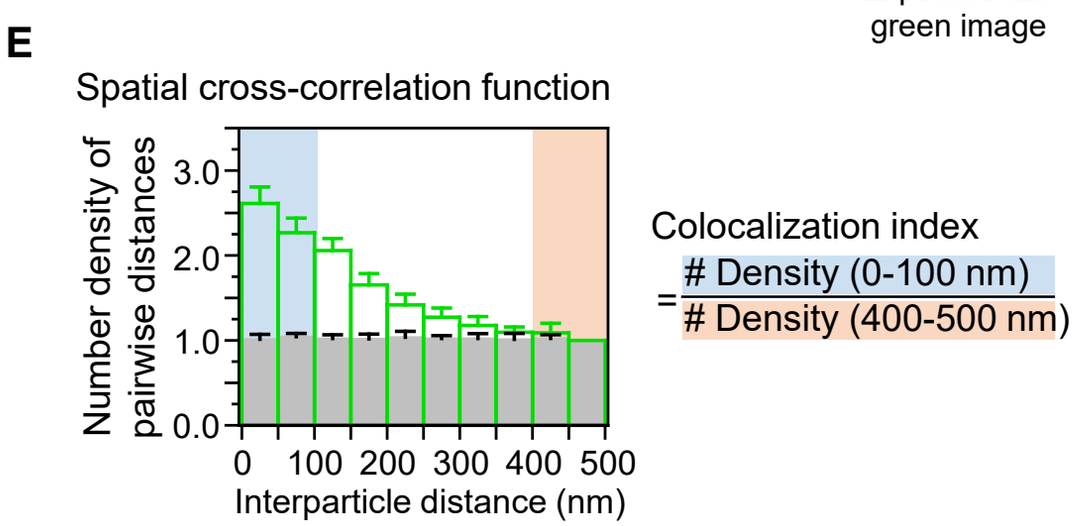
E
Spatial cross-correlation function
Number density of pairwise distances
3.0
2.0
1.0
0.0
0
100
200
300
400
500
Interparticle distance (nm)
Colocalization index
= # Density (0-100 nm) / # Density (400-500 nm)

Fig. S2

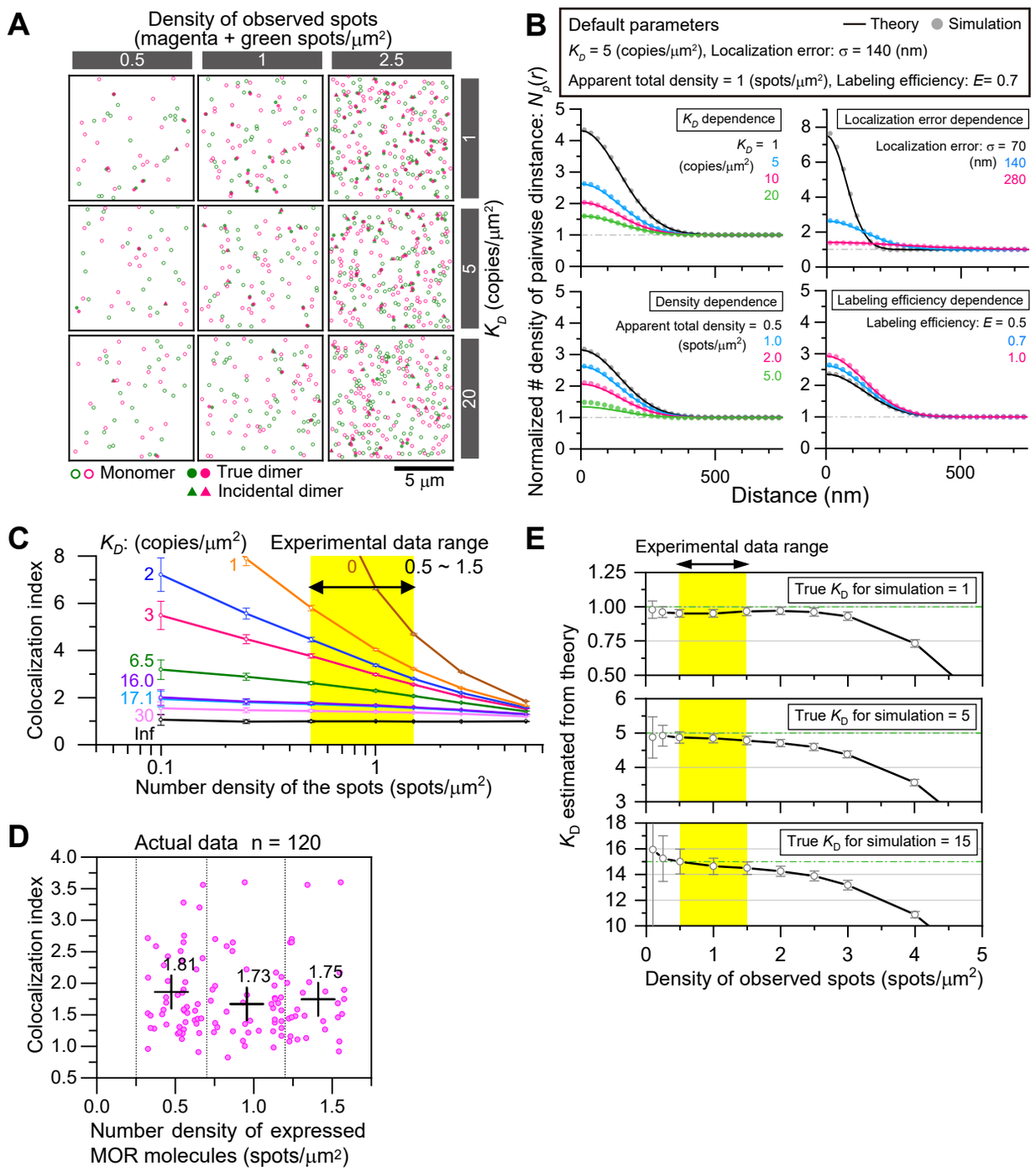
A
Density of observed spots
(magenta + green spots/μm²)
0.5
1
2.5
1
5
20
K_D (copies/μm²)
Monomer
True dimer
Incidental dimer
5 μm
B
Default parameters
Theory
Simulation
K_D = 5 (copies/μm²), Localization error: σ = 140 (nm)
Apparent total density = 1 (spots/μm²), Labeling efficiency: E= 0.7
Normalized # density of pairwise dinstance: $N_p(r)$
K_D dependence
K_D = 1
(copies/μm²)
5
10
20
Localization error dependence
Localization error: σ = 70
(nm)
140
280
Density dependence
Apparent total density = 0.5
(spots/μm²)
1.0
2.0
5.0
Labeling efficiency dependence
Labeling efficiency: E = 0.5
0.7
1.0
Distance (nm)
C
K_D: (copies/μm²)
Experimental data range
0.5 ~ 1.5
Colocalization index
Number density of the spots (spots/μm²)
Inf
D
Actual data n = 120
Colocalization index
1.81
1.73
1.75
Number density of expressed
MOR molecules (spots/μm²)
E
Experimental data range
True K_D for simulation = 1
True K_D for simulation = 5
True K_D for simulation = 15
K_D estimated from theory
Density of observed spots (spots/μm²)

Fig. S3

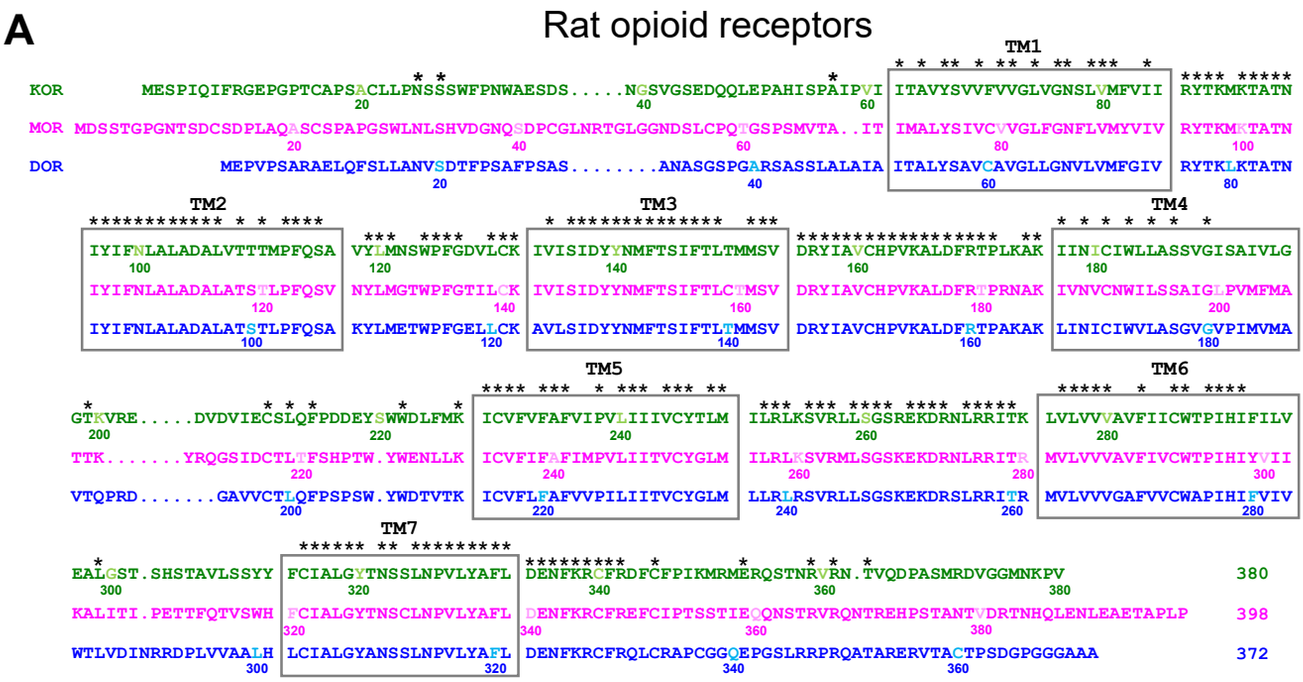
A
Rat opioid receptors
TM1
TM2
TM3
TM4
TM5
TM6
TM7
KOR
MOR
DOR

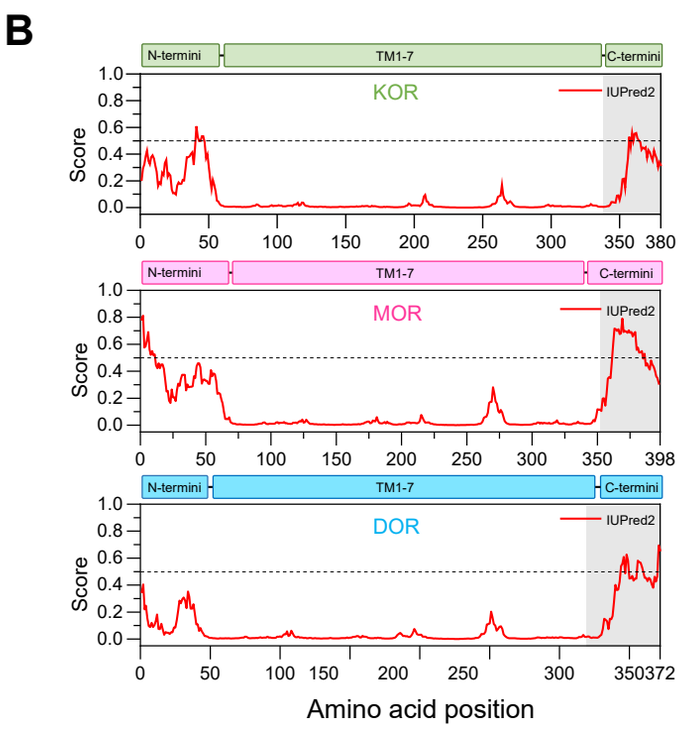
B
N-termini
TM1-7
C-termini
KOR
MOR
DOR
IUPred2
Score
Amino acid position

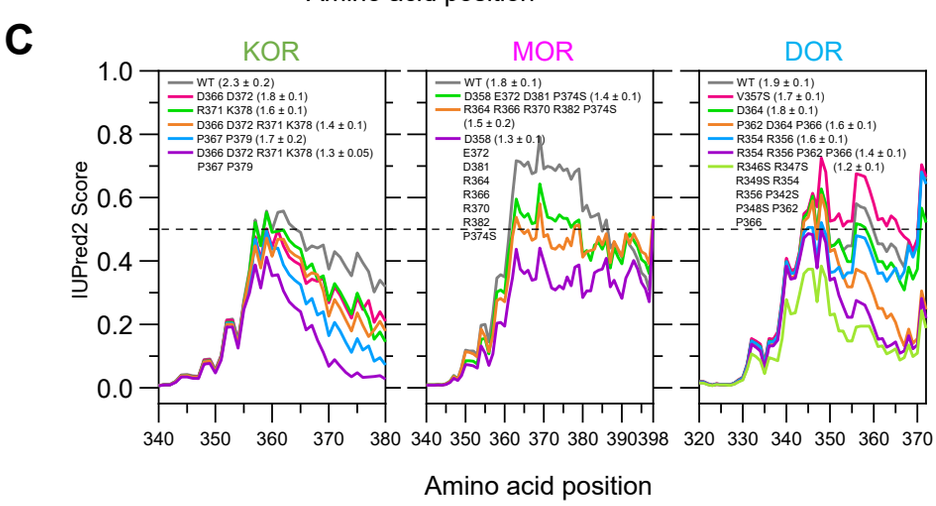
C
KOR
MOR
DOR
IUPred2 Score
WT (2.3 ± 0.2)
D366 D372 (1.8 ± 0.1)
R371 K378 (1.6 ± 0.1)
D366 D372 R371 K378 (1.4 ± 0.1)
P367 P379 (1.7 ± 0.2)
D366 D372 R371 K378 (1.3 ± 0.05)
P367 P379
WT (1.8 ± 0.1)
D358 E372 D381 P374S (1.4 ± 0.1)
R364 R366 R370 R382 P374S
(1.5 ± 0.2)
D358 (1.3 ± 0.1)
E372
D381
R364
R366
R370
R382
P374S
WT (1.9 ± 0.1)
V357S (1.7 ± 0.1)
D364 (1.8 ± 0.1)
P362 D364 P366 (1.6 ± 0.1)
R354 R356 (1.6 ± 0.1)
R354 R356 P362 P366 (1.4 ± 0.1)
R346S R347S
(1.2 ± 0.1)
R349S R354
R356 P342S
P348S P362
P366
Amino acid position

Fig. S4

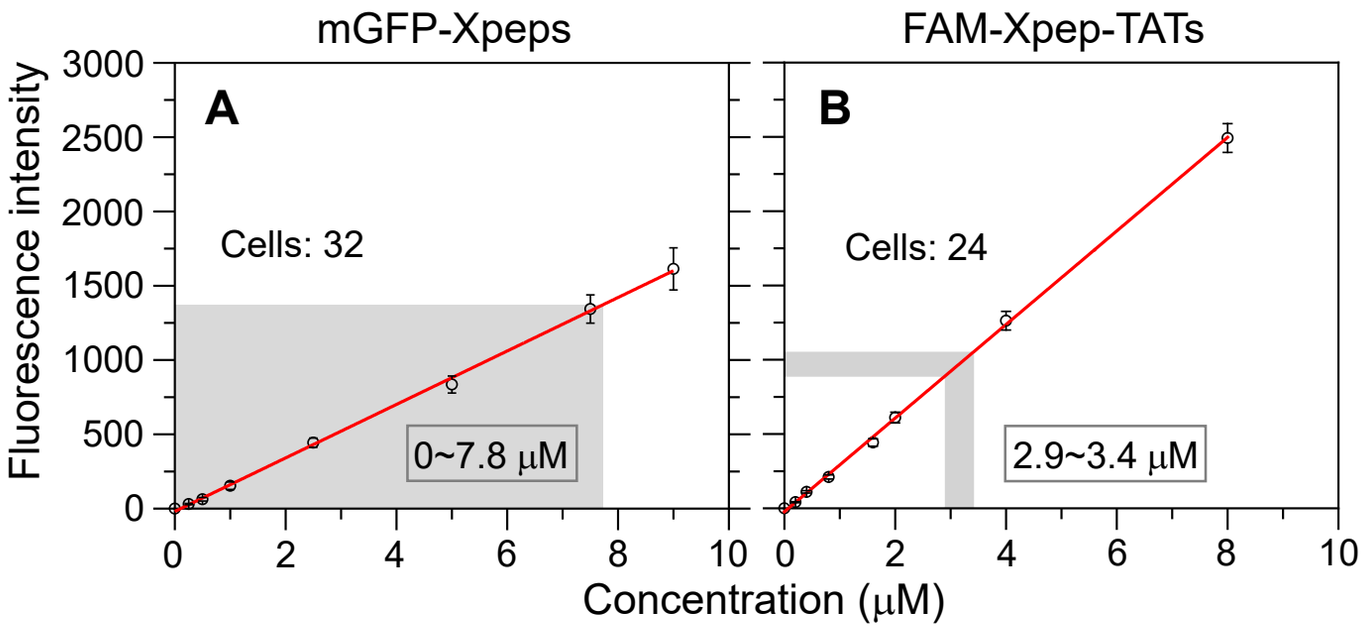
mGFP-Xpeps
FAM-Xpep-TATs
A
B
Cells: 32
Cells: 24
0~7.8 μM
2.9~3.4 μM
Fluorescence intensity
Concentration (μM)
0
500
1000
1500
2000
2500
3000
0
2
4
6
8
10

Fig. S5

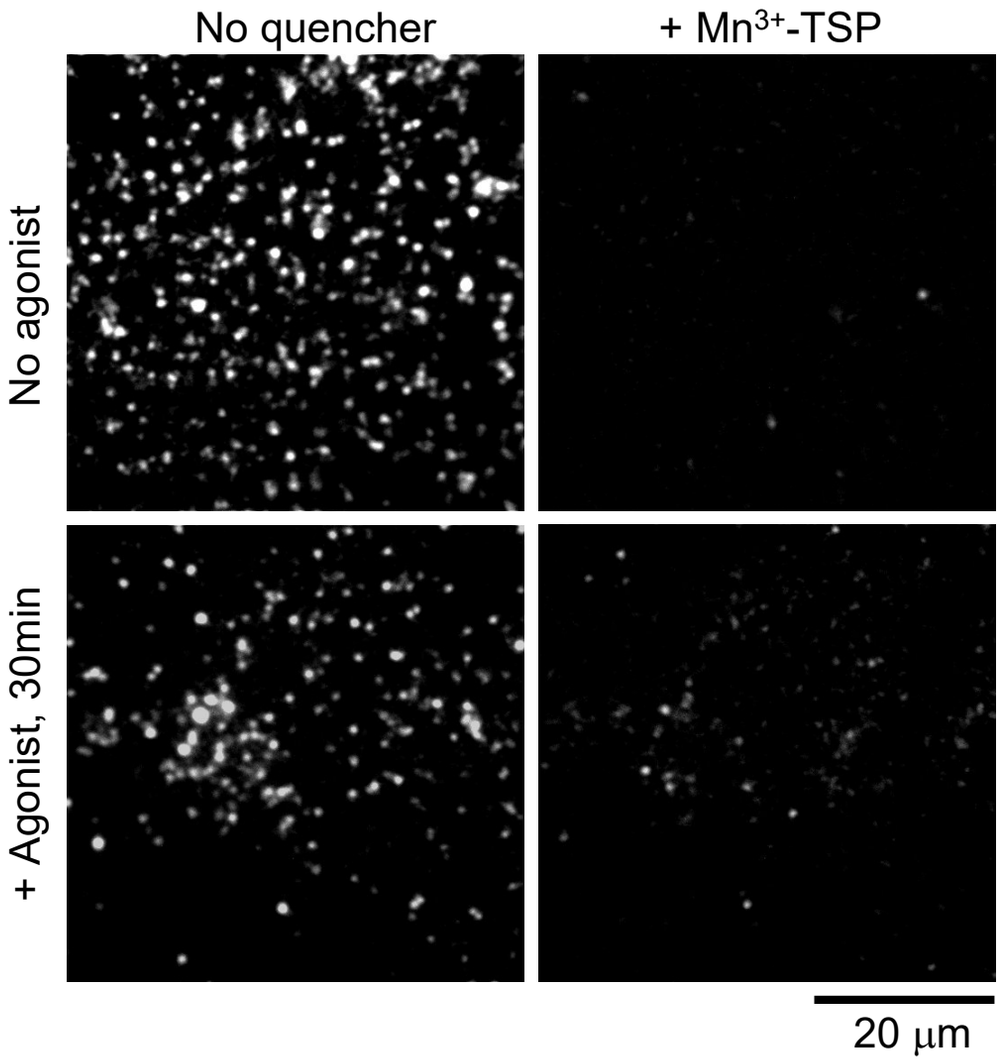

Fig. S6

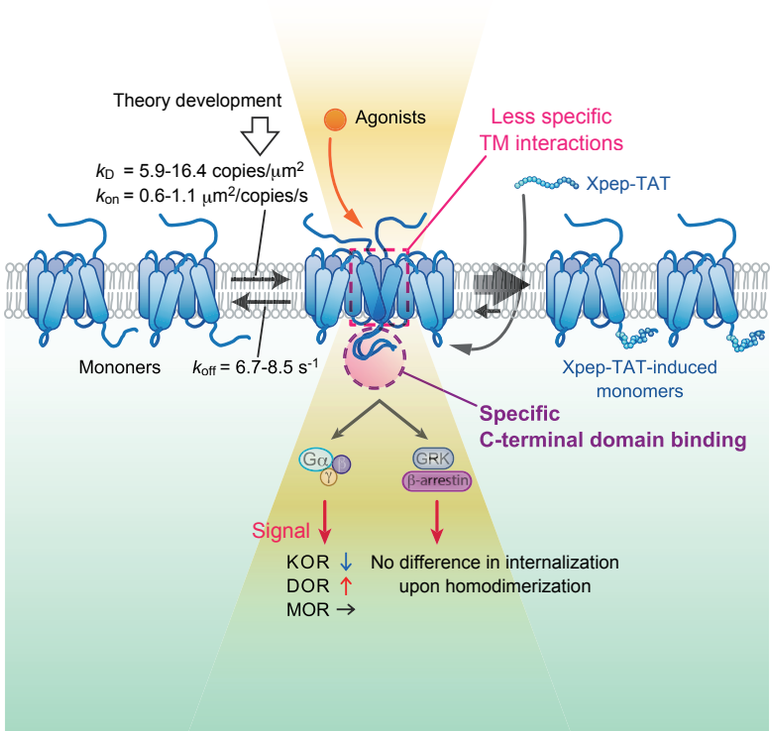
Theory development
k_D = 5.9-16.4 copies/μm^2
k_{on} = 0.6-1.1 μm^2/copies/s
Agonists
Less specific
TM interactions
Xpep-TAT
Mononers
k_{off} = 6.7-8.5 s^{-1}
Xpep-TAT-induced
monomers
Specific
C-terminal domain binding
Gα
β
γ
GRK
β-arrestin
Signal
KOR ↓
DOR ↑
MOR →
No difference in internalization
upon homodimerization

Single-molecule detection of transient dimerization of opioid receptors 1: Homodimers' effect on signaling and internalization

Peng Zhou[1], Taka A. Tsunoyama[1], Rinshi S. Kasai[2,3,4], Koichiro M. Hirosawa[4], Ziya Kalay[5], Amine Aladag[1], Takahiro K. Fujiwara[5], Simone Pigolotti[6], and Akihiro Kusumi[1,5]

[1]Membrane Cooperativity Unit, Okinawa Institute of Science and Technology Graduate University, Onna-son, Okinawa 904-0495, Japan. [2]Institute for Life and Medical Sciences, Kyoto University, Kyoto 606-8507, Japan. [3]Division of Advanced Bioimaging, National Cancer Center Research Institute, Tokyo 104-0045, Japan. [4]Institute for Glyco-core Research (iGCORE), Gifu University, Gifu 501-1193, Japan. [5]Institute for Integrated Cell-Material Sciences (WPI-iCeMS), Kyoto University, Kyoto 606-8501, Japan. [6]Biological Complexity Unit, Okinawa Institute of Science and Technology Graduate University, Onna-son, Okinawa 904-0495, Japan.

Graphical Abstract

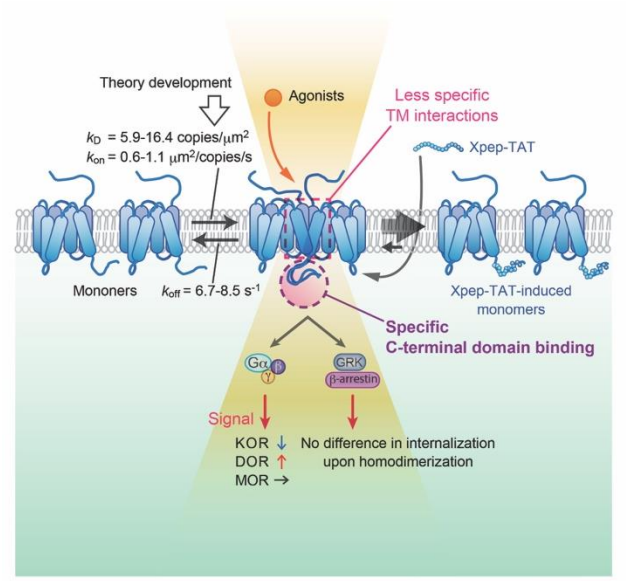

Highlights

- Opioid receptors rapidly interconvert between monomers and transient homodimers
- We developed theories for evaluating the dimer k_{off} and K_D in the plasma membrane
- C-terminal cytoplasmic domains are involved in specific homodimerization
- Homodimer blocking peptides modulate signaling but not receptor internalization

SUMMARY

Opioid receptors (ORs) are critical for endogenous and synthetic analgesics. Their homodimerization is considered important for their pharmacological diversities, but whether they form homodimers remains controversial. Here, we established that the three classical ORs, μ-, κ-, and δ-ORs (MOR, KOR, and DOR, respectively) undergo repeated transient (120-180 ms) homodimerizations every few seconds. This was done by using single-molecule imaging and developing theories for analyzing single-molecule colocalization data, which provide the key parameters, homodimer-monomer dissociation equilibrium constants and rate constants. Their 9-26 amino-acid C-terminal cytoplasmic domains, without sequence similarities, are involved in specific homodimerization, whereas the transmembrane domains provide less specific affinities. Using the membrane-permeable peptides mimicking the C-terminal homodimerization sequences which block homodimerizations, functions of monomers and homodimers were dissected. KOR and DOR homodimers, but not MOR homodimers, activate downstream G-proteins differently from monomers upon agonist addition, without influencing OR internalization. These findings could guide strategies to enhance OR-based analgesia.